

NEUROMUSCULAR DYNAMICS IN THE CONTEXT OF MOTOR
REDUNDANCY

by

Cornelius Raths (Kornelius Rácz)

A Dissertation Presented to the
FACULTY OF THE USC GRADUATE SCHOOL
UNIVERSITY OF SOUTHERN CALIFORNIA
In Partial Fulfillment of the
Requirements for the Degree
DOCTOR OF PHILOSOPHY
(NEUROSCIENCE)

August 2012

Für Włodek Bzówka (21.06.1979 - 26.12.2007)

Acknowledgements

In the spring of 2007, having completed three lab rotations, I met with Professor Gerald Loeb to break to him my decision to join his lab, in which I had done my second lab rotation, working on the machine learning problem of predicting elbow angles from shoulder coordinates. My overly idealistic plan for my dissertation project was to develop a neural hand prosthesis, having worked on the development of Brain-Computer Interfaces for my Master's thesis in Computer Science. Professor Loeb correctly pointed out that the neural control of the hand was poorly understood (and additionally, I was hardly familiar with what was understood), rendering the development of such a prosthesis premature. To alleviate my shortcomings and enable me to potentially embark on this project in the long-term future, he introduced me to Francisco Valero-Cuevas, who was soon going to join the Biomedical Engineering Department at USC. Having completed a successful and very instructive fourth lab rotation in the summer of 2007, and been very much involved in the establishment of the new Brain-Body Dynamics Lab, I decided to join.

I have always admired Francisco for his intuition: where it took me hours to come up with an idea of how to analyze or interpret data, he suggested an excellent solution within minutes, if not seconds. Many times, this has reinvigorated my enthusiasm for the projects described in this dissertation. Furthermore, I would like to thank him for his kind and generous attitude, allowing me to complete two Master of Science degrees

in addition to the PhD, and the many pleasant conversations we had, sometimes outside the scope of our immediate work.

Naturally, I extend my thanks to the person to whom I owe having met Francisco: Professor Gerald Loeb, who did however serve on my Guidance Committee. While Francisco was a great source of encouragement for my ideas and plans, Professor Loeb was antipodal in that in our numerous and lengthy discussions (or should I say, lessons), he challenged them, based on scientific principle and experience. The challenges were never general, always addressing details, but also providing ideas to overcome demonstrated shortcomings. When it comes to muscle physiology, his knowledge is unmatched.

Another important source of scientific challenge, but also of means to "get things done", joined our lab in the summer of 2008: Jason Kutch, then a post-doc, now a professor in the Biokinesiology division. I had first met Jason at a workshop on mathematics and biosciences at Ohio State University earlier that year, when he had just completed his PhD. His combined mathematics and physiology background allowed Jason more than anybody to identify appropriate ways to model and simulate scientific phenomena and to test hypotheses. Without his ideas, much of the work presented here would not have been possible. I am grateful that he served on my Dissertation committee.

Speaking of interdisciplinarity, I would also like to express my gratitude to Professor Madhusudan Venkadesan, Francisco's PhD student at Cornell University until 2007 and now a Professor at the National Centre for Biological Sciences in Bangalore, India. Although we talked only briefly at a noise and balance workshop in Banff, Alberta, Canada, these conversations proved to be some of the most important of my entire PhD. While the idea that motor variability in terms of muscle and endpoint force reflects fatigue mitigation mechanisms and is not simply uncorrelated noise came to me previously, it was thanks to Madhu that I started thinking of using differential equations to model fatigue and recovery and combine these models with optimization.

While I was not short of projects and work, a conversation between Francisco and Professor Nina Bradley, of the Biokinesiology Division, in 2009, would lead to a very fruitful collaboration on the motor development of domestic chick. This project taught me a lot about the use of statistics in life science research and I am deeply grateful to Nina for her devotion to precision both methodologically and in terms of expressing scientific findings. Naturally, I would also like to thank her to have served on my Guidance and Dissertation Committees, in fact, as the chair on the latter.

Besides faculty, I am indebted first of all to Sudarshan Dayanidhi, who joined the lab and graduated at the same time as I. During those 5 years in between, we became close friends and I will never forget that he attended my wedding in China in the fall of 2010, and served as one of the best men. Besides this, he has always found the time for a discussion on physiology or science in general, being an excellent Physical Therapist, and to participate in one of my experiments. I hope that my presence in the lab was half as useful to his work as my presence was to his.

Those 5 years I also shared with Manish Kurse, who had accompanied Francisco from Cornell, having joined the lab the year before. Manish helped me tremendously in modeling isometric motor task, with his excellent background in mechanics and optimization. Furthermore, I will always kindly remember his cheerful personality.

Besides, I would like to thank Josh Inouye, for having designed and built the second generation of the TIM grasping device. Moreover, his productivity, work ethic and determination towards his work have been inspirational. I would also like to thank Dan Brown, formerly at Cornell and whom unfortunately I have never met, for having built the first generation of the TIM and having mathematically modeled the motor task of simultaneous tripod grasp and thumb oscillation.

None of university research would be possible without the contribution of administrators, who make sure that stipends are paid, equipment is purchased and forms are

filled out. In this regard, I would like to mention the great work done by Adriana Cisneros, at the RTH Business Center, and Vanessa Clark, at the Neuroscience Graduate Program. But most of all, I would like to thank Linda Bazilian, especially for helping me stay at USC when there was a chance of my having to drop out due to university regulations. I am grateful to the Neuroscience Program as a whole for having provided this awesome opportunity and having accepted me into the program.

Finally, I owe much of the happiness of the last 6 years to Jingyang Zhong, whom I met on August 2, 2006, when we both started our PhDs in Neuroscience and whom I married on September 29, in Hangzhou, China. Facing similar challenges in our PhDs, but fortunately (!) pursuing very different interests scientifically, we found in each other sources of constant and unconditional support.

Kornelius Rácz

Los Angeles, 2012

Table of Contents

Dedication	ii
Acknowledgements	iii
List of Tables	xi
List of Figures	xii
Abstract	xvi
Chapter 1: Introduction, Background and Prior Work	1
1.1 Motor Redundancy	1
1.2 Muscle Fatigue	4
1.3 Experimental Evidence: Leveraging Muscle Redundancy for Fatigue Mitigation	8
1.4 Modeling and Simulation: Muscle Redundancy and Muscle Fatigue	10
Chapter 2: Fatigue Dynamics Have Profound Consequences for Muscle Coordination and Theories of Motor Control	14
2.1 Abstract	14
2.2 Introduction	15
2.3 Methods	19
2.3.1 Modeling a redundant neuromuscular system	19
2.3.2 Mathematical modeling of fatigue	25
2.3.3 Simulating muscle activation dynamics in isometric knee extension subject to optimization	27
2.3.4 Parameter search	29
2.4 Results	30
2.4.1 Eureqa-extracted dynamics of muscle fatigue and recovery	30
2.4.2 Running the nominal model subject to optimized activation	32
2.4.3 Parameter search results	34
2.5 Discussion	39

Chapter 3: Biomechanics Rather Than Neurophysiology Explains the Abolishment of Alternating Activation of Synergistic Muscles in Submaximal Fatiguing Isometric Contractions	45
3.1 Abstract	45
3.2 Introduction	46
3.3 Methods	48
3.3.1 Modeling a redundant neuromuscular system	48
3.3.2 Muscle necessity analysis	50
3.3.3 Sensitivity analysis	51
3.3.4 Data collection	52
3.3.5 Data analysis	54
3.4 Results	54
3.4.1 Muscle necessity analysis	54
3.4.2 Sensitivity analysis	54
3.4.3 Experimental results	54
3.5 Discussion	57
Chapter 4: Temporal Analysis Reveals a Continuum, Rather Than a Separation, of Task Relevance	63
4.1 Abstract	63
4.2 Introduction	64
4.3 Methods	67
4.3.1 Data collection	67
4.3.2 Data preprocessing	68
4.3.3 Data analysis	70
4.3.4 Identification and modeling of the mechanical requirements of the task and its nullspace	72
4.4 Results	74
4.4.1 Principal component analysis of simulated normal forces	74
4.4.2 Principal component analysis of experimental forces	76
4.4.3 Detrended Fluctuation Analysis of time series projected onto principal components	82
4.5 Discussion	85
Chapter 5: An Involuntary Stereotypical Grasp Strategy Pervades Voluntary Dynamic Multifinger Manipulation	90
5.1 Abstract	90
5.2 Introduction	91
5.3 Methods	92
5.3.1 Experimental procedure	92
5.3.2 Mechanical Analysis	97

5.3.3	Equations of motion for a 2-D system of three links connected via a common hinge	99
5.3.4	Simulations	102
5.3.5	Data analysis	104
5.4	Results	107
5.4.1	Analytical Solution and Simulations	107
5.4.2	Principal component associated with the <u>modeled ideal</u> performance of the task.	109
5.4.3	Summary of experimental PCA result and comparison with the modeled ideal performance of the task	110
5.4.4	Experimental PCA result and comparison with the modeled ideal performance of the task	110
5.4.5	Comparison with the modeled imperfect performance and the experimentally grounded task	113
5.4.6	Comparison with the simple static hold control tasks	116
5.4.7	Comparison with the alternating index/middle finger normal force task	119
5.4.8	Comparison with voluntarily oscillated grasp force	120
5.5	Discussion	121
5.5.1	Ruling out potential confounds	123
5.5.2	Grasp Mode variability reveals fundamental challenges to controlling dynamic multifinger manipulation	126

Chapter 6: Prenatal Motor Development Under Different Incubation Periods Affects Postural Control in Domestic Chick	129	
6.1	Abstract	129
6.2	Introduction	130
6.3	Methods	132
6.3.1	Subjects	132
6.3.2	Incubation Conditions	133
6.3.3	Acceleration of embryogenesis through light exposure	133
6.3.4	Quiet Stance Training	133
6.3.5	Data collection	134
6.3.6	Data processing	138
6.3.7	Center of pressure dynamics analysis: classical approach	139
6.3.8	Center of pressure dynamics analysis: perturbation response	141
6.3.9	Statistical Analysis	142
6.4	Results	144
6.4.1	Quiet stance experiment	144
6.4.2	Stance perturbation experiment	145
6.5	Discussion	147

Chapter 7: Summary and Conclusions	155
Bibliography	159

List of Tables

Table 4.1: List of relevant constraints in static grasp	74
Table 5.1: Explanation of tests and simulations used to support hypothesis . .	98

List of Figures

Figure 1.1: Levels of redundancy	3
Figure 1.2: Hyperbolic relationship between force and endurance	5
Figure 1.3: EMG recorded from 12 finger muscles	9
Figure 1.4: Muscle activation pattern vector direction	9
Figure 1.5: Experimental setup	11
Figure 1.6: Quadriceps EMG of 1 h of isometric knee extension	11

Figure 2.1: Muscles contributing to isometric knee extension	24
Figure 2.2: Model MVC decline	31
Figure 2.3: Model MVC recovery	31
Figure 2.4: Model fatigue dynamics	32
Figure 2.5: Model recovery dynamics	32
Figure 2.6: Sum of squared activation muscle dynamics	34
Figure 2.7: Sum of activation muscle dynamics	35
Figure 2.8: Constant activation proportions dynamics	36
Figure 2.9: Constant muscle forces dynamics	37
Figure 2.10: Objective functions error comparison	38
Figure 2.11: Objective functions switching dynamics comparison	39
Figure 3.1: Experimental setup	53
Figure 3.2: Muscle necessity analysis result at 15% MVC	55
Figure 3.3: Muscle necessity analysis result at 41% MVC	56
Figure 3.4: Vasti muscles sensitivity analysis	57
Figure 3.5: Rectus femoris sensitivity analysis result	58
Figure 3.6: Representative EMG recordings at 2.5% MVC	59
Figure 3.7: Representative EMG recordings at 10% MVC	60
Figure 3.8: Representative EMG recordings at 15% MVC	61

Figure 4.1: Experimental Setup	69
Figure 4.2: Task simulation	75
Figure 4.3: Normal force modes	77
Figure 4.4: Representative data for simple grasp	79
Figure 4.5: Representative data for grasp with visual feedback	80
Figure 4.6: Distribution of data principal components	81
Figure 4.7: Proportions of variance explained	82
Figure 4.8: Representative plot of projected data	83
Figure 4.9: DFA scaling exponent distribution	86
Figure 5.1: Experimental setup	94
Figure 5.2: Force space	103
Figure 5.3: Sample time histories	105
Figure 5.4: Overview of the 3 force variability modes	108
Figure 5.5: Results summary	113
Figure 5.6: Results of the original task	114
Figure 5.7: Results of the original task simulation	115
Figure 5.8: Results of the simulation with signal-dependent noise added	117
Figure 5.9: Results of the original task with device attached to ground	118
Figure 5.10: Results of the static hold task	119
Figure 5.11: Results of the alternating forces task	121

Figure 6.1: The incubator	135
Figure 6.2: Chick on force platform	136
Figure 6.3: Sample center-of-pressure data	137
Figure 6.4: Sample perturbation response	143
Figure 6.5: Mean distance distribution	145
Figure 6.6: Mean speed distribution	146
Figure 6.7: Sway area distribution	147
Figure 6.8: Sample pre- and post-perturbation center-of-pressure data	148
Figure 6.9: 2nd peak magnitude distribution	149
Figure 6.10: 2nd peak to 1st peak magnitude ratio distribution	150
Figure 6.11: 2nd peak to perturbation magnitude ratio distribution	151
Figure 6.12: Post-perturbation sway area distribution	152
Figure 6.13: Individual chick performances	153
Figure 6.14: Absence of learning effects	154

Abstract

Motor redundancy in neuromuscular systems exists on multiple levels. The term "motor redundancy" represents the availability of infinitely many different solutions to perform a motor task. This dissertation is concerned with three particular of those levels: muscle redundancy, wrench redundancy and posture redundancy, which are successively more general forms of redundancy, each of which will be explained in detail.

The first level corresponds to the phenomenon that for a given constant vector of *submaximal* limb endpoint force in *isometric* tasks, an infinite multitude of muscle coordination patterns exists. The motor control research community refers to this kind of redundancy as **muscle redundancy**, and traditionally, the selection of a particular muscle coordination pattern has been considered a computational problem for the nervous system. Mathematically, the possible muscle activations span an n-dimensional space - n being the number of independently controlled muscles - and the mapping between this space and that of isometrically generated endpoint forces is projective, therefore giving rise to a null space. The null space comprises those muscle activation vectors that do not have an effect on the endpoint forces, due to the mutual cancellations of generated forces. Specifically, the space of endpoint force vectors is 6-dimensional, consisting of three linear and three rotational components, leaving n-6 degrees of freedom. In the present work, I am studying a potential benefit of muscle redundancy, namely

the mitigation of muscle fatigue through the dynamic switching between muscle activation patterns. Based on my results, I am proposing to abandon the view of muscle redundancy as a computational problem for the nervous system, since in the presence of muscle fatigue even the alleged simplification of this problem, that is, dimension reduction through muscle synergies requires awareness of the full dimensionality of the motor task. Instead, future research should focus on how the nervous system responds flexibly to the challenge of time-variance due to fatiguing and actually leverages muscle redundancy.

The second level of motor redundancy is concerned with the phenomenon that in addition to the redundancy of muscles, infinitely many different combinations of endpoint forces and moments all achieve successful task performance. Again, this redundancy has been considered a computational problem for the nervous system and various ways of how it simplifies the selection of a particular wrench have been proposed. Note that the selected solution in terms of endpoint forces constrains the muscle coordination solution space, in which a particular solution has to be found. Hence, wrench redundancy is a generalization of muscle redundancy. In the case of three-finger grasp, for instance, different fingertip force vector combinations result in an absence of net forces and moments applied to a grasped object, due to mutual cancellation of forces and moments applied by the fingertips. For example, one way to vary the applied forces is to squeeze the object harder and still succeed at the motor task of static grasp. I refer to this kind of redundancy as **wrench redundancy**: the same 6-dimensional wrench vector applied to an object can be produced by a multitude of force vectors individually acting on the object. Wrench redundancy can possibly help to mitigate effects of fatigue, namely through the dynamic shifting between endpoint force vector combinations, just like shifting between coordination patterns achieves this at the muscle level. In the present work, however, I am pursuing a different path of research: In

the first study, looking at the normal force dynamics in static tripod grasp, I will show how mathematically independent wrench space dimensions are actually controlled in quite different ways, reflecting their specific roles in achieving dexterous manipulation. This work shows that a purely spatial analysis of endpoint force variability is not sufficient and that temporal correlations can reveal important aspects of motor control. In particular, the dynamics of forces indicate a hierarchy of task dimensions in terms of task-relevance and contradict the view held by some that task variables can be separated into task-relevant and -irrelevant (i.e. the Uncontrolled Manifold Hypothesis). According to this view, large variability in a mechanically task-irrelevant dimension reflects the lack of control of this dimension by the nervous system. Based on these results, I am proposing to abandon the view of wrench redundancy as a purely spatial problem and to espouse the use of time series analysis to determine neural control strategies. In the second study of wrench dynamics, I will show how in a non-redundant dexterous manipulation task, where all wrench dimensions are task-relevant due to simultaneous force and motion requirements, the control of different task dimensions is likely coupled through neurophysiological pathways, whose separation during evolution has been incomplete. Specifically, I will show how different wrench space dimensions of the motor task, though mathematically independent, are nevertheless coupled in the performance of the task, thus limiting the ability to match the perfect mechanical solution of the task. We see here an important interaction between the wrench and the muscle level: when the wrench level becomes non-redundant, the muscle level also seems to hit a boundary and reveals limitations in the independence of control of muscles across fingers.

Finally, the third level is concerned with **postural redundancy**, meaning that during the performance of a motor task the task goal can be achieved with different limb configurations, described in terms of joint angles. Once again, this level of redundancy

is a generalization of the previous level and potentially extends the potential benefits of the former: a selected posture that enables motor task performance will constrain the admissible endpoint force space, which in turn will constrain the muscle coordination space. One common task taking advantage of postural redundancy is quiet stance. During quiet bipedal stance, two-legged animals are usually swaying or shifting from one posture to another, the former of which can be attributed to motor noise and the latter of which is likely a fatigue mitigation strategy. In this dissertation, I will present results of an analysis of postural control in one-day old domestic chicks (*Gallus gallus*) that reveal differences in prenatal motor development, which were induced by different amounts of light exposure during incubation.

In summary, it can be said that the nervous system is remarkable in that it is capable of monitoring and reconciling continuously multiple levels of redundancy during performance of common motor tasks, in particular, since the kinematic degrees of freedom of limbs are not controlled directly by the brain. Instead, their actuation is achieved through a complex mapping starting with the degrees of freedom found at the brain level, where the task is likely represented very differently from joint angles. Importantly however, not even the three levels studied and discussed here are exhaustive: at one end, muscle redundancy specializes to the little studied motor unit redundancy, whereby different subsets of motor units in a single muscle generate the same muscle force. Motor units represent the control subunits that make up and provide graded control of muscle activity. At the other end of the redundancy spectrum, postural redundancy generalizes to behavioral redundancy, that is, using different strategies to achieve a task, for instance, walking vs. running, etc. Personally, I found that the separation of motor control into different levels of redundancy espoused here to be uncommon in the literature and the field, although it has helped me tremendously in forming hypotheses, designing experiments and attributing causes of failure in motor tasks to specific neuromuscular factors,

and would certainly help the field of motor control research as well. I hope that the following work induces the reader to consider adopting this hierarchical view of motor redundancy, which is different from, and can potentially exist alongside other, hierarchical views of the neuromuscular system.

Chapter 1

Introduction, Background and Prior Work

1.1 Motor Redundancy

Manipulating objects with the fingertips (**dexterous manipulation**) is an awe-inspiring sensorimotor ability that is essential to the activities of daily living. Multifinger dexterous manipulation arises from dynamical interactions among muscles within and across fingers to produce accurate fingertip forces (and motions). Arguably, the simplest of dexterous manipulation tasks is the static grasp of rigid objects: it nevertheless requires the accurate orchestrations of forces across the two or three fingertips involved [Cutkosky, 1985, Raibert and Craig, 1981, Yoshikawa, 1990, Goddard et al., 1992, Murray et al., 1994], having selected an appropriate posture, such that the grasped object does not move or turn. Many investigators have studied finger biomechanics (e.g., [Berme et al., 1977, Minami et al., 1983, An et al., 1985, Schuind et al., 1992, Valero-Cuevas et al., 1998, Sancho-Bru et al., 2001]), neuromuscular control (e.g. [Cole and Abbs, 1986, Darling et al., 1988, Burstedt et al., 1999, Zatsiorsky et al., 2000, Venkadesan and Valero-Cuevas, 2008, Winges et al., 2009, Keenan et al., 2009]), and the role of brain function during their use (e.g., [Binkofski et al., 1999, Ehrsson et al., 2000, Talati et al., 2005]). In addition, the coordination of two, three or more fingers as they hold an object is the

subject of multiple studies (e.g., [Johansson and Birznieks, 2004, Winges et al., 2009, Latash and Zatsiorsky, 2009]).

Understanding **redundancy** (i.e., how the nervous system selects and implements a specific *posture*, a specific *wrench* and a specific *muscle coordination pattern* from among the many possible options that all achieve successful motor task performance) has been the central problem of neuromuscular control for at least four decades (e.g., [Bernstein, 1967, Chao and An, 1978, Hogan, 1985, Valero-Cuevas et al., 1998, Todorov and Jordan, 2002, Seth and Pandy, 2007]). I illustrate the different levels of redundancy with a simple example (Figure 1.1): quiet stance. With regards to *postural redundancy*: the task of standing quiet and upright can be achieved by many leg joint angle configurations, where some might be more suited than other for specific purposes, such as resisting perturbations, for instance, or reducing the level of stress on the joints and muscles. With regards to *wrench redundancy*: during standing, the body weight can be shifted from one leg to the other, allowing for infinitely many weight distributions that produce the same functional outcome. Lastly, with regards to *muscle redundancy*: again, the forces necessary to stabilize the legs in quiet stance can be achieved by different muscle coordination patterns, and once again, different patterns provide different benefits.

The complexity of the human hand, the system, whose redundancy we study in chapters 4 and 5, far exceeds that of the legs and apparently exacerbates the problem of redundancy for dexterous manipulation due to the large number of muscles and kinematic degrees of freedom involved. The triple challenge of task complexity, anatomical complexity and muscle redundancy has delayed a rigorous understanding of how we coordinate finger musculature for dexterous manipulation. Moreover, understanding how the redundancy problem is solved in the context of dexterous manipulation remains a critical limitation to our understanding of the mechanisms of impairment and clinical treatment

Kinematic redundancy

Posture redundancy

Wrench redundancy

Muscle redundancy

Motor unit redundancy

Figure 1.1: The three levels of redundancy studied in this work and embedded into the next more general and more specific levels of redundancy, respectively. The most specific level is muscle redundancy, i.e. the availability of infinitely many different muscle coordination patterns producing the same endpoint force. This kind of redundancy is embedded into wrench redundancy, i.e. the availability of infinitely many different endpoint force vectors satisfying the motor task constraints. Wrench redundancy, in turn, specializes posture redundancy, i.e. the availability of infinitely many different static postures in an isometric task, for each of which endpoint force vectors can be found that satisfy the constraints of the motor task. Also shown are the next more special and general levels of redundancy, respectively.

of hand disability (some reviews include [Spoor, 1983, Schieber and Santello, 2004, Valero-Cuevas et al., 2009a, Latash and Zatsiorsky, 2009]). I am careful to explicitly delineate the aspects of redundancy I will address in the following chapters of this dissertation.

More general than the selection of a static posture, the choice of a particular motion pattern (i.e. a sequence of postures) constitutes the next higher level of redundancy.

On the other hand, more specific than the selection of a particular muscle coordination pattern, we have at the single-muscle level the so-called motor unit redundancy: since a muscle is composed of a large number of muscle fibers, different activation patterns of the associated motor units can generate the same submaximal single-muscle output force (a maximal force would obviously involve all fibers of a muscle). The dynamic phenomenon associated with motor unit redundancy is also known as motor unit rotation or substitution [Sale, 1987, Westgaard and De Luca, 1999], hypothesized to spread the work load.

1.2 Muscle Fatigue

For the purposes of this work, I adopt the definition of **muscle fatigue** as the exercise-induced reversible decline of the maximum force a muscle can generate [Vollestad, 1997]. In the performance of submaximal motor tasks, this decline in performance is not immediately apparent, but eventually muscle fatigue will lead to the inability to maintain the force required for the task. This phenomenon is referred to as exhaustion [Bigland-Ritchie et al., 1986]. Fatigue is a phenomenon mostly [Merton, 1954] occurring in the muscle itself rather than the central nervous system, i.e. in the neurons and the brain, and has therefore been studied almost exclusively in isolated muscle tissue. Since the central aspects of fatigue are poorly understood, and since I believe that the plant should be understood before the controller, I focus on the peripheral aspects of fatigue and disregard central aspects.

At the task level, in submaximal activity, the fatigue state cannot be directly observed but only estimated through the interpolation of occasional maximal contractions. After exercise, there is usually a phase of recovery that is nearly complete within minutes and

sometimes a much slower component [Edwards et al., 1977, Allen et al., 2008]. Usually recovery of maximum force is virtually complete by 30 minutes, and it is possible to perform repeated fatigue runs with nearly similar time courses after this recovery [Allen et al., 2008].

Studies at the physiological level, in turn, indicate that different fatigue mechanisms, which are not fully understood, but involve the depletion of Ca^{2+} and ATP, cascade so as to give rise to a hyperbolic relationship between force (Figure 1.2) and endurance time [Enoka and Stuart, 1992], which indicates the onset of exhaustion. In the following, I will explain the known mechanisms briefly and specifically highlight differences between the two major fiber types found in human muscle.

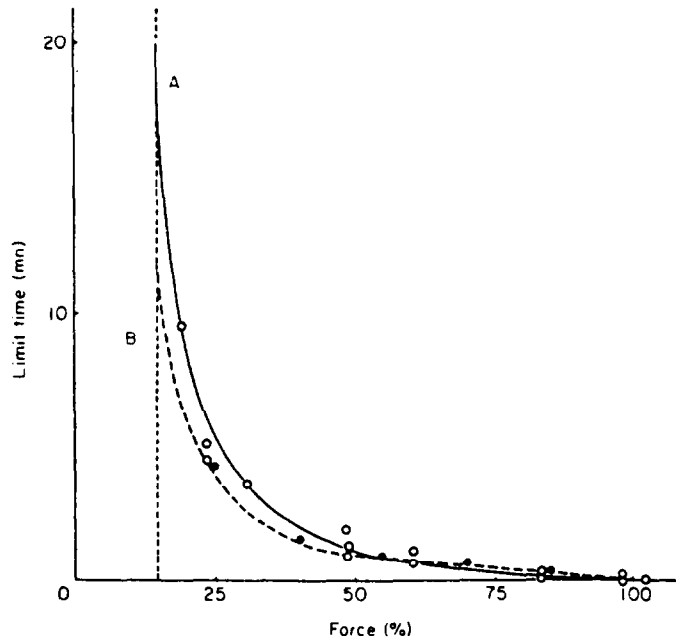


Figure 1.2: The relationship between force requirement and endurance time is hyperbolic, indicating that fatigue benefits can be achieved by reducing force in a muscle, which makes activation pattern shifts a reasonable option (Diagram from [Dul et al., 1984]).

Cross-bridge cycling in myocytes, which generates the force produced by muscles through contraction, can only occur in the presence of Ca^{2+} , which is released from the Sarcoplasmatic Reticulum (SR) in response to a muscle action potential (AP) and then pumped into the SR again. Since the time constants of Ca^{2+} release (< 20 ms) and re-uptake (80 - 200 ms, [Baker et al., 1995]) differ greatly, the net result of sustained muscle contraction - especially under a fused tetanus - is a depletion of available Ca^{2+} . The amount of available Ca^{2+} is further reduced due to the gradual depletion of ATP, since ATP is needed for Ca^{2+} re-uptake into the SR through the pumps as well as the release of cross-bridges.

To maintain a constant force level under fatigue, the activation of the muscle has to be increased, which will increase the rate of Ca^{2+} and ATP depletion even more, leading to a "vicious circle". Importantly, the muscle fibers, which the muscle is composed of, fatigue at different rates and can be categorized into slow-fatiguing (aerobic) [Bevan, 1991], or slow-twitch, and fast-fatiguing (anaerobic), or fast-twitch, types. According to the size principle [Henneman, 1957], fast-fatiguing fibers being larger than slow-fatiguing ones, they are recruited at higher activation levels. Therefore, tasks with very low force requirements can be performed virtually infinitely, with very limited amounts of fatiguing [Sjogaard et al., 1986].

The slow-twitch fibers owe their endurance to the following qualities: a) a high oxidative capacity due to a large number of mitochondria [Bezanilla et al., 1972, Essen et al., 1975], b) a much greater amount of Ca^{2+} stored in rested muscle (70% of maximum capacity vs. 20% [Bhagat and Wheeler, 1973] in fast-fatiguing fibers) and c) a smaller Ca^{2+} release time constant (1/3 of that of fast-twitch muscles [Bianchi and Narayan, 1982]). Furthermore, the rate and amount of SR Ca^{2+}

release per AP is approximately three times higher in fast-twitch fibers than in slow-twitch fibers [Baylor and Hollingworth, 2003]. A feature of fast muscle but also a drawback, from a fatigue point of view, is that it can consume ATP, and thereby produce ADP and P_i (Phosphate) much faster than it can regenerate it, hence the above difference in time constants applies to the consumption (fast) and regeneration (slow) of ATP as well.

Lastly, this difference between slow and fast fibers is also attributable to the higher density of both DHPR/voltage sensors and Ca^{2+} release channels in fast-twitch fibers [Lamb and Walsh, 1987, Lamb, 1992, Margreth et al., 1993, Delbono and Meissner, 1996]. The rapid contraction of fast-twitch fibers requires the presence both of fast MHC (type II) isoforms and fast Ca^{2+} release. Slow-twitch fibers, on the other hand, have fewer Ca^{2+} binding sites on troponin C and the SR pumps, and thus, a lower rate and amount of Ca^{2+} release suffices for contraction, particularly given the much slower contraction rate of the predominant MHC isoform (type I) present [Bortolotto et al., 2000, Bottinelli and Reggiani, 2000]. Thus SR and contractile properties in a given fiber are generally well matched [Trinh and Lamb, 2006].

In conclusion, an appropriate modeling of fatigue needs to take into account oxygen-dependence and differential rates of fatigue among fibers and the proportions of these fibers present in contributing muscles: in the slow-twitch fiber-dominated muscle, time-variance of the EMG-to-muscle force relationship is hardly attributable to fatigue. Isometric tasks involving muscles with a high proportion of fast-twitch fibers, on the other hand, will be strongly affected by fatigue, unless they have low force requirements, in which case only the non-fatiguable slow-twitch fibers in that muscle are activated. In consequence, as the fast-twitch-fiber-dominated muscle progressively fatigues, the activation of that muscle has to be increased (Figure 1.3) to maintain a constant muscle force. In turn, the resulting recruitment of additional motor units gives rise to the increase in EMG occurring when muscles sustain force at a given submaximal level.

Somewhat surprisingly however, the discharge rate of originally active motor units can decrease during prolonged submaximal contractions, since twitch time constants increase with fatigue, despite the fact the overall excitatory drive to the motor neuron pool increases as fatigue develops [Garland et al., 1994]. It is the increased excitatory drive and the concurrent increased recruitment that is measured by the EMG, but not the (decreased) discharge rates of individual motor units. The reduction of discharge rate in motor units is normally well-matched to the slowing of relaxation that occurs with muscle activation (increase of twitch time constant), such that the stimulation rate remains just sufficient to give a fused tetanus of close to maximum force possible at that point in time [Bigland-Ritchie et al., 1983, BiglandRitchie and Woods, 1984, Balog et al., 1994]. This phenomenon is often called "muscle wisdom" [Enoka and Stuart, 1992, Gandevia, 2001]. There exists evidence that the reduction in motor unit activation is mediated through group III/IV afferents reflex inhibition [Garland and McComas, 1990, Gandevia, 1990, Garland, 1991, Hayward et al., 1991] as their discharge rates decline during the initial phase of fatigue, and muscle spindle afferents later in fatigue [Gandevia, 1990, Macefield et al., 1991].

1.3 Experimental Evidence: Leveraging Muscle Redundancy for Fatigue Mitigation

At the level of muscle redundancy, there currently exists one study involving tripod grasp, [Santos et al., 2010] that has investigated the neuromuscular system's ability to traverse the muscle solution space, for a constant endpoint force output. Subjects were asked to produce a constant submaximal normal force output, while minimizing tangential force, with three fingers in a grasp posture until exhaustion. Fine-wire EMG was recorded from 10 muscles and subsequently, the relative muscle activation contributions

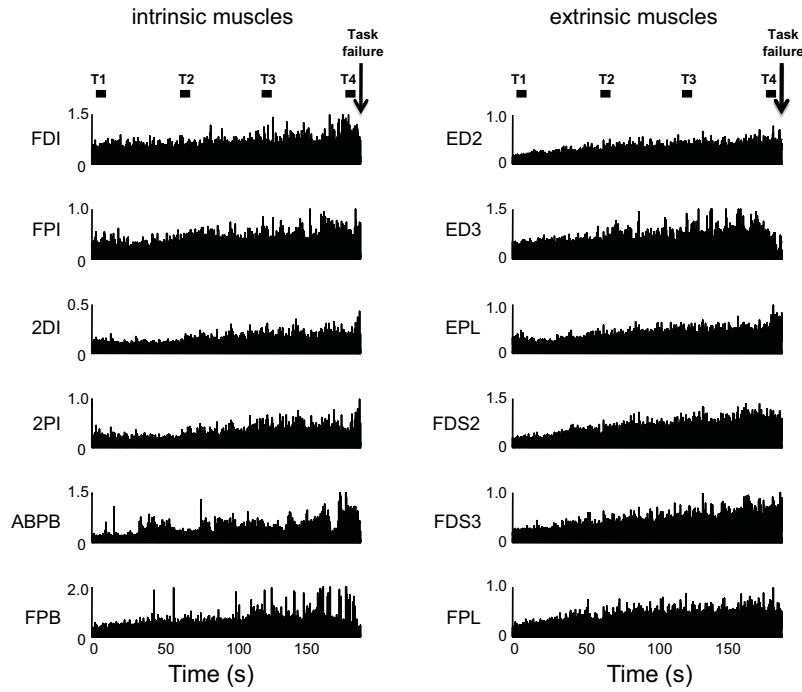


Figure 1.3: All 12 muscles measured in [Santos et al., 2010] show an increase in EMG activity as the muscles gradually fatigue, while producing the same isometric force output.

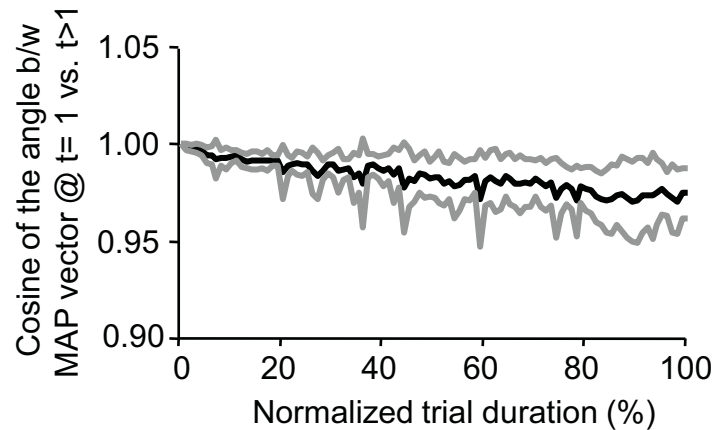


Figure 1.4: The activation pattern of the 12 muscles does not change, despite the overall increase in EMG, as evidenced by an only minimal change in the activation pattern direction vector (diagram from [Santos et al., 2010]).

were computed to determine if the activation pattern changed. The results indicate that although the activations of all contributing muscles increased as time passed, the relative contributions did not change. We will show in Chapter 3, for the simpler task of isometric knee extension, how a target force of only 15% MVC already constrains the solution space such that dynamic muscle activation becomes severely limited.

The dynamics of muscle coordination in the context of isometric knee extension have been extensively studied by Kouzaki, Shinohara and others [Kouzaki et al., 2002, Kouzaki et al., 2004, Kouzaki and Shinohara, 2006]. The authors showed that involuntary alternation between synergist quadriceps muscles, rectus femoris and vastus lateralis, occurs during very low-level sustained knee extension, between 4 and 11 times during the one hour long trial. Subjects were asked to generate an extremely low isometric 2.5% MVC force for 1 hour, whereupon MVC force was measured again, to determine if fatigue had occurred. Interestingly, the reduction in MVC was inversely correlated with the frequency of alternation, indicating that alternation did provide the benefit of reducing fatigue, for instance, by enabling recovery of the temporarily silent muscle. While these results are very encouraging, the authors have not provided a formal generative mechanism or model to explain and interpret those results.

1.4 Modeling and Simulation: Muscle Redundancy and Muscle Fatigue

Modeling of isometric force sharing under fatigue minimization was first done in Dul et al. [Dul et al., 1984]. Their minimum-fatigue criterion was formulated as the maximization of the endurance time across a group of synergistic muscles. The endurance time is a function of both the force generated by the muscle (inversely proportional)

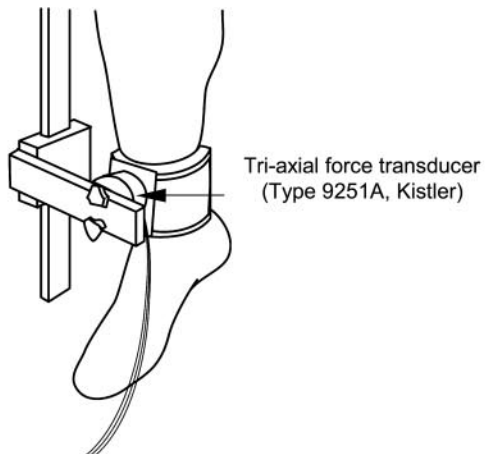


Figure 1.5: The experimental setup for the isometric knee extension task described in [Kouzaki et al., 2002].

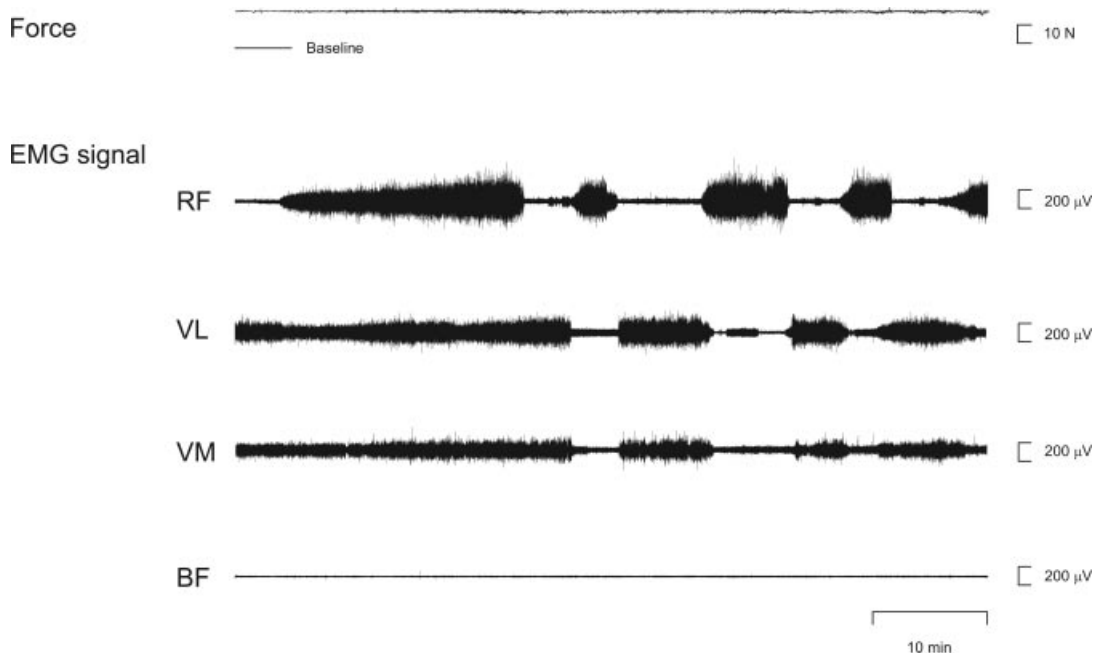


Figure 1.6: During one hour of 2.5 % MVC force production, alternations between synergistic muscles were observed (diagram from [Kouzaki and Shinohara, 2006]).

and its percentage of slow-fatiguing aerobic fibers (proportional), based on observations and curve fitting. Not surprisingly, the optimal activation of muscles in an isometric knee flexion task, according to a nonlinear (i.e. maximization of a minimum)

optimization scheme, tended to favor force production in muscles with a higher percentage of slow fibers and muscles with large volumes, predicting nonetheless synergistic activation among muscles. Finally, the predicted time to failure and the predicted forces agree with values from the literature, underlining the physiological correctness of this optimization criterion further confirmed elsewhere [Prilutsky et al., 1997, Prilutsky and Zatsiorsky, 2002]. These studies found that fatigue, along with stress, energy expenditure and perceived effort [Prilutsky and Zatsiorsky, 2002], were the best predictors in static optimization schemes. The major drawback of modeling studies in fatigue-minimization in isometric tasks are their staticness, as they predict a single fatigue-minimizing activation pattern that is held until failure, and do not consider by design dynamic changes in the pattern as the isometric task progresses that could improve performance and time to failure. Therefore, so far no model has been able to reproduce the activation pattern [Kouzaki et al., 2002]. In Chapter 2, I will address the problem of static optimization, based on the incorrect assumption of time-invariance of the neuromuscular system and show in particular, how the concept of synergies strongly conflicts with the control of a time-varying system. Synergies, in short, are understood as the rigid co-activation of muscles, basically treating a group of muscles as one muscle and thereby simplifying the muscle redundancy problem [Bizzi et al., 2002, d'Avella et al., 2003]. .

With respect to redundancy at the *wrench level*, there are currently no studies which directly investigating possible dynamic strategies in a *fatiguing, isometric, and submaximal* task or consider the specifics of muscle fatigue and recovery dynamics. Instead, studies at this level of redundancy focus on the effect of fatigue on the variability along different task-relevant and task-irrelevant dimensions of a motor task, in the context of the Uncontrolled Manifold Hypothesis [Scholz and Schner, 1999]. Two studies by Danion et al. [Danion et al., 2000, Danion et al., 2001] explicitly looked at the effects

of fatigue on a redundant task. The first study involved two fatiguing force production exercises, one at the distal and one at the proximal phalanges, both with four fingers and single fingers. While force enslaving [Zatsiorsky et al., 2000] across fingers remained unaffected by fatigue at the phalanx involving the exercise, enslaving increased at the other phalanx. Furthermore, the difference between the MVC generated by all four fingers in unison and the larger sum of single-finger MVCs increased. These results indicate a neural level reorganization that aims to "preserve" a force production synergy across fingers. The other study involved fatiguing exercises at the same distal and proximal sites by the index finger only. This resulted in reduced enslavement of the index finger in an all-finger force production task, and a reduction in its contribution to the total sum of forces, leading the same authors to reach the opposite conclusion: that fatigue leads to a reorganization at the neural level that "progressively removes" the fatigued finger from a synergy (so that it can be "reintegrated into the synergy" faster due to a swift recovery).

Another study, by [Singh et al., 2010] found that unfatigued fingers in multi-finger force production tasks adaptively increase their force variability, so as to match the fatigue-induced increase in variability in the fatigued finger. This adaptive behavior helps to maintain a balance of variability, i.e. a synergy and to protect the task-relevant dimensions from fatigue effects. While the authors certainly admit the benefits of redundancy in fatigue mitigation, they fail to investigate the specific dynamics of wrench along the task-irrelevant directions.

In conclusion, the findings of these studies therefore necessitate further investigation into wrench redundancy and the opportunities for the nervous system to mitigate the effects of fatigue at this level of control.

Chapter 2

Fatigue Dynamics Have Profound Consequences for Muscle Coordination and Theories of Motor Control

2.1 Abstract

In submaximal motor tasks, the nervous system is believed to be confronted with the computational challenge of selecting a particular from infinitely many distinct muscle coordination patterns. Muscle redundancy, as this phenomenon is known, has led researchers to hypothesize either the minimization of cost functions to find a solution, or control strategies such as muscle synergies, whereby muscles are co-activated in a stereotypical fashion, thus reducing computational complexity.

Here, we investigate the consequences of these hypotheses in the light of the hitherto oft-overlooked interplay between muscle coordination and fatigue. Simulations of submaximal isometric knee extension with realistic fatigue and recovery show that the nervous system continuously needs to respond to the complex changes in force production capability experienced by muscles, to lengthen the time to failure.

First, we find that adherence to a synergy in activation space or muscle force space requires either non-synergy-like muscle activations or muscle forces, respectively. We

conclude that synergies can only be enforced in a single space (muscle activations or forces). This challenges the hypothesis that synergies can serve to simplify and guide the selection of muscle coordination patterns.

Secondly, the adherence to a synergy leads to early task failure, if compared to other strategies of pattern selection (for instance, energy minimization), which do not restrict dynamics in any space. This result indicates the disadvantage of suppressing changes in the levels and proportions of muscle activations or force when enforcing the constraints of the task.

Thirdly, and somewhat surprisingly, we find that intuitive cost functions, some of which have been proposed in the literature and are based on physiological considerations, actually prevent muscle recovery. We conclude that one needs to recognize the impact of fatigue on redundancy when proposing optimization strategies.

Together, the results not only cast doubt on the utility of synergies and highlight a major disadvantage, but challenge their association with computational benefits. Therefore, the results encourage abandoning the view of redundancy as a computational challenge, and instead encourage us to study associated opportunities in the mitigation of muscle fatigue and to find relevant and appropriate objective functions capable of reproducing the dynamics in time-variant neuromuscular systems.

2.2 Introduction

The problem of motor redundancy has been a longstanding one in motor control research [Bernstein, 1967, Tresch and Jarc, 2009], ever since it had been observed that in repeatedly performed motor tasks, humans never seem to use the exact same coordination pattern of joints to achieve the task goal [Bernstein, 1967]. Redundancy refers to the multitude of muscle activation or muscle force patterns that all give rise to the

same endpoint force vector in submaximal and otherwise underspecified tasks, due to the mutual cancellation of muscle actions. The perceived computational "problem" of motor redundancy now is that the nervous system is confronted with having to choose one from many possible muscle coordination patterns.

Having observed that despite motor output variability (be it kinematic or kinetic), muscle activation patterns are similar across repetitions of a motor task and across people, scientists have proposed the existence of an underlying optimizing principle as a means to determine a unique solution [Chao and An, 1978, Crowninshield and Brand, 1981, Dul et al., 1984, Prilutsky and Zatsiorsky, 2002]. This solution minimizes or maximizes a proposed objective function, which is selected based on various neurophysiological or energetic considerations. It has been shown in numerous studies that experimentally observed muscle coordination patterns can (at least nominally) be found through the optimization of different objective functions [Crowninshield and Brand, 1981, Dul et al., 1984, Anderson and Pandy, 2001]. However, these studies fail to address the possibility that there exist sufficiently many constraints to the task (e.g. high force, resistance to perturbations, posture) to uniquely determine a solution [Loeb, 2000], regardless of the objective function. Furthermore, optimization is commonly employed to compute a single static solution, based on the often implicit assumption that the neuromuscular system does not undergo changes over time, during repeated or continuous task performance. However, allowing for time-variance in the system might actually help to further constrain the search space of potential objective functions, since the ability to reproduce experimentally observed muscle activation patterns provides another selection criterion.

Assuming that there exists an underlying principle of optimization in the selection of muscle coordination, scientists have proposed for the purpose of computational simplicity the concept of muscle synergies. Subject to a synergy, muscles

are always co-activated in specific patterns [Bizzi et al., 2002, d’Avella et al., 2003, Chhabra and Jacobs, 2006, Tresch and Jarc, 2009]. The combination of different distinct synergies enables variable and dynamic muscle coordinations, while simultaneously reducing the number of variables in optimization. One criticism of synergies is firstly the assumption that high dimensionality poses a computational problem [Bizzi et al., 2002], an assumption that remains to be supported by evidence. Secondly, while allowing for motor variability, synergies constrain the muscle activation or force spaces in specific ways, which greatly restricts potential beneficial or even necessary variability [Kutch and Valero-Cuevas, 2012]. Numerous studies have shown that the role of an individual muscle relative to another (synergist or antagonist) depends on posture [Hasan and Enoka, 1985], torque [Caldwell and Van Leemputte, 1991] or direction of force application [Theeuwen et al., 1994], and in fact, synergists like gastrocnemius medialis and soleus can become functional antagonists [Schieppati et al., 1990, Kutch and Valero-Cuevas, 2011].

In the present work, we firstly explore the potential consequences of one way in which neuromuscular systems are time-varying: muscle fatigue, which we understand as the exercise-induced decline of the maximum force of a muscle. The primary effect of fatigue is to reduce the proportionality between muscle activation, measured through EMG, and muscle force [Dideriksen et al., 2010]. Hence, to maintain a given force level, the activation of each fatigued muscle has to be increased, to recruit more motor units or increase the firing rate of already recruited ones. Since synergistic muscles fatigue at different rates, due to the demands of the task and the proportion of fatigable vs non-fatigable fibers [Johnson et al., 1973, Housh et al., 1995, Loeb and Ghez, 2000], we hypothesize that the increase in activation occurs at different rates across muscles.

Specifically, we hypothesize that including fatigue-based time-variance in modeling exposes an important drawback of adhering to a single initial solution, and simply scaling it up to maintain a force, in the presence of reduced muscle output as it fatigues. This strategy will lead to comparatively early failure, and exposes the requirement for continuous optimization, or more generally, continuous adaptation. Besides, adding time-variance to musculoskeletal models provides another constraint to identify valid approaches to the finding of a solution.

Secondly, we show that due to the time-variance of the mapping from muscle activation to muscle force, only one domain (muscle force or activation) at a time can be controlled synergistically, while the other varies dynamically, thus making obvious the inevitability of dynamical changes in either activity or force, with important consequences to the study of computational complexity in motor function. Furthermore, we hypothesize that the restriction on the solution space imposed by synergies will lead to a relatively early task failure. It is important to note that we consider the adherence to a synergy to be equivalent to the adherence to a static optimal solution: if an "optimal" synergy fails, then a random synergy is all the more likely to fail, as the co-activation pattern in that case is not even adapted to the task. This result suggests the need for and the benefits of dynamic activation strategies in submaximal tasks, for which there exists evidence from isometric knee extension EMG recordings [Sjogaard et al., 1986, Kouzaki, 2005, Kouzaki and Shinohara, 2006].

2.3 Methods

2.3.1 Modeling a redundant neuromuscular system

Assumptions

For the purposes of modeling a redundant motor task subject to fatiguing, we adopt the definition of **muscle fatigue as the exercise-induced decline of the maximum force a muscle can generate** [Vollestad, 1997]. In turn, this requires an increase of activation of that muscle to maintain the force, as has been observed previously [Dideriksen et al., 2010, Danna-Dos Santos et al., 2010, Rudroff et al., 2010]. Muscle recovery, on the other hand, occurs only in the total absence of activation [Dideriksen et al., 2011], while at very low muscle forces, the muscle neither fatigues nor recovers, due to the reliance on slow-twitch fibers, also known as indefatigable fibers [Loeb and Ghez, 2000].

We selected the task of isometric knee extension, because there exists prior evidence, in the absence of a mathematical model, that the nervous system leverages redundancy for the mitigation of fatigue [Sjogaard et al., 1986, Kouzaki, 2005, Kouzaki and Shinohara, 2006]. Besides, from a modeling point of view, knee extension has favorable properties: it allows for isolation of muscle redundancy and a relatively clean separation from endpoint force vector redundancy, whereby different force vectors can all achieve successful task performance. Specifically, the muscles actuating knee extension (vasti and rectus femoris) are largely similar in terms of their mechanical action - in particular, these muscles don't add/abduct or rotate the leg. Therefore, dynamic activation of RF and the Vasti in isometric knee extension is unlikely to give rise to undesirable tangential endpoint force component, which helps to keep this vector constant.

Furthermore, we assume the following:

Independence of muscles: The 31 muscles actuating the modeled limbs (actually 33, but see below) are assumed to be controlled independently. However, it has been observed in numerous studies that the activations of muscles correlate to some degree. Whether these correlations are a function of the particular motor task [Kutch et al., 2008, Valero-Cuevas et al., 2009b] or the common input at a higher center [Winges et al., 2006], is currently unclear. The only exception we make to this assumption is that the three Vasti muscles are controlled together and basically treated as one muscle [Hoffer et al., 1987a, Hoffer et al., 1987b]. This reduces the original number of 33 muscles to 31.

Knowledge of muscle state is unaffected by noise and neural delays: since the neural delays involved in transmitting information about the muscle state to a central controller are negligible (on the order of ms) compared to the time scale of fatiguing (on the order of 10s of seconds to minutes) and force modulation (isometric task), we do not include them in our model. Furthermore, we disregard noise, either in the muscle activation signal or the endpoint force fluctuation (signal-dependent noise [Jones et al., 2002]), based on the observation that the magnitudes of relative shifts in muscle activation are much larger than the fluctuations about the mean force level generated by a muscle. Nevertheless, noise and delays might influence the amplitude, frequency or timing of activation pattern dynamics but are unlikely to prevent such high-amplitude, low-frequency dynamics altogether.

Leg consisting of rigid, supported links with ball and hinge joints: for an isometric task, this assumption has been shown to be sufficient and valid [Valero-Cuevas et al., 1998]. This assumption allows us to use a simple three-dimensional geometric model to model the mapping from joint torques to limb endpoint forces. Furthermore, since we model a seated posture, with knee and hip flexed at right angles, the leg is completely supported and no torques are necessary to maintain posture.

Linearity: It has been shown previously that in isometric force production, the mapping from muscle activation to the endpoint wrench is approximately linear [Valero-Cuevas et al., 1998], which entails that the mapping from muscle activation to limb endpoint force can be described by matrix multiplication. Force-velocity curves do not play a role in isometric tasks and the force-length curve properties are captured by the changes of the moment arms as the posture varies.

Post activation potentiation: Under activation, the maximum force a muscle can generate initially increases [Brown and Loeb, 1998], before the onset of fatigue. We assume here that the muscle has been activated accordingly and is capable of generating its maximum force.

Mathematical modeling of isometric knee extension

The leg model consists of two joints, a ball joint at the hip and a hinge joint at knee, but no ankle joint, since none of the knee extensors crosses this joint. The knee and hip joint are both flexed at 90°. The two joints actuate a rigid two-link system, with the upper and lower leg being 0.437 m and 0.37 m long, respectively [Ward et al., 2009]. The particular endpoint coordinates and limb orientation x, y, z, α at the lower end of the shin are a function of the four joint angles $\vec{q} = [q_1, q_2, q_3, q_4]$ (i.e. hip add/abduction, rotation, flexion/extension and knee flexion/extension) [Valero-Cuevas, 2009]. This relationship is expressed by the geometric relationship ($s(q) = \sin(q)$, and $c(q) = \cos(q)$):

$$\vec{x} = \begin{bmatrix} x \\ y \\ z \\ \alpha \end{bmatrix} = \begin{bmatrix} G_x(\vec{q}) \\ G_y(\vec{q}) \\ G_z(\vec{q}) \\ G_\alpha(\vec{q}) \end{bmatrix} = \begin{bmatrix} L_1 c(q_1)c(q_2) + L_2[s(q_4)(s(q_1)s(q_2) - c(q_1)c(q_3)s(q_2)) + c(q_1)c(q_2)c(q_3)] \\ L_1 s(q_2) + L_2[c(q_4)s(q_2) + c(q_2)c(q_3)s(q_4)] \\ -L_1 c(q_2)s(q_1) + L_2[s(q_4)(c(q_1)s(q_3) + c(q_3)s(q_1)s(q_2)) - c(q_2)c(q_4)s(q_1)] \\ c(q_1)q_3 + s(q_1)(q_2 + q_4) \end{bmatrix}$$

where the L_i are the link lengths. The change in endpoint coordinates and orientation, as a function of the change in joint angles can be expressed by the Jacobian [Yoshikawa, 1990], i.e. the partial derivatives of the above geometric relationship:

$$\dot{\vec{x}} = J(\vec{q})\dot{\vec{q}} = \begin{bmatrix} \frac{\partial G_x(\vec{q})}{\partial q_1} & \frac{\partial G_x(\vec{q})}{\partial q_2} & \frac{\partial G_x(\vec{q})}{\partial q_3} & \frac{\partial G_x(\vec{q})}{\partial q_4} \\ \frac{\partial G_y(\vec{q})}{\partial q_1} & \frac{\partial G_y(\vec{q})}{\partial q_2} & \frac{\partial G_y(\vec{q})}{\partial q_3} & \frac{\partial G_y(\vec{q})}{\partial q_4} \\ \frac{\partial G_z(\vec{q})}{\partial q_1} & \frac{\partial G_z(\vec{q})}{\partial q_2} & \frac{\partial G_z(\vec{q})}{\partial q_3} & \frac{\partial G_z(\vec{q})}{\partial q_4} \\ \frac{\partial G_\alpha(\vec{q})}{\partial q_1} & \frac{\partial G_\alpha(\vec{q})}{\partial q_2} & \frac{\partial G_\alpha(\vec{q})}{\partial q_3} & \frac{\partial G_\alpha(\vec{q})}{\partial q_4} \end{bmatrix} \dot{\vec{q}}$$

The Jacobian $J(\vec{q})$ is nonlinearly dependent on the posture \vec{q} . The endpoint wrench \vec{w} in knee extension, i.e. the four-dimensional vector consisting of 3 forces and 1 moment applied by the shin, is also related to the joint torques $\vec{\tau}$ by the Jacobian, taking its inverse transpose:

$$\vec{w} = J(\vec{q})^{-T} \vec{\tau}$$

These torques, in turn, are generated about the hip and knee joints by the tendon tensions \vec{f} , where \vec{f} is an n-dimensional vector and n the number of muscles ($n = 31$):

$$\vec{\tau} = R(\vec{q})\vec{f} = \begin{bmatrix} r_{11} & \dots & r_{1n} \\ \vdots & \ddots & \vdots \\ r_{31} & \dots & r_{3n} \end{bmatrix} \vec{f}$$

Here, $R(\vec{q})$ is the moment arm matrix and the r_{ij} are the moment arms of the j-th muscle acting about the i-th joint. Since muscle moment arms change with muscle lengths, which in turn depend on the posture and thus the joint configuration, the moment arm matrix is posture-dependent, but we simplify it to R . We used moment arms for the 31 muscles for this particular posture (90° knee and hip flexion) based on published values [Arnold et al., 2010]. In our model, the 31 muscles generate 4 joint

torques (hip add/abduction, rotation, flexion/extension and knee flexion/extension), corresponding to an underdetermined mapping from activation to torques.

Finally, the tendon tensions \vec{f} generated by the muscles are related to the muscle activations \vec{a} ($0 \leq a_i \leq 1$) through a diagonal mapping F_0 :

$$F_0 \vec{a} = \begin{bmatrix} F_{11} & 0 & \dots & 0 \\ 0 & F_{22} & \dots & 0 \\ \vdots & \vdots & \ddots & \vdots \\ 0 & 0 & \dots & F_{nn} \end{bmatrix} \vec{a}$$

where the entry F_{ii} corresponds to the maximum muscle tension of the i -th muscle. This value scales the individual muscle activations, which are between 0 and 1, to the force generated by the muscle. The diagonality of this mapping reflects the above mentioned assumption of independent muscle control. The maximum muscle tension values are computed as the product of the physiological cross-sectional areas (PCSA) of the muscles and the muscle stress, the values of which can be found in [Arnold et al., 2010].

If we allow for fatigue dynamics, which we describe in the next section, the matrix F_0 becomes time-varying, since the maximum tension a muscle can generate will decrease or increase depending on its activation level, as per our adopted definition of fatigue, hence $F_0(t)$. Initially, muscles are assumed to be unfatigued and capable of producing maximum force [Brown and Loeb, 1998]. Incorporating muscle fatigue and recovery dynamics in this way reflects the assumption of immediate knowledge of muscle state (above).

In conclusion, the linear mapping from muscle activations \mathbf{a} to the 4-dimensional endpoint wrench \mathbf{w} , applied by the ventral aspect of the lower leg, in an isometric knee extension task, can be described by the product of the 3 above matrices:

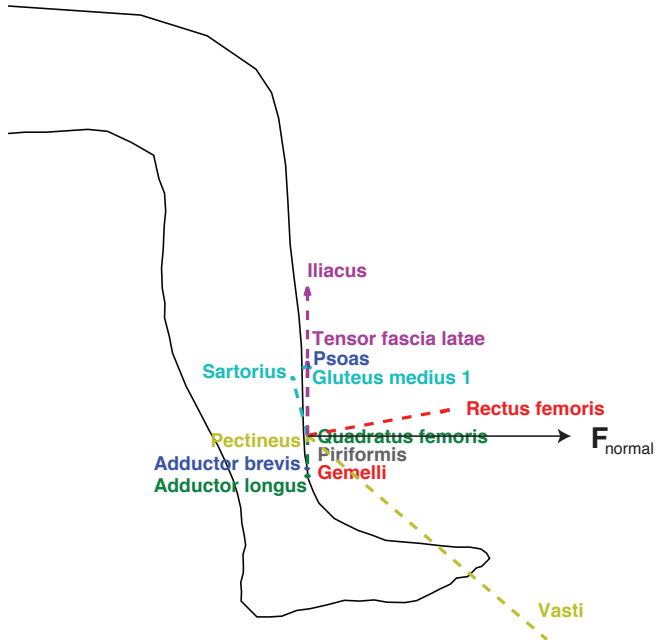


Figure 2.1: Muscles contributing to knee extension and their vectors of force application (if knee and hip are flexed at right angles), based on the linear model and selected by various optimization functions (described below). Also shown is the direction of normal force application (black arrow), just above the malleolus. Note that some of these vectors, those associated with adductors and abductors, point out of the plane.

$$\mathbf{w} = J^{-T} R F_0(t) \cdot \mathbf{a}$$

In our modeling approach of knee extension, where 31 muscles actuate the hip and knee joints to generate a wrench, the redundancy, i.e. the infinity of possible solutions, can then be mathematically illustrated as follows:

$$\begin{aligned}
\mathbf{w} &= J^{-T} R F_0(t) \cdot \mathbf{a} \\
\mathbf{w} &= J^{-T} R F_0(t) \cdot \mathbf{a} \\
&= J^{-T} R F_0(t) \cdot (\mathbf{y} + \mathbf{z}) \\
&= J^{-T} R F_0(t) \mathbf{y} + J^{-T} R F_0(t) \mathbf{z} \\
&= J^{-T} R F_0(t) \cdot \mathbf{y} + \mathbf{0} \\
&= J^{-T} R F_0(t) \cdot \mathbf{y}
\end{aligned}$$

where an 31-dimensional muscle activation vector $\mathbf{a} = \mathbf{y} + \mathbf{z}$ can be decomposed into two vectors, one of which \mathbf{z} is an **arbitrary** vector from the null space of the matrix $J^{-T}RF$, which has $31 - 4 = 27$ basis vectors. Note that due to the $[0, 1]$ -constraint on the activations the solution space is constrained and moreover, because of the time-dependence of $F_0(t)$, the solution space of the matrix is shrinking and expanding in various dimensions as the muscles fatigue and recover.

2.3.2 Mathematical modeling of fatigue

To extract realistic fatigue and recovery dynamics, represented by a set of differential equations, we implemented and ran a recently published model [Dideriksen et al., 2011] of single-muscle force production and fatigue. This model extends a common motor unit-based model of muscle force generation [Fuglevand et al., 1993] by dynamics of muscle cell metabolite uptake and release rates, which in turn depend on the muscle activation level. Accumulation of metabolites decreases the twitch amplitude and increases the twitch time constant of each motor unit. We simulated the decrease in MVC force,

and thus fatigue, by continuously activating the muscle activated at 10 different, but constant levels, from 0.1 to 1.0, i.e. full activation, where full activation is the level of activation necessary to achieve the maximum firing rate in all of the motor units of the muscle. We simulated the time course of MVC force increase due to recovery, on the other hand, by leaving an initially fully fatigued muscle deactivated for a sufficiently long time. The fatigue and recovery profiles are shown in figures 2.2 and 2.3. Note that the fully fatigued muscle is still capable of generating low amounts of force, which reflects the contribution of indefatigable slow fibers [Loeb and Ghez, 2000]. The fatigue dynamics at high forces initially match the activation-dependent exponential profile proposed elsewhere [Freund and Takala, 2001]. The recovery, on the other hand, follows an initial exponential increase, which is followed by a slow linear phase. The linear phase represents the change in the amplitude in the H-reflex [Duchateau et al., 2002].

Based on these time series of muscle fatigue and recovery, we used the EUREQA software [Schmidt and Lipson, 2009] to find possibly non-linear differential equations $\frac{dF_0}{dt} = f(F_0(t), a(t)) \cdot a(t)$ and $\frac{dF_0}{dt} = f(F_0(t))$ representing fatigue and recovery, respectively. EUREQA implements a machine learning technique known as symbolic regression that uses genetic programming to evolve analytical expressions to model the available data. A population of models is evaluated iteratively to find a set of models that best map the inputs to the outputs. This is unlike other machine learning techniques that use a "black box" approach to model input-output relationships because it avoids overfitting in attempting to uncover the underlying physics by not espousing any one specific form of the equations.. The optimization criterion we used to fit the dynamics was the maximization of the R-squared goodness-of-fit metric, as this provided the best trade-off between minimizing the fitting error and model complexity, i.e. the over-fitting of the simulation time series.

2.3.3 Simulating muscle activation dynamics in isometric knee extension subject to optimization

We integrated the previously obtained differential equations with a simple Euler scheme, implemented in the MATLAB© (Natick, MA) environment. The activation dynamics at each time step, which we set to 10 s (i.e. small relative to time constants of muscle fatigue and recovery), were found using the constrained optimization functions `linprog()` and `quadprog()`, minimizing linear or quadratic objective functions, respectively. These objective functions represent simple control strategies and ways to overcome or leverage, respectively, motor redundancy. The following constraints applied:

$$J^{-T} RF_0(t)_{x,y} \mathbf{a}(t) = 0$$

$$J^{-T} RF_0(t)_\alpha \mathbf{a}(t) = 0$$

$$J^{-T} RF_0(t)_z \mathbf{a}(t) = c$$

i.e. the normal force component of the vector generated at the leg endpoint needs to be kept constant at c N (Figure 2.1), where c represents a percentage of MVC force, while keeping tangential force components F_x and F_y and the endpoint torque at zero. Furthermore, the 31 muscle activations $\mathbf{a}(t)$ are constrained to fall in the $[0, 1]$ interval, i.e.:

$$0 \leq a_i(t) \leq 1$$

We simulated activation dynamics based on the instantaneous minimization of six objective functions at each time point of simulation, *static* variations (muscle forces being static) of which have been proposed previously [Prilutsky and Zatsiorsky, 2002]:

- 1) $\sum_i a_i(t)^2$ (sum of activations squared)
- 2) $\sum_i a_i(t)$ (sum of activations)
- 3) $\sum_i (F_i(t)a_i(t))^2$ (sum of muscle forces squared)
- 4) $\sum_i F_i(t)a_i(t)$ (sum of muscle forces)
- 5) $\sum_i \left(\frac{a_i^*}{\sum_i a_i^*} - \frac{a_i(t)}{\sum_i a_i(t)} \right)^2$ (constant activation proportions)
- 6) $a_i(t) = F_i^*/F_i(t)$ (constant muscle force)

where the a_i^* and F_i^* are initial muscle activations and muscle forces computed for the unfatigued muscle, by minimization of objective function 1). Note that in 5), activation proportions rather than actual activations are kept constant, since the latter would lead to immediate task failure, i.e. activations need to increase from task beginning to compensate for fatigue. Objective functions 5) and 6) represent synergistic strategies of task performance, by either keeping all muscle activation contributions equal, as in 5) or keeping the force produced by each muscle constant. In [Danna-Dos Santos et al., 2010], the authors claim to have found evidence for the former strategy, while synergies can also be understood as occurring at the muscle force level, as in 6), or yet another level of the control hierarchy.

Running the muscle activation dynamics based on these objective functions, we quantified the performance of each control strategy in terms of i) failure times, i.e. the time point at which the 31 muscles were no longer capable of generating the forces necessary to produce the isometric knee extension force, ii) cumulative error, that is, the cumulative absolute difference between the generated force and the target forces, iii)

the number of changes in the order of individual muscle activation proportions, iv) the number of changes in the order of individual muscle forces, v) the summed difference in activation at the beginning and the time of failure and vi) the same as v), but for muscle force. Synergies would aim to keep the latter four metrics at zero, due to "hard-wired" muscle co-activation, which intends to prevent any dynamics in activation or muscle force. Specifically, we would expect objective function 5) to keep at zero the number of activation order switches and objective function 6) the number of muscle force order switches.

2.3.4 Parameter search

Since the model [Dideriksen et al., 2011] simulates the force, activation, fatigue and recovery dynamics of the first dorsal interosseous (FDI) muscle, the extracted differential equations cannot be simply applied to any muscle of the human body without some degree of adjustment. Therefore, to test the sensitivity of our obtained results to parameters, we reran the above described simulations over a range of values. Most importantly, we ran simulations at different submaximal activation levels, expressed as percentages of normal force MVC. Gradually increasing the activation level has the effect of reducing the volume of the solution space of admissible muscle coordination patterns [Valero-Cuevas, 2009]. Specifically, we hypothesize that at high activation levels, different optimization functions all converge to the same activation dynamics, due to the lack of solutions. Furthermore, we tested different ratios of the dominant time constants of fatigue and recovery, thus gradually approaching a scenario without muscle recovery. Lastly, we explored the sensitivity to a parameter we refer to as the "fatigue threshold", whereby muscles do not fatigue if their activation is below this value (Figure 2.2, at low activations) [Housh et al., 1995]. This reflects the contribution or proportion of slow-twitch (or non-fatiguable) motor units, which are variable in the human

body [Johnson et al., 1973]. We hypothesize that since the above objective functions do not explicitly take into account the muscle physiology, a change in this value will not have an obvious effect on the computed muscle coordination patterns. The specific parameters and value ranges tested are shown in table 2.3.4.

Parameter	Range
MVC percentage	0.01 - 20 %
$\tau_{\text{recovery}}/\tau_{\text{fatigue}}$	0.5 - 10
Non-fatiguable activation level	0.01 - 0.3

2.4 Results

2.4.1 Eureqa-extracted dynamics of muscle fatigue and recovery

We first ran the motor-unit model [Dideriksen et al., 2011] at different activation levels, to obtain curves of decrease and increase of maximum muscle force representing fatigue and recovery (Figures 2.2 and 2.3).

Based on these curves, we ran Eureqa for approximately 9 hours on an Apple Macbook Pro with a 4-core 2.53 Ghz Intel Core i5 and selected a fit that achieved the best trade-off between low error and complexity:

$$\frac{dF_0}{dt} = \tau_{\text{fatigue}} F_0(t) e^{-(2.451F_0(t)^2 a(t) - 0.5933)^2} a(t)$$

where $\tau_{\text{fatigue}} = -0.00905$ for the nominal fatigue dynamics. Similarly, we ran Eureqa on the muscle recovery curve for 4 hours to obtain:

$$\frac{dF_0}{dt} = \tau_{\text{recovery}} \text{erfc}(15.18F_0(t)^2 - 11.66F_0(t))$$

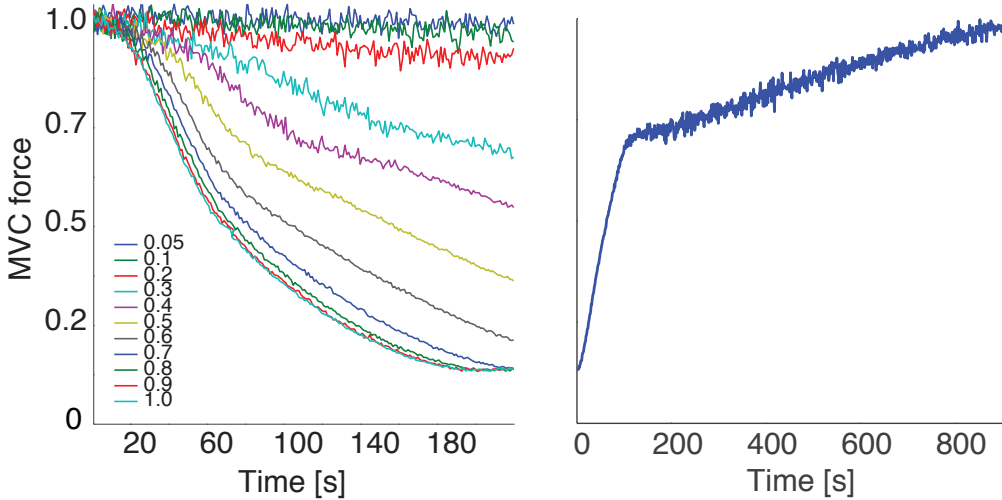


Figure 2.2: Fatigue dynamics. Decline in MVC force for various constant muscle activations, based on the model in [Dideriksen et al., 2010]. Note that at low activation levels ($a(t) \leq 0.2$), the muscle almost doesn't fatigue and that even if fully activated, the muscles maximum force declines to a non-zero level. These phenomena likely reflect the contribution of slow-twitch fibers.

Figure 2.3: Recovery dynamics. Incline in MVC force in the absence of muscle activation. Note the much longer time scale compared to muscle fatiguing. Also note that an initial exponential increase in MVC force is followed by a long linear increase.

where $\text{erfc}(x)$ represents the complementary error function, i.e. $\text{erfc}(x) = \frac{2}{\sqrt{\pi}} \int_x^{\infty} e^{-y^2} dy$ and $\tau_{\text{recovery}} = 0.00448$ for the nominal recovery dynamics (Figure 2.5).

Lastly, we extended the fatigue differential equation by a conditional operations, whereby fatigue dynamics were suppressed if the activation level of the muscles was below the fatigue threshold h described above, i.e. $a(t) \leq h$. Moreover, we extended the recovery differential equation by another conditional operator to suppress recovery if the activation was different from zero, i.e $a(t) = 0.0$.

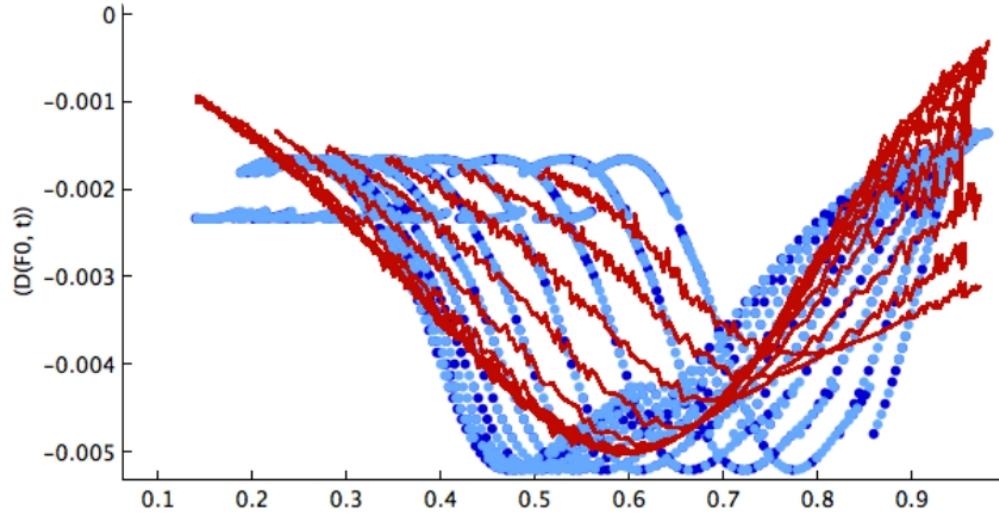


Figure 2.4: Observed fatigue dynamics $\frac{dF_0}{dt}$ in the simulations of [Dideriksen et al., 2011], and the fit (red) obtained using Eureqa.

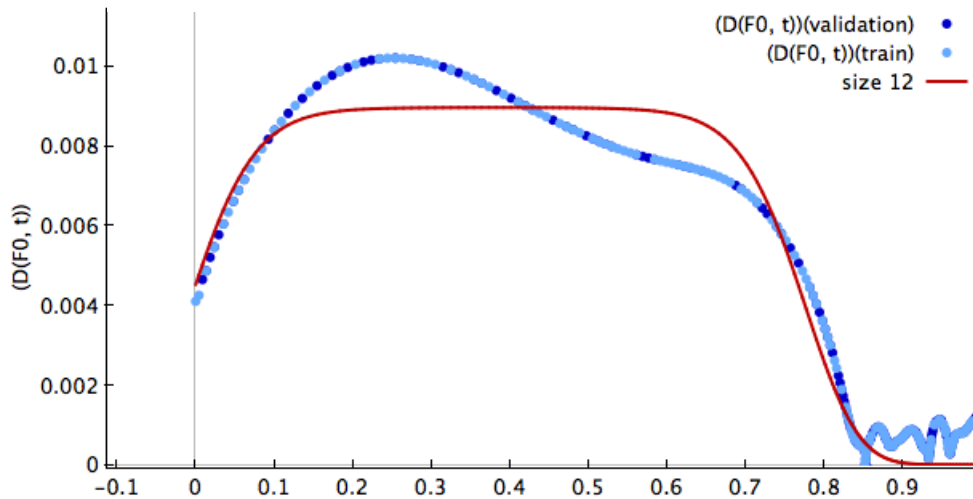


Figure 2.5: Observed recovery dynamics $\frac{dF_0}{dt}$ in the simulations of [Dideriksen et al., 2011], and the fit (red) obtained using Eureqa.

2.4.2 Running the nominal model subject to optimized activation

At each time step of simulation, where $dt = 10$ s, we ran MATLAB's `linprog()` and `quadprog()` functions, minimizing the above described objective functions, subject

to the above mentioned constraints and using the current maximum muscle forces $F_{0_i}(t)$. Next, we computed the instantaneous fatigue or recovery increment or decrement from the Eureqa-extracted differential equations (previous section). In Figures 2.6 and 2.7, we observe a clear difference in muscle activation dynamics, based on the objective function minimized. All objective functions rely mostly on the rectus femoris and the vasti, as expected. None of the objective functions, however, gives rise to the activation of hamstring muscles, which are hip extensors. Their activation would be expected, based on the fact that rectus femoris also acts as a hip flexor and this flexion needs to be counteracted. However, it has been found [Andersen et al., 1985] that the hamstrings remain silent in knee extension in this posture and that RF basically acts as a monoarticular muscle. Here, the upward component of the rectus femoris is mostly counteracted by its synergists, the vasti, and other muscles.

Importantly, synergy-based activation dynamics, i.e. keeping constant the proportions of muscle activations or the force produced by each muscle, succeed at their respective objectives (Figures 2.8 and 2.9). However, we observe that the former also entails non-constant contributions of individual muscles in terms of force, while the latter entails non-constant contributions in terms of activation. In other words, synergy-based objectives can only be met in one domain, while requiring dynamic changes in others. Furthermore, the constant activations proportion objective function almost immediately gives rise to a tangential force component, thus violating the task constraints (Figure 2.8).

Another important observation is that not only do different objective functions give rise to different activation dynamics, but they also rely on vastly different numbers of muscles. For instance, minimizing the sum of activations, a linear objective function, involves only 4 muscles, while minimizing the sum of squared activations, a quadratic objective function, involves 13 muscles (Figures 2.7 and 2.6).

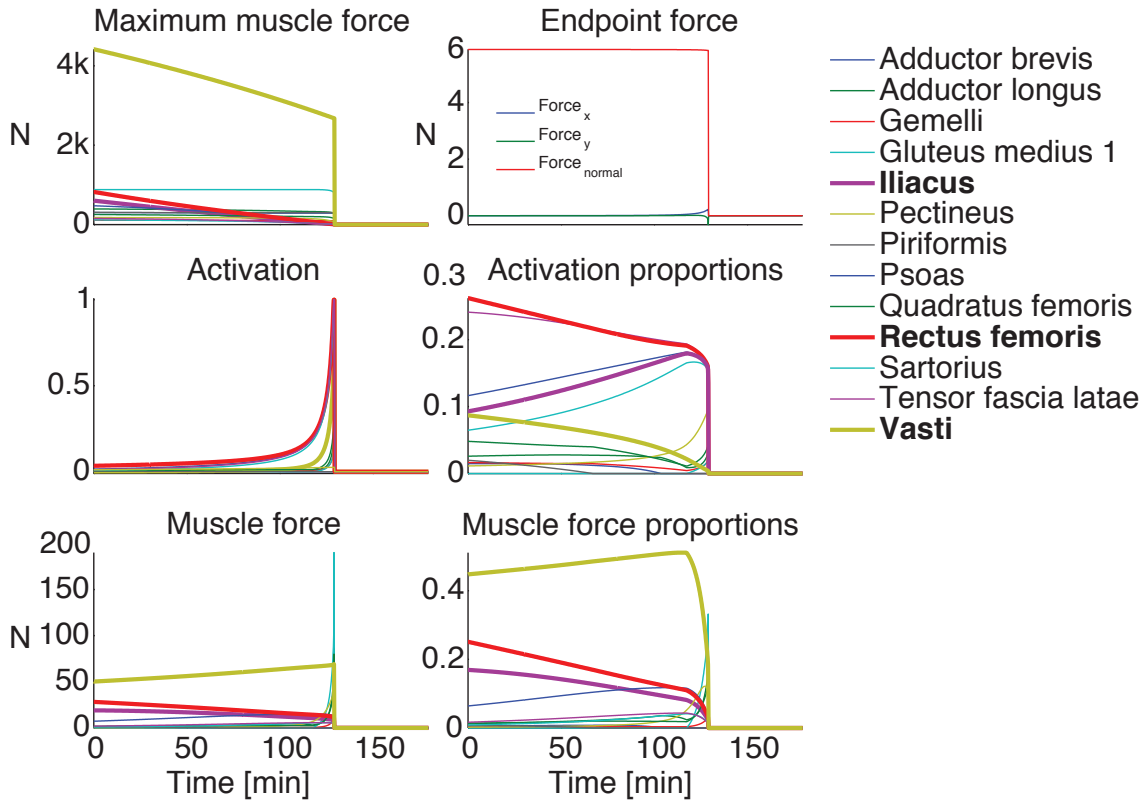


Figure 2.6: Sum of squared activations objective function muscle activation and force dynamics. Muscle activation and force dynamics are highly dynamic, quite different from a static optimization approach that ignores time-variance due to muscle fatigue.

2.4.3 Parameter search results

Even more strikingly, relying on just 4 muscles at the lowest force levels, the sum of activations objective function fails at the task significantly later than its quadratic counterpart (Figure 2.10), and for that matter, all other objective functions. It does so consistently across all levels of force. This can be attributed to the fact that minimizing this criterion is actually the only one tested here that leverages the ability of muscles to recover, here specifically the rectus femoris and the vasti (Figure 2.7), to a considerable degree, reaching the maximum recovery rate at levels between 10 and 20 % of MVC force (Figure 2.11). Note that at lower force levels, recovery is necessary to a lesser

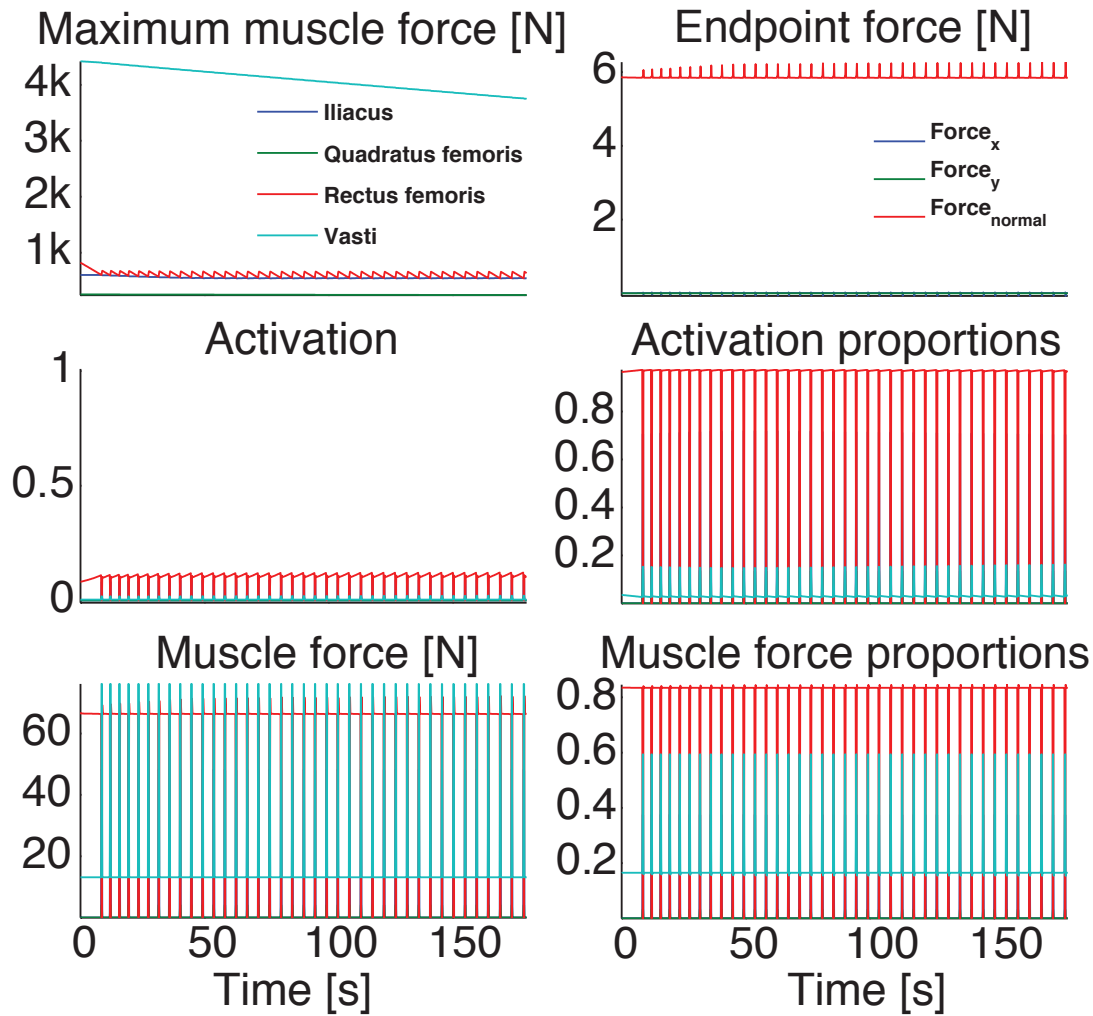


Figure 2.7: Sum of activations objective function muscle activation and force dynamics. Note the rapid switching between rectus femoris and vasti muscles and the fact that this strategy only relies on 4 muscles for successful task performance. The brief switching off of rectus femoris allows it to recover slightly, before being reactivated.

degree, due to the fatigue threshold described above. The decline of recovery at higher forces can be attributed to the lack of available muscle coordination patterns that achieve the task, while the lower rate at low forces reflects the contribution of muscles activated sufficiently low to avoid fatiguing.

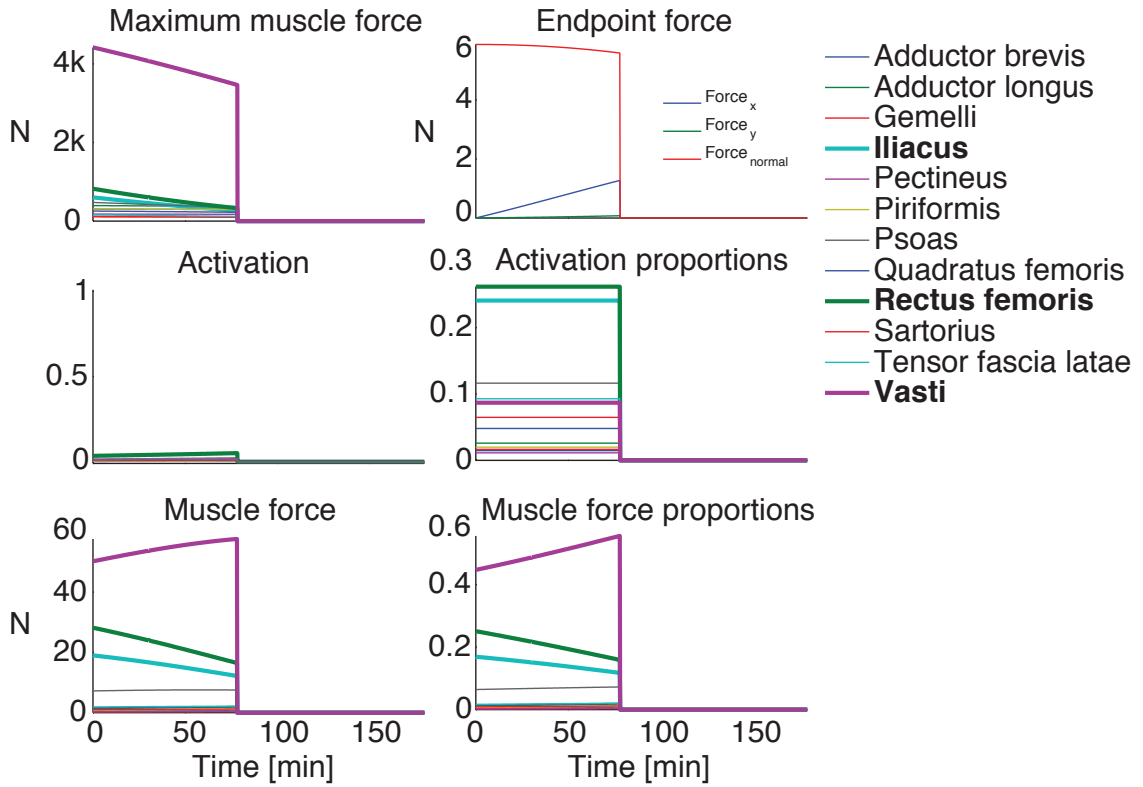


Figure 2.8: Constant activation proportions objective function muscle activation and force dynamics. Note that this objective functions leads to both a relatively early task failure and a large task error in terms of normal force and one of the tangential components of force. Finally, it involves complex dynamics in muscle force space.

All objective functions perform better than the constant muscle force objective function, in terms of failure time and better than the constant activation proportions objective function, in terms of error rate (Figure 2.10). As a matter of fact, note that while the constant activation proportions function seemingly fails later than all other activation schemes, it consistently does so by violating the task constraint of zero tangential force (Figure 2.8), thus giving rise to a large error rate at all MVC force percentage levels (Figure 2.10). Interestingly, while succeeding at enforcing their respective synergy, synergies do however involve either activation or muscle switching and thus give rise to "undesirable" computational complexity.

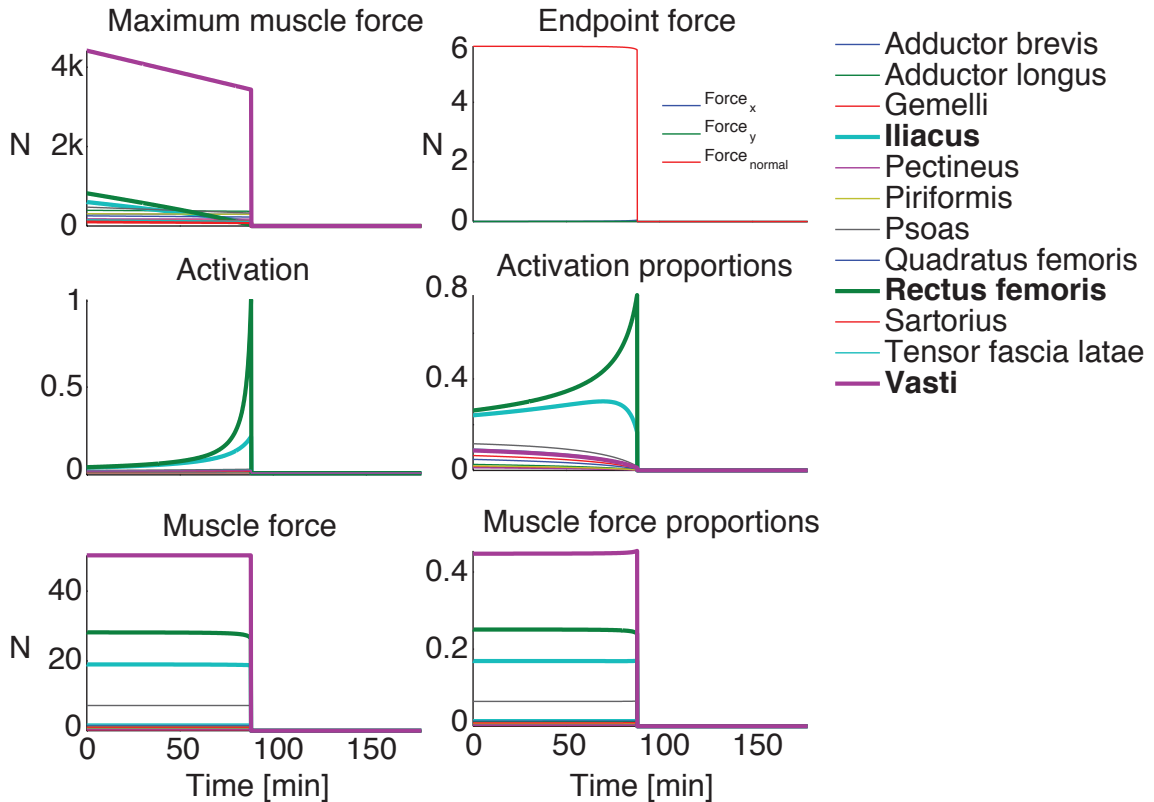


Figure 2.9: Constant muscle forces objective function muscle activation and force dynamics. This objective function leads to a relatively early task failure and involves complex dynamics in muscle activation space.

Lastly, varying the ratio of recovery and fatigue time constants and the fatigue threshold have far smaller influence on the results, giving almost the same results for all values in terms of the metrics computed here (results not shown). This is hardly surprising, since only one of the objective functions, minimizing the sum of activations, actually leverages muscle recovery dynamics. Thus, its dynamics are the only ones that do show some effect of increasing the recovery time constant, specifically a reduction in switching behavior and a reduction in the recovery rate.

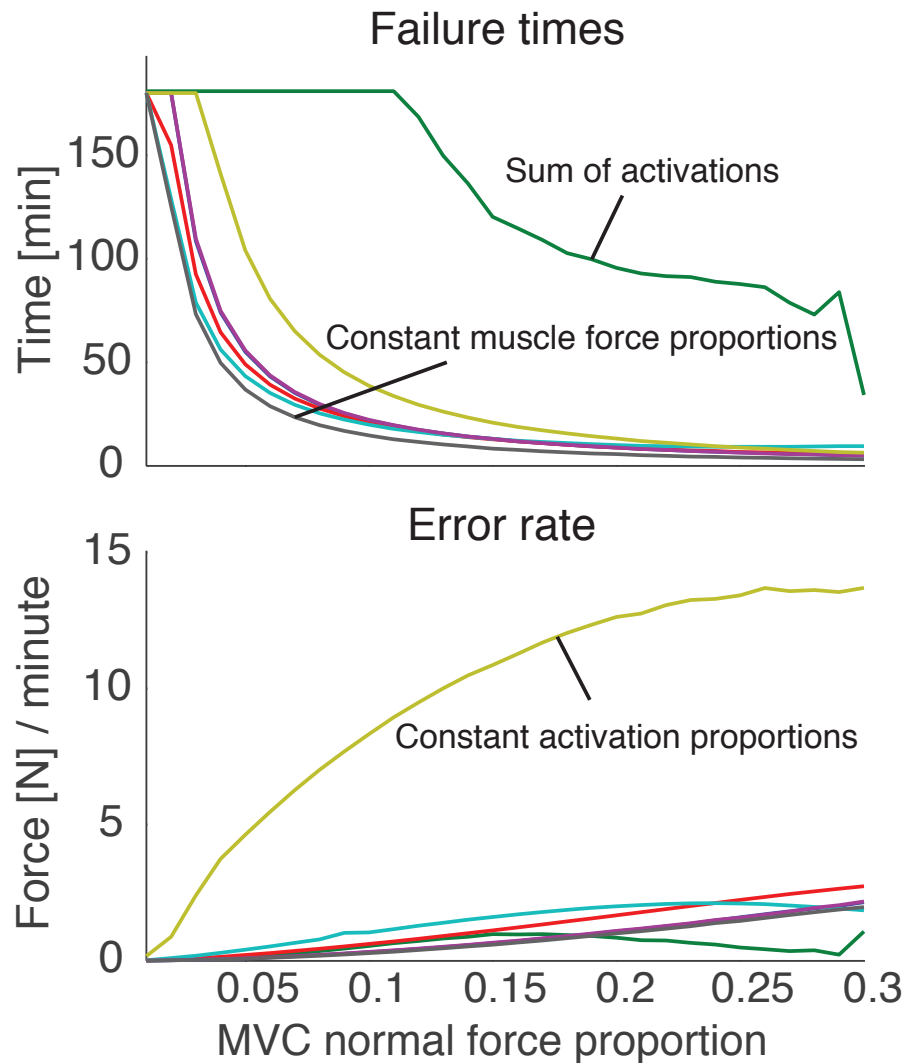


Figure 2.10: Comparison of failure times and error rates over a range of target normal force MVC proportions. While naturally, all dynamics fail progressively earlier as the force demands of the task increase, the linear sum of activations objective functions performs the longest. Note that while the synergistic constant activation proportion objective function seemingly performs well in terms of time-to-failure, it has by far the largest error rate, due to its inability to enforce the zero tangential force constraint (Figure 2.8)

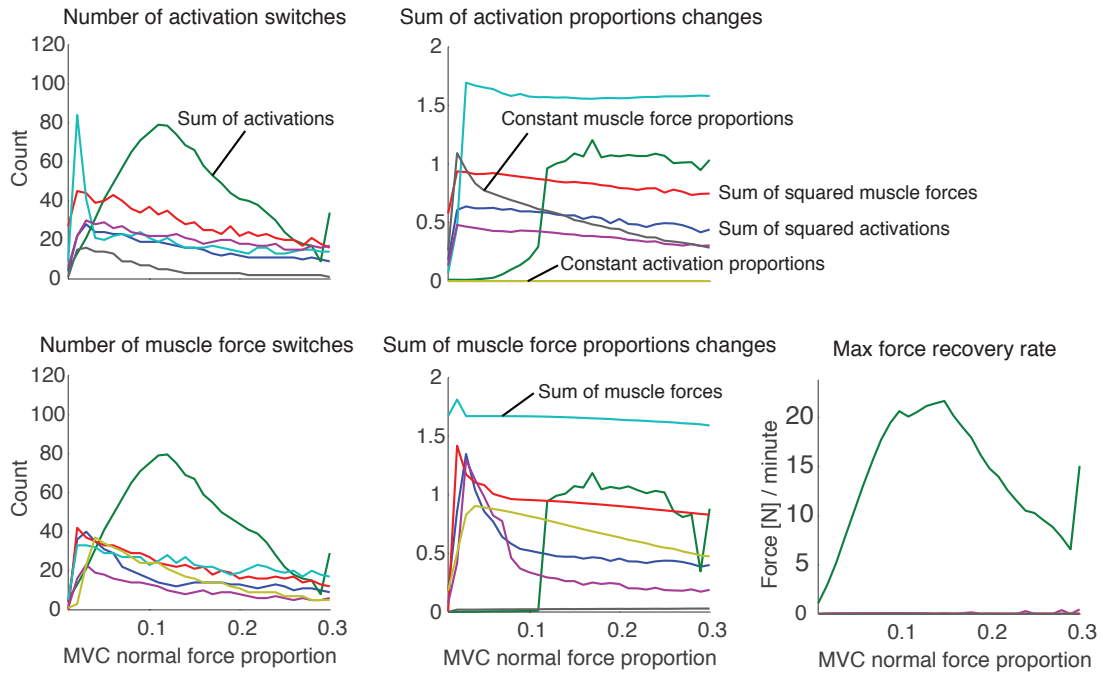


Figure 2.11: Comparison of activation and muscle force dynamics at different target normal force MVC proportions. Note that as the target force level increases, only the linear sum of activations objective functions increasingly relies on switching between muscles in terms of both activations and force. At low force levels, this function is actually less dynamic than most others, while achieving similar failure times and error rates (Figure 2.10)

2.5 Discussion

In submaximal tasks, the reality of fatigue and recovery in neuromuscular systems and the resultant time-variance of maximum muscle forces necessitates an adaptive response by the nervous system to select muscle activations based on the instantaneous state of the system, to maintain a desired output. This is contrary to the currently dominant thinking about optimization for neuromuscular systems, whereby a single optimal solution is relied on for the entire duration of task performance [Prilutsky and Zatsiorsky, 2002]. Importantly, the need for dynamic muscle activations and forces doesn't arise simply to

ensure increased activation to compensate for muscle fatigue [Dideriksen et al., 2010]: since muscles fatigue differentially [Housh et al., 1995], the compensatory increase in activation needs to be individually tuned. Mathematically, the activation pattern can be represented by a vector, whose direction is determined by the individual muscle activation contributions and whose magnitude represents the overall activation [Valero-Cuevas et al., 1998, Valero-Cuevas, 2000]. Based on this interpretation, the need for continuous adaptation is expressed by the need for both changes in direction of the vector and increase in its magnitude. A single static optimal solution, on the other hand, is expected to yield an optimal result only for the instantaneous state of the system and thus proves suitable only in the prediction of muscle forces, when the relationship between activation and force is ignored (e.g. [Prilutsky and Zatsiorsky, 2002]), or in the prediction of activation in tasks of short duration.

Incorporating sophisticated state-of-the-art dynamics of fatigue and recovery [Dideriksen et al., 2011] in a realistic linear model of isometric knee extension [Yoshikawa, 1990, Arnold et al., 2010], we simulated continuous optimization for a variety of objective functions and showed that fatigue-induced time-variance inevitably, regardless of the objective, leads to complex dynamics of activation and individual muscle force contribution (Figures 2.6 and 2.7).

Importantly, synergy-based co-activation of muscles, such as maintaining constant muscle activation proportions or individual muscle forces, is equivalent to adhering to an initial solution found through static optimization. While synergies indeed succeed at minimizing dynamics in their respective domains, the dynamics in the respective other domains are clearly not synergy-like (Figure 2.8 and 2.9). However, combining the contributions of individual muscles into a desired endpoint force output, the nervous system cannot ignore any of the domains. Therefore, the results presented here for even a simple motor task indicate that the computational benefits associated with synergies

are restricted to a single domain. However, the fact that humans are capable of performing motor tasks continuously or repeatedly show that the nervous system is capable of processing time-varying relationship between high-dimensional muscle activation and muscle force spaces.

How could the neuromuscular system still achieve simultaneous simplicity in the muscle force and the activation dynamics? One possibility is that despite their differential activation, contributing muscles all fatigue at the same rate, which in turn requires equal increases in activation across muscles to compensate for the loss in muscle force. Given the possibility that some muscles are activated at levels sufficiently low to avoid fatiguing and thus make unnecessary the increase in activation [Housh et al., 1995], this seems highly unlikely. The other possibility is that the mapping from muscle activation to muscle force, which is known to be complex and time-variant [Dideriksen et al., 2010], is adjusted such that synergies can be maintained in both domains simultaneously. Apart from the lack of evidence for such a complex and unnecessary adjustment, it again requires knowledge of individual muscle states and thus information about the full dimensionality of the problem.

Moreover, synergistic objective functions either lead to relatively early task failure, as in the case of constant muscle forces, or they fail to meet the task constraints, as in the case of constant activation proportions (Figure 2.10). Alternatively, this can be considered an immediate task failure. Since fatiguing depends functionally on the muscle force, a constant muscle force strategy will leave resources in less activated muscles unused and this strategy will fail by the time one of the muscles reaches full activation and fatigue cannot be compensated any more. A constant activation proportion strategy, on the other hand, cannot meet task constraints due to the above mentioned differential fatiguing in muscles, almost immediately producing force in undesired directions. For these reasons, lack of computational simplification and early failure, synergies (and thus

single static optimization) are at best unnecessary but at worst outright detrimental for motor task performance.

It can be argued nevertheless, that shifting between synergies might help to alleviate this problem. While there exists evidence for switching between specific activation patterns [Akima et al., 2011], this strategy raises the question of how many synergies are necessary to perform a task and where the difference lies between shifting between synergies and dynamic activation.

Why have these necessary consequences of differential fatiguing seldom been observed previously? One possibility is the lack of redundancy in previously studied tasks: for instance, the task posture or the force requirement might only admit a very limited number of solutions [Loeb, 2000, Kutch and Valero-Cuevas, 2011] (Figure 3.2). While these solutions likely require differential activation of contributing muscles, leading to differential fatiguing, the observed activation dynamics might approximate those of synergistic activation, i.e. a simple scaling up of the muscle coordination pattern [Rudroff et al., 2010, Danna-Dos Santos et al., 2010], due to the limited resolution of surface EMG [Farina et al., 2004].

Unexpectedly, while it did enable relatively longer task performance, continuous optimization of most objective functions tested here did not leverage the availability of muscle recovery. Only minimizing the sum of activations function gave rise to the required disabling of muscles. While, on the one hand, being one of the least complex strategies, involving the fewest number of muscles, it also came closest to reproducing the dynamics observed in [Kouzaki and Shinohara, 2006], namely the switching between rectus femoris and the vasti (Figure 2.7). As we increased the force requirement, this switching gradually disappeared (Figure 2.11), reflecting the need to keep all quadriceps muscles activated and reducing the space of available solutions. The ability

to leverage redundancy for optimal use of resources provides another important aspect in the debate on optimization as a means to solve the redundancy problem.

There exists peripheral evidence for the underlying mechanisms that give rise to activation shifts between muscles. Selective fatiguing through electric stimulation of the vastus lateralis [Akima et al., 2002] and biceps brachii [Aymard et al., 1995] has been shown to increase recruitment of synergists, while the selective fatiguing of first dorsal interosseous has been shown to increase the α -motoneuron excitability of the non-fatigued neighboring abductor pollicis brevis [Duchateau and Hainaut, 1993]. The former observations have been attributed to the decrease in inhibition of group Ia afferents between synergists, with the inhibition between antagonists remaining unaffected [Aymard et al., 1995], while the latter are due to the activation of group III and IV afferents under fatigue, which in turn inhibit the fatigued muscle. Further evidence suggests that an observed alternating activity between synergistic muscles, such as the switching between rectus femoris and the vasti (as seen in the optimization of the sum of activations function), when we optimized the sum of activations objective function, serves to prolong task performance, as the switching frequency negatively correlated with the post-trial decrease in MVC force [Kouzaki and Shinohara, 2006].

Concluding, our results encourage us to view redundancy as an opportunity for mitigation of fatigue in neuromuscular systems, rather than a computational problem. However, the results furthermore indicate that even if the neuromuscular system does not leverage redundancy, a controller nevertheless needs to be fully aware of the high-dimensional dynamics in muscle force and activation spaces and the time-varying relationship between the two. Future efforts at discovering a potential optimization principle underlying muscle activations in motor tasks should therefore investigate the interplay between redundancy and muscle recovery at submaximal forces. However, computational models are required to design experiments to ensure the availability of multiple

solutions in a given motor task, so as to avoid falsely concluding that synergies are a consequence of nervous system control, as well as the drawbacks of the limited resolution of EMG.

Chapter 3

Biomechanics Rather Than Neurophysiology Explains the Abolishment of Alternating Activation of Synergistic Muscles in Submaximal Fatiguing Isometric Contractions

3.1 Abstract

Several publications in the last two decades have demonstrated slow dynamic reweighting of muscle activation among synergists in fatiguing low-force isometric tasks. Furthermore, some of these studies have found evidence that switching between synergists serves as a fatigue mitigation mechanism, as the frequency of switching is inversely related to the decrease in MVC force during the trial. Potentially, muscles that are switched off can recover from fatigue to some degree. However, the switching between synergists largely disappears at approximately 10% of MVC [Kouzaki et al., 2002], a phenomenon hitherto not understood.

It is a well-known that at lower force levels, multiple muscle coordination patterns can generate the same force output. Here, we show, based on the prediction of a realistic biomechanical model of isometric knee extension, that although multiple muscle

coordination solutions do exist at the 15% MVC force level, each of them requires all synergists involved in knee extension to be activated, thus precluding muscle coordination patterns in which individual muscles are switched off.

We then used surface EMG to determine experimentally the muscle activations in isometric knee extension and successfully reproduced the switching dynamics observed in previous studies of isometric knee extension. We find that, as predicted by the model, switching largely disappears between 10 % and 15 % of MVC force.

Hence, we provide a simple biomechanical rather than a complex neurophysiological explanation for the abolishment of muscle switching at higher force levels. This result has important implications for our understanding of how the nervous system deals with muscle redundancy: specifically, we show that the assumption of neurophysiological factors is unnecessary in the explanation of the abolishment of muscle switching. This enables us to view control by the nervous system as being mainly constrained by biomechanical factors, while being able to play an active role in the mitigation of fatigue.

3.2 Introduction

Involuntary low-frequency alternations in recruitment of different parts of the quadriceps during submaximal isometric knee extension were first reported in [Sjogaard et al., 1986]. Since then, such changes in muscle activation in isometric tasks have been reproduced in the same task [Kouzaki and Shinohara, 2006], as well as observed in other isometric tasks such as elbow flexion [Semmler et al., 2000] and ankle extension [Tamaki et al., 1998]. In particular, in the former two studies the observed changes were statistically associated with a reduced decrease in post-trial MVC [Kouzaki and Shinohara, 2006] or increased endurance [Semmler et al., 2000].

These results have important and hitherto overlooked implications for motor control, specifically the way in which the nervous system handles the redundancy problem [Bernstein, 1967], i.e. the seemingly infinite number of muscle activation patterns that all generate the same endpoint force vector in submaximal tasks. The results indicate that the nervous system is actually capable of leveraging redundancy for the mitigation of fatigue, i.e. employing the switching between synergists to mitigate fatigue and extend the time to exhaustion in submaximal tasks.

Besides, these results cast doubt on the validity of using optimization to determine a unique solution to the redundancy problem [Prilutsky and Zatsiorsky, 2002], since traditional approaches in biomechanics disregard the time-varying nature of neuromuscular systems subject to fatigue and thus do not allow for dynamic muscle activation or at least, the switching between solutions. This mismatch between prediction and observation also applies to the idea of muscle synergies [Tresch and Jarc, 2009], i.e. the rigid co-activation of muscles, since synergies can be considered as static solutions to the redundancy problem.

Importantly, however, the endurance-enhancing muscle switching between synergists has only been observed at very low forces, at no more than 10% of MVC force [Kouzaki et al., 2002]. Why alternating recruitment has not been observed at higher force levels, is currently unclear, but [Kouzaki et al., 2002] suggest that these dynamics are related to the balance between neural inputs from peripheral afferents and the voluntary drive. Specifically, inhibition between synergist muscles decline as voluntary contraction levels increase [Gritti and Schieppati, 1989, Schieppati et al., 1990].

Here, we test a simpler hypothesis for the observed abolishment of switching at higher contraction intensities. In particular, we hypothesize that the neuromuscular system simply requires all synergists, i.e. rectus femoris and the vasti, to produce the desired force. To generate a specific endpoint force vectors, a subtle combination of

muscles whose individual vectors point in the approximate direction is required. While at low forces, combinations exist that do not necessarily involve all synergists, at higher force the neuromuscular system simply runs out of solutions of this kind. This prediction is based on a simple linear and redundant, but realistic model of isometric knee extension [Yoshikawa, 1990, Valero-Cuevas, 2009].

3.3 Methods

3.3.1 Modeling a redundant neuromuscular system

Assumptions

For the purposes of modeling a redundant motor task subject to fatiguing, we adopt the definition of **muscle fatigue as the exercise-induced decline of the maximum force a muscle can generate** [Vollestad, 1997]. In turn, this requires the increase of activation of that muscle to maintain the force generated by it, as has been observed previously [Dideriksen et al., 2010, Danna-Dos Santos et al., 2010, Rudroff et al., 2010]. Muscle recovery, on the other hand, occurs only in the total absence of activation [Dideriksen et al., 2011]. At very low muscle forces, the muscle neither fatigues nor recovers, due to the reliance on slow-twitch fibers, also known as indefatigable fibers [Loeb and Ghez, 2000].

We selected the task of isometric knee extension, because there exists prior evidence that the nervous system leverages redundancy for the mitigation of fatigue [Sjogaard et al., 1986, Kouzaki, 2005, Kouzaki and Shinohara, 2006]. Besides, from a modeling point of view, knee extension has favorable properties: it allows for isolation of muscle redundancy and a clear separation from endpoint force vector redundancy, whereby different force vectors can all achieve successful task performance.

Specifically, the muscles actuating the knee (vasti and rectus femoris) are largely similar in terms of their mechanical action and additionally, these muscles don't add/abduct or rotate the leg. Therefore, dynamic activation of rectus femoris and the vasti in isometric knee extension is unlikely to give rise to undesirable tangential endpoint force component, which helps to keep this vector constant.

Furthermore, we assume the following:

Independence of muscles: Muscles actuating the modeled limbs are assumed to be controlled independently. However, it has been observed in numerous studies that the activations of muscles correlate to some degree. Whether these correlations are a function of the particular motor task [Valero-Cuevas et al., 2009b, Kutch et al., 2008] or the common input at a higher center [Winges et al., 2006], is currently unclear. The only exception we make to this assumption is that the three vasti muscles are controlled together and basically treated as one muscle [Eccles et al., 1957, Hoffer et al., 1987a, Hoffer et al., 1987b].

Leg consisting of rigid, supported links with ball and hinge joints: for an isometric finger task, this assumption has been shown to be sufficient and valid [Valero-Cuevas et al., 1998]. This assumption allows us to use a simple three-dimensional geometric model to model the mapping from joint torques to limb endpoint forces. Furthermore, since we model a seated posture, with knee and hip flexed at right angles, the leg is completely supported and no torques are necessary to maintain posture.

Linearity: It has been shown previously that in isometric force production, the mapping from muscle activation to the endpoint wrench is approximately linear [Valero-Cuevas et al., 1998], which entails that the mapping from muscle activation to limb endpoint force can be described by matrix multiplication. Force-velocity curves do not play a role in isometric tasks and the force-length curve properties are captured by the changes of the moment arms as the posture varies.

Mathematical modeling of isometric knee extension

The modeling of isometric knee extension has been described in the previous chapter, in a section with the same title.

3.3.2 Muscle necessity analysis

We used the nominal matrix $J^{-T}R(\vec{q})F_0$ to determine whether specific muscles, namely the rectus femoris and the vasti are necessary for a given desired output force using standard tools in computational geometry. The muscle redundancy problem can be expressed as a set of linear inequalities [Chao and An, 1978, Spoor, 1983]. These inequality constraints enforce firstly, that the activation for each muscle lie between 0 and 1, secondly, that the actual output normal force is equal to the desired force, in terms of the percentage of MVC normal force, thirdly, the tangential components of the endpoint force vector are zero and finally, that no torque is applied about the endpoint. The inequality constraints define a region in muscle activation space called the task-specific activation set: any point inside that set will produce the desired output force [Kuo and Zajac, 1993, Valero-Cuevas et al., 1998, Valero-Cuevas, 2000, Valero-Cuevas, 2005]. We computed the vertices defining the task-specific activation set using a vertex enumeration algorithm [Avis and Fukuda, 1992]. We then found the task-specific activation ranges to achieve the desired output force for each muscle by projecting all vertices onto the 31 muscle coordinate axes to determine the minimum and maximum task-specific activations. We used the necessity analysis of the nominal model to determine a set of candidate muscles for the subsequent sensitivity analysis (below). Since running vertex enumeration to test the robustness of muscle necessity results is computationally too costly, we tested the necessity of a few individual muscles only, which we identified by the low force at which they became necessary. Lastly, due

to the computational cost, we performed the necessity analysis on a reduced model with 15 muscles, including all muscles that have a moment about the knee plus some of the hip muscles, mainly hip flexors and extensors.

3.3.3 Sensitivity analysis

To test how sensitive the muscle necessities of the most necessary muscles found through vertex enumeration are to variations in task posture, muscle moment arms and maximum muscle forces, we perturbed the column vectors of the matrix $J^{-T}R(\vec{q})F_0$, by adding random vectors drawn from a zero-mean normal distribution. Since the action matrix is formed by the product of the posture-dependent Jacobian inverse transpose, the muscle moment arm matrix and the diagonal matrix of maximum muscle forces, perturbing this product is equivalent to randomly varying these parameters in isolation.

To determine necessity of individual muscles, we ran MATLAB's `linprog()` constrained linear optimization algorithm. Specifically, we minimized the sum of muscle activations $\sum c_i a_i$ subject to the above described muscle activation, torque and tangential constraints. However, all coefficients c_i , except the one for the muscle of interest (rectus femoris and vasti) were set to zero, therefore the objective function becomes simply $c_i a_i$. Thus, the objective is to minimize the contribution of the muscle of interest, while allowing other muscles to contribute an arbitrary amount of force, as long as the constraints are satisfied. If the contribution of the muscle of interest cannot be reduced to zero, that muscle needs to be considered necessary under the given constraints.

Besides varying the perturbation intensity from zero (nominal model) to 20% of each action matrix column vector's length, we also varied the output normal force in terms of the percentage of MVC normal force, which the particular perturbed model could generate, to determine for each perturbation intensity the percentage at which a muscle becomes necessary.

3.3.4 Data collection

Data were obtained from 3 young adult male subjects (ages 23, 32 and 33, all right-dominant) during sustained knee extension at three different MVC percentage levels (2.5%, 10% and 15%), below and just above the predicted level at which the vasti muscles became necessary to perform the task.

We measured subjects' MVC torque using a CYBEX Humac Norm system (Cybex, Medway, MA). They were asked to produce maximum isometric knee extension torque with their dominant leg and with hip and knee flexed at 90° for 5 seconds. This was repeated 3 times and the maximum obtained value was used as the MVC torque. Based on the MVC knee extension torque and the moment arm length, i.e. the distance between knee and the location of force application just above the malleolus, we computed the MVC normal force by dividing the torque by the moment arm length.

Subjects were seated in a chair, hip joint flexed at 90° and the knee of the dominant leg flexed at slightly less than 90°. Subjects were not strapped to the chair, to ensure that they voluntarily maintained that posture and could not rely on postural changes to mitigate fatigue. However, the lower leg was immobilized between the force sensor and the leg rest of the chair. Subjects exerted force with the ventral aspect of their lower dominant leg just above the medial malleolus (Figure 3.1) against a 6-axis force transducer (JR3, Woodland, CA). Simultaneously, we recorded bipolar surface electromyogram (EMG) using a Delsys system (Delsys, Boston, MA) from the muscle bellies of rectus femoris (RF), vastus lateralis (VL), vastus medialis (VM), biceps femoris (BF) and semitendinosus (ST), while the common reference electrode was placed on the skin around the olecranon. Because of its deep location, we were unfortunately not able to record from iliacus via surface EMG. EMG and force data were sampled at 1000 Hz using a 16-bit data acquisition system (National Instruments 6259) and stored and analyzed on a computer.

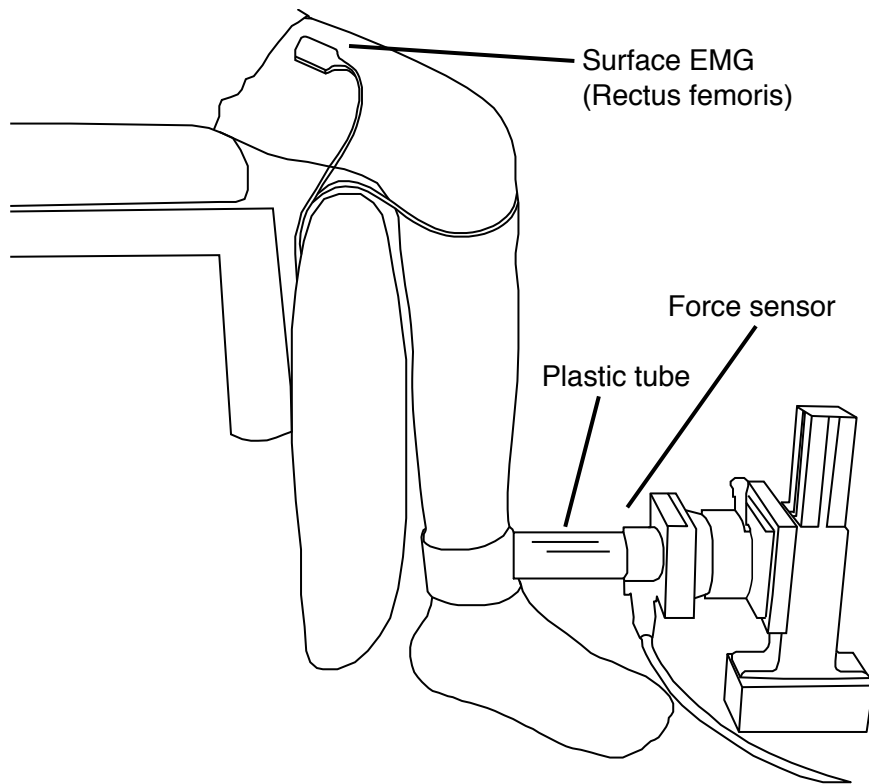


Figure 3.1: Experimental setup. Subjects were seated on a chair, with the backrest set to vertical, to help them maintain a posture of 90° hip flexion and near 90° knee flexion. They exerted a force directed forward against a tube that was attached to a force sensor, set to the appropriate height above ground. The dominant leg, with which subjects exerted force, was immobilized between the tube and the leg rest. To prevent discomfort caused by the force exertion, a strap was tied around the leg above the malleolus.

Subjects maintained the 2.5% MVC normal force for 1 hour, the 10% for 20 minutes, and the 15% MVC for 15 minutes or until exhaustion. Subjects were given visual feedback on the normal force: a horizontal line on the screen representing the applied normal force had to be aligned with a horizontal target force line, as closely as possible. While subjects did perform a short 1-minute learning trial, they were not given directions during the actual trial.

3.3.5 Data analysis

3.4 Results

3.4.1 Muscle necessity analysis

The muscle necessity analysis reveals that first, the vasti become necessary, near 12% MVC normal force and next, both rectus femoris and iliacus become necessary at 41% (Figures 3.2 and 3.3). None of the other muscles that have a moment about the knee joint, such as the hamstrings, for instance, become necessary at these force levels. In fact, at 41% MVC, all muscles except the three mentioned above can be arbitrarily activated and a suitable solution still be found. Therefore, for the subsequent sensitivity analysis, we investigated the robustness of the necessity results for the vasti, rectus femoris and iliacus.

3.4.2 Sensitivity analysis

Our sensitivity analysis based on randomized perturbations to the model of isometric knee extension suggests that it is the vasti which are the determining factors in the disappearance of muscle switching, since they become necessary at lower MVC normal force levels than the rectus femoris.

3.4.3 Experimental results

Subjects' MVC normal forces were found to be 440 N, 481 N and 951 N, respectively. All three subjects were able to maintain the required force for the duration of the trial at the 2.5 and 10% MVC target forces. When the task was performed until exhaustion, the subjects only failed to maintain the required force at the very end. Exhaustion only occurred when 15% MVC normal force was the target force.

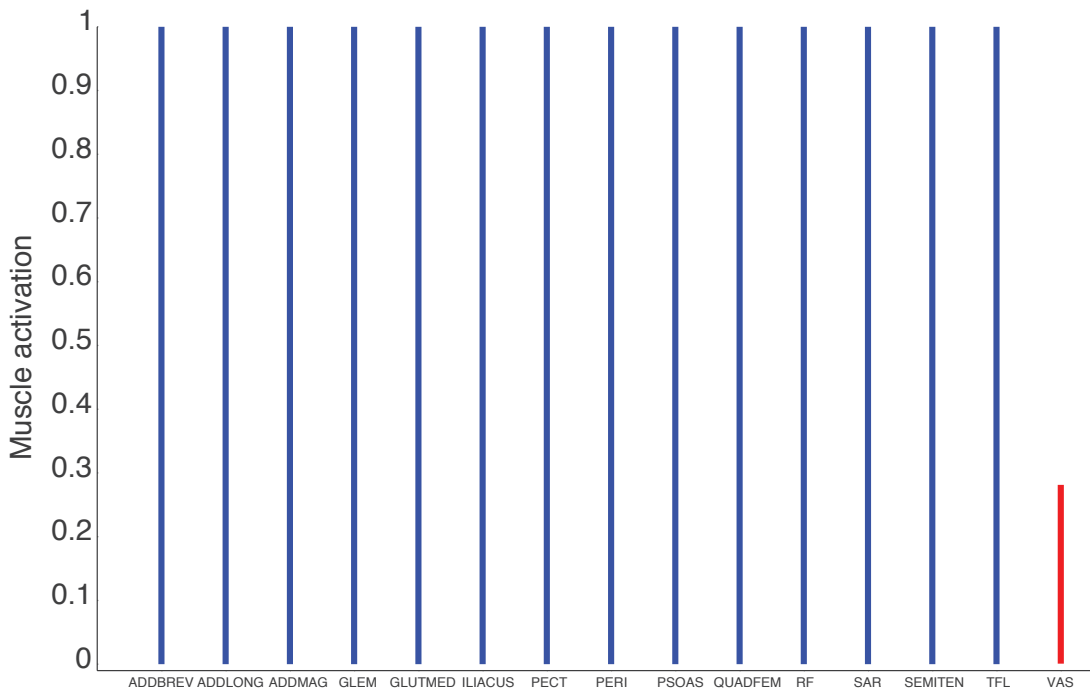


Figure 3.2: Muscle necessity analysis result at 15% of MVC normal force. The admissible activation ranges for necessary muscles are colored red. At this force level, the vasti muscles (VAS) become necessary for any muscle coordination pattern, and thus cannot be switched off for potential recovery from fatigue. Note that all other muscles can be activated at any level and a suitable coordination pattern can still be found.

Plotting the EMG traces for the three force levels of 2.5%, 10% and 15% of MVC normal force (Figures 3.6 - 3.8), we see a gradual change from very pronounced switching dynamics among the rectus femoris and the two vasti at low force, becoming less pronounced as the force increases to a complete disappearance at the highest force level. Instead, the high force is maintained by gradually increasing the activation of all synergistic muscles, thus confirming our hypothesis that at least one of the synergists becomes necessary at this force level. Thus, the switching off of a muscle would lead to violation of the task constraints.

More specifically, the observed switching occurred mainly between the rectus femoris and the two of the vasti muscles, possibly all three of

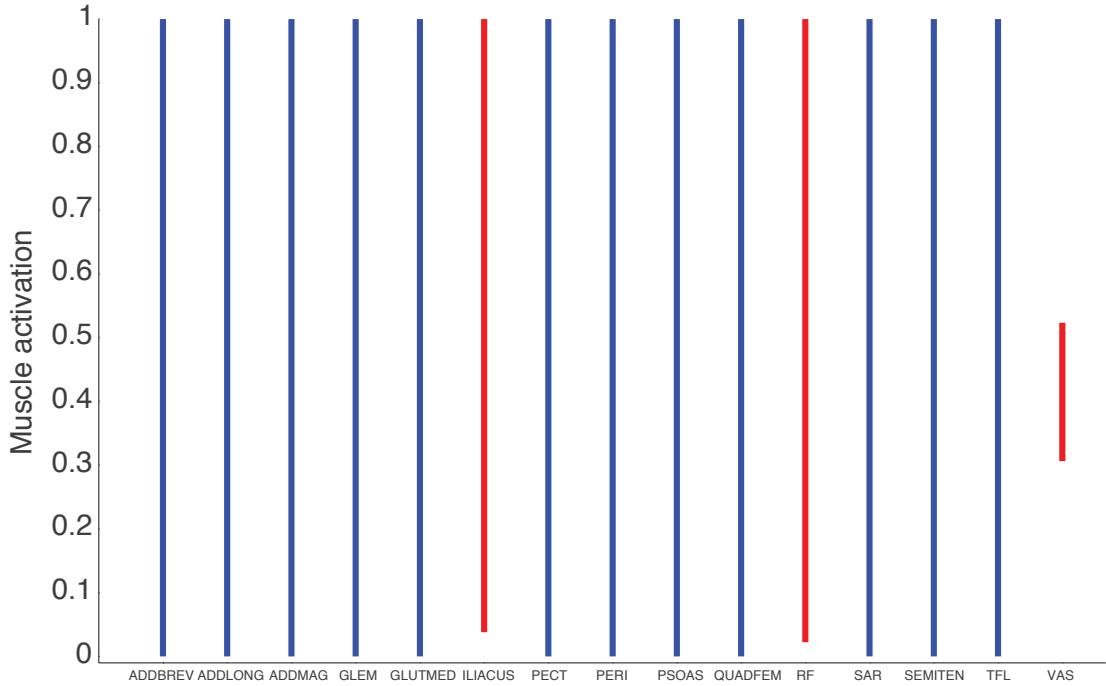


Figure 3.3: Muscle necessity analysis result at 41 % of MVC normal force. The admissible activation ranges for necessary muscles are colored red. Besides the vasti (VAS), the rectus femoris (RF) and the illiacus (ILIACUS) become necessary, too, while all other muscles can be activated at any level.

them [Akima et al., 2011], due to the common innervation of these muscles [Hoffer et al., 1987a, Hoffer et al., 1987b, Eccles et al., 1957]. This confirms the observations in [Kouzaki et al., 2002, Kouzaki and Shinohara, 2006, Akima et al., 2011], where the observed switching frequency among the vasti was near zero. Moreover, the switching activity between muscles, when it occurred, never began immediately or soon after the start of the trials, but 15 minutes into the trial at medium force levels (Figure 3.7) and even later at the lowest force level (Figure 3.6, 25-30 minutes), suggesting that the switching is induced by fatigue.

Finally, the finding of our sensitivity analysis that the vasti become necessary at lower force levels than the rectus femoris is reflected by the comparatively greater modulation of RF activation (Figures 3.6 and 3.7), i.e. the difference in activation between

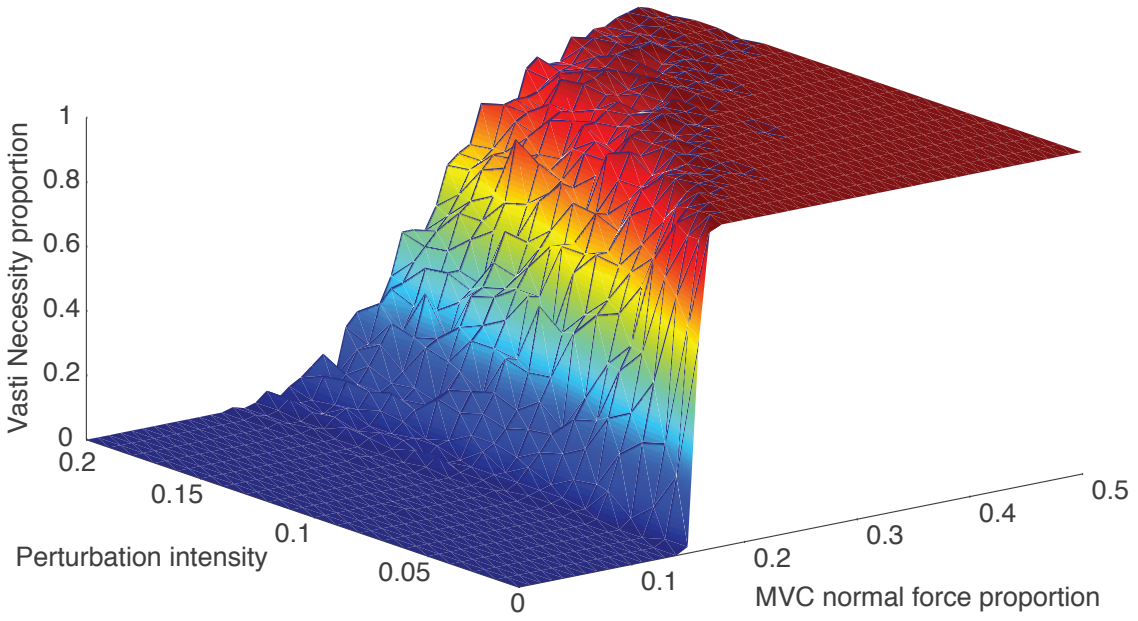


Figure 3.4: Sensitivity analysis for the vasti muscles. For a given MVC normal force proportion between 0 and 0.5, the column vectors of the matrix $J^{-T}RF_0$ were perturbed by vectors of length 0 to 0.2 of the nominal vector length. For each perturbation length, the perturbation was repeated 100 times and at each iteration the necessity of the vasti was determined. The z-axis represents the proportion of iterations for which the vasti were necessary. We see that the vasti become necessary at the lowest force level for the unperturbed nominal model, near 0.12 of its MVC normal force.

"on" and "off" phases is more pronounced in the latter. This confirms that more muscle coordination patterns exist in the absence of RF activation than do in the absence of vasti activation.

3.5 Discussion

In this work, we have found evidence for a simple biomechanical explanation for the abolition of muscle activation alternation among synergists. Specifically, our 31-muscle model of isometric knee extension predicts the necessary activation of some of

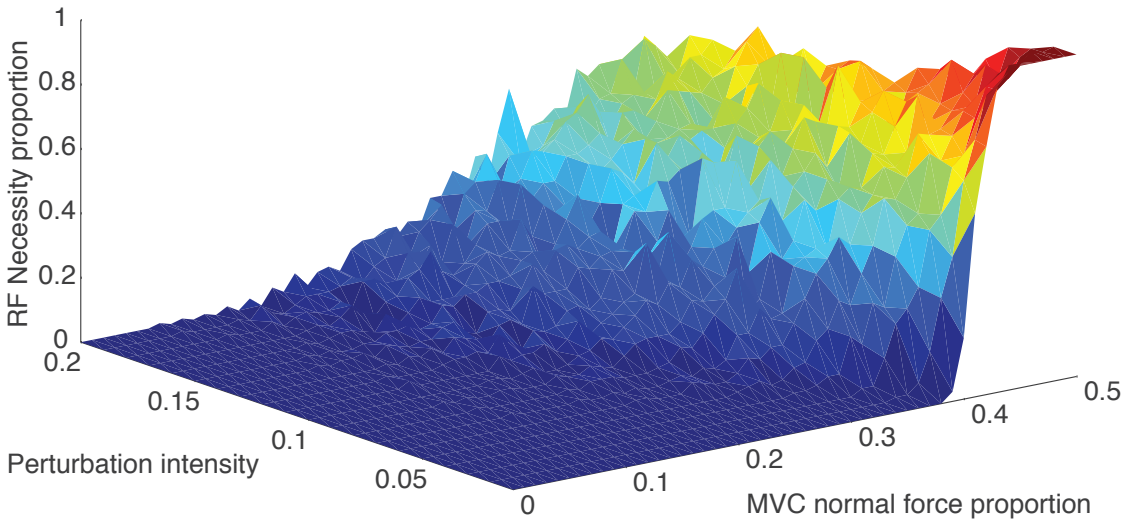


Figure 3.5: Sensitivity analysis for rectus femoris. Contrary to the vasti, in the nominal model the rectus femoris becomes necessary at the highest MVC normal force proportion, between 0.35 and 0.4, while in the most perturbed model, the RF can be necessary at force levels as low as 0.1.

the involved muscles, which prevents their deactivation and thus the alternation among synergists.

Alternating activation between synergistic muscles in fatiguing submaximal isometric tasks is a phenomenon that has been observed in multiple studies [Sjogaard et al., 1986, Tamaki et al., 1998, Kouzaki et al., 2002]. It has been suggested that the alternation serves as an endurance-enhancing mechanism, whereby deactivated muscles recover some of their force-generating capability that decreased under fatigue. The underlying physiological mechanisms giving rise to the alternation phenomenon are currently unclear, but it has been hypothesized that muscle afferents send fatigue-related information to the α -motoneurons of all synergists via interneurons. In particular, a potential mechanism is the fatigue-induced disinhibition of afferents between synergists [Schieppati et al., 1990, Pascoe et al., 2006]. According to this interpretation, the alternation between synergists occurs due to the reciprocal decrease in

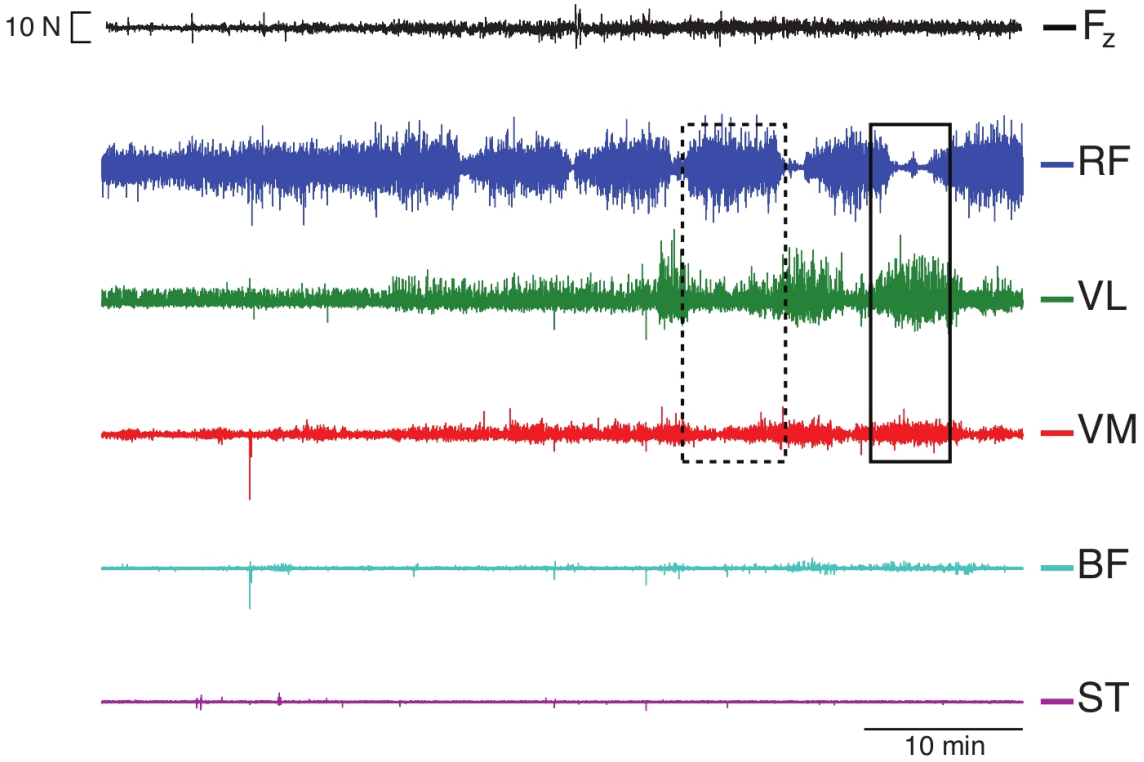


Figure 3.6: Representative EMG recordings at 2.5% MVC normal force. The subject maintained this force level for 60 minutes. Between 20 and 30 minutes into the trial, we see activation rotation between the RF and the two vasti, becoming more pronounced as the trial progresses. Two sample coordination patterns are highlighted: *dashed rectangle*: RF activated, vasti deactivated, *solid rectangle*: RF deactivated, vasti activated

inhibition, but since muscles fatigue at different rates, they inhibit each other differentially. Not surprisingly, the reason for the disappearance of alternation at approximately 10% MVC is even less understood. It has been found that the blood flow to muscles is significantly reduced at 10% MVC [Sjgaard et al., 1988]. This in turn would require larger activation of the muscle. It has been found [Gritti and Schieppati, 1989, Schieppati et al., 1990] that besides fatigue, greater muscle contraction also as the effect of disinhibition among synergists. Therefore, the constant disinhibition due the larger activation overrides the effect of the periodic disinhibition due to fatigue.

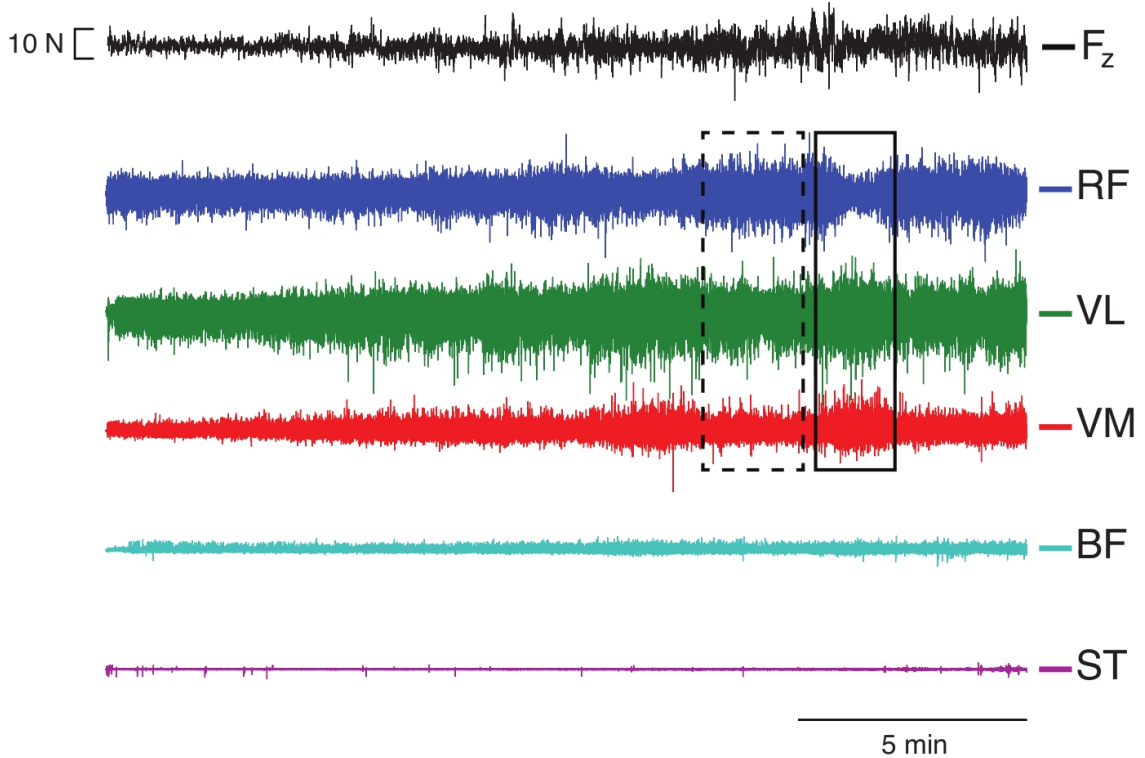


Figure 3.7: Representative EMG recordings at 10% MVC normal force. The subject maintained this force level for 20 minutes. The switching between RF and the vasti now begins around 10 to 15 minutes into the trial, but is less pronounced. Two sample coordination patterns are highlighted: *dashed rectangle*: RF activated, vasti deactivated, *solid rectangle*: RF deactivated, vasti activated

While this interpretation might be true, we argue that it is too complex and incorrectly assumes that alternation would still occur if not for the abolishment of inhibition between synergists by high muscle activation. Indeed, a larger desired output force requires greater activation. but based on the experimentally confirmed biomechanical model of isometric knee extension, we argue that the primary reason for the absence of alternation between the rectus femoris and the vasti muscles is the necessity for vasti activation. Given that rectus femoris occupies only 15% of the volume of the quadriceps [Akima et al., 2007], it appears obvious that the knee extension force generated at

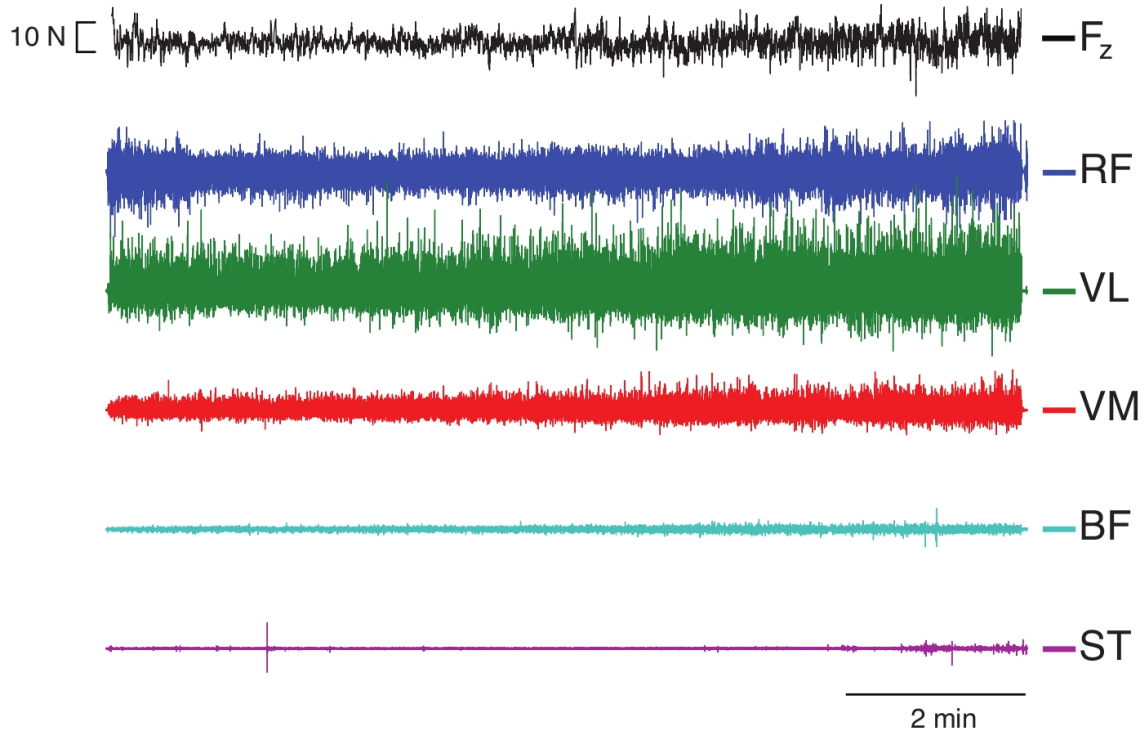


Figure 3.8: Representative EMG recordings at 15% MVC normal force. The subject maintained this force level for 10 minutes. Assuming that switching serves as a fatigue mitigation mechanism, we expect it to begin progressively earlier as the force level is increased. However, no switching occurs at this force level.

higher levels needs to originate somewhere and cannot solely come from rectus. However, since the rectus femoris is not necessary at the low force levels studied here (Figure 3.3), this muscle could still be deactivated on its own, while the activation of the vasti would be accordingly modulated to compensate. While modulation is indeed more pronounced in RF (Figure 3.7), we hypothesize that disinhibition due to high activation [Gritti and Schieppati, 1989, Schieppati et al., 1990] still plays a role in preventing the complete deactivation of rectus femoris at higher force levels.

The importance of biomechanics in the explanation of neural control strategies seen here emphasizes the need for a controller capable of a flexible response to the complex and interdependent requirements imposed by the mechanics of the task, the

redundancy of muscles and the time-variance due to muscles fatiguing at different rates, proportional to their individual activation. Indeed, there exists some indication for a great degree of flexibility in the activation of synergistic and thus, redundant, muscles. In [Schieppati et al., 1990], it was found that gastrocnemius and soleus are not necessarily synergists under all conditions: as the force requirements of the task increase, the inhibition between synergists disappears, thus altering the relative function of the two muscles, which become more synergistic. Furthermore, selective fatigue of biceps brachii has been shown to increase the activation of unfatigued synergists [Aymard et al., 1995], while the same has been shown in the quadriceps [Akima et al., 2002], potentially due to the disinhibition mechanism described above. In summary, these findings strongly argue against a rigid co-activation by muscles, as suggested by optimization [Prilutsky and Zatsiorsky, 2002] and the muscle synergy concept [Tresch and Jarc, 2009]. Instead, they indicate that i) the biomechanical requirements of the task, in particular the desired output force level, need to be taken into consideration in trying to determine a muscle coordination pattern, and ii) the time-varying nature imposed by fatigue on neuromuscular systems does not allow for a static solution without violation of task constraints. On the other hand, the ability to respond in a flexible way affords the nervous system a means to proactively leverage muscle redundancy, specifically a dynamic activation of muscles, to enhance the endurance of the system [Kouzaki and Shinohara, 2006].

Chapter 4

Temporal Analysis Reveals a Continuum, Rather Than a Separation, of Task Relevance

4.1 Abstract

The Uncontrolled Manifold and Principle of Minimal Intervention hypotheses propose that the observed differential variability across task relevant (i.e., task goals) vs. irrelevant (i.e., in the nullspace of those goals) variables is evidence of a separation of task variables for efficient neural control strategies. Support for this comes from spatial domain analyses of kinematic, kinetic and EMG variability. While proponents admit the possibility of *preferential* as opposed strictly "uncontrolled" variables, such distinction has not been quantified or considered when inferring control action. Here we extend analysis of task variability to the temporal domain and show that, even for steady-state 3-finger static grasp, the variability in "task-irrelevant" variables exhibits a structure indicative of corrective action at par with that for "task-relevant" variables. The spatial fluctuations of fingertip forces show, as expected, greater ranges of variability in "task-irrelevant" variables ($> 98\%$ associated with changes in total grasp force; vs. only $< 2\%$ in "task-relevant" changes associated with acceleration of the object). At some time scales, however, the temporal fluctuations of "task-irrelevant" variables can exhibit negative correlations clearly indicative of corrective control (Hurst

exponents < 0.5); and temporal fluctuations of "task relevant" variables can exhibit neutral and positive correlations clearly indicative of absence of corrective control (Hurst exponents ≥ 0.5). We conclude that we must revise our understanding of task relevance in the context of task variability, and that we must consider both spatial and temporal features of all task variables when inferring control action and understanding how the CNS handles task redundancy.

4.2 Introduction

In motor control research, redundancy has traditionally been viewed as its "central problem" [Bernstein, 1967]. Here, we understand the term "redundancy" as the availability of infinitely many different solutions to the performance of a motor task, as opposed to muscle redundancy, which refers to the multitude of muscle coordination patterns producing the same endpoint force. The "problem" in either type of redundancy is selecting a unique solution. In multifinger grasp, which has been studied extensively from a redundancy point of view [Park et al., 2010, Santello and Soechting, 2000, Latash and Zatsiorsky, 2009], a solution consists of finding a configuration of n fingertip force vectors, whose summation will create a net force and moment vector that leads to successful task performance. For instance, in static three-finger grasping of rigid objects studied here, one can squeeze an object harder, without translating or rotating it, or the pressing of a key can be performed as long as the normal force is sufficiently large and the tangential force components are inside the friction cone.

Mathematically, the redundant space of all applicable forces can be separated into the mutually orthogonal subspaces of force variability that has no effect on the task (e.g. squeezing the object in static grasp) and force variability that violates the task

constraints. We refer to the former subspace as the task-irrelevant space, or "null space". Faced with the above mentioned "problem" of selecting particular solutions, researchers have suggested that the nervous system only needs to identify and control the latter, task-relevant subspace, and can disregard the former subspace, thereby simplifying the control task. This idea of control is known as the "Uncontrolled Manifold" hypothesis [Scholz and Schner, 1999, Scholz et al., 2002, Latash et al., 2010] or "Principle of minimal intervention" [Jordan, 2003, Valero-Cuevas et al., 2009b]. Studies have considered as evidence for this strategy the observation that task-irrelevant dimensions exhibit relatively larger variability than task-relevant dimensions [Scholz and Schner, 1999]. Such stratified variability has been demonstrated in analyses of kinematic [Tseng and Scholz, 2005], kinetic [Santello and Soechting, 2000] and EMG variability [Valero-Cuevas et al., 2009b]. In this sense, large variability in a task dimension reflects the absence of control of this dimension during successful task performance. On the other hand, even a task-relevant dimension will exhibit some amount of variability. Therefore, the magnitude of variability is not necessarily a good predictor of task-relevance and in fact, proponents of the UCM hypothesis admit the possibility of *preferential* as opposed to a separation into strictly controlled and uncontrolled variables [Latash et al., 2010]. Despite this admission, a specific quantification that would allow us to predict task-relevance based on variability is currently missing.

However, little attention has so far been directed at the temporal structure of variability in the task null space. Being considered uncontrolled, the implicit assumption is that task-irrelevant variability exhibits the properties of either a white noise process, consisting of uncorrelated samples, or Brownian motion, formed by the integration of uncorrelated samples [Kantz and Schreiber, 2004]. Conversely, a controlled process, continuously or intermittently controlled [Collins and De Luca, 1994, Milton et al., 2009], will exhibit correlations between time samples. Both linear

and nonlinear time series analysis have been commonly employed to reveal temporal correlation structure indicative of control strategies, primarily in postural control research [Jeka et al., 2004, Collins and De Luca, 1994]. For instance, in a seminal paper by Collins and de Luca [Collins and De Luca, 1994] the authors demonstrated a complex correlation structure in the center-of-pressure time series recorded during quiet stance, a highly redundant task.

Here, we test the hypothesis that a time-series, or temporal, analysis of forces in the "task-irrelevant" subspace of static tripod grasp reveals more than just an uncorrelated process with relatively large variance. We selected the task of static tripod grasp, because it is one of the most common but simple motor tasks. Yet at the same time, it allows for multiple solutions in terms of fingertip force vector configurations, since the object can be squeezed harder or the intersection point of the three force vectors can move, without imparting a moment or acceleration on the object [Yoshikawa and Nagai, 1991, Flanagan et al., 1999]. Thus, static tripod grasp has an intuitive associated task null space. To reveal temporal correlation and thus structure indicative of control, we apply Detrended Fluctuation Analysis (DFA) [Kantelhardt et al., 2001] to the time series of mechanically task-irrelevant variables to reveal long-range correlations indicative of corrective feedback control of these variables. Such temporal structure of task-irrelevant variability challenges the thinking that task-irrelevant variables are not controlled. Instead, these results suggest that task-relevance needs to be understood more broadly than just mechanically and is incommensurate with a simple separation into task-relevant and task-irrelevant variables. Rather, task variables need to be ranked according to this extended understanding of relevance. We speculate that the control of mechanically irrelevant variables can help to improve task performance.

4.3 Methods

4.3.1 Data collection

We asked 12 young subjects (ages 20-36, 6 male, 9 right-handed) to perform a static tripod grasp of an instrumented object designed and built in our lab (Figure 4.1). While performing the grasp, the thumb, index and middle finger were in contact with three ATI Nano17 6-axis force transducers (Apex, NC, USA) locked in a configuration comfortable for each subject. The angle between index and middle finger was approximately 30°, while the angles formed with the thumb by each finger were approximately 165°. Each force transducer was coated with a teflon surface to reduce reliance on friction by the subjects to achieve a stable grasp. The force transducers were connected to a 16-bit National Instruments 6225 M-series data acquisition card (National Instruments, Austin, TX, USA). Attached to the object were three markers for motion capture, forming an equilateral triangle, whose plane was parallel to the grasp plane of the three fingertips. 7 motion capture cameras (Vicon, Oxford, UK) allowed us to measure the object's position and orientation to quantify how well the subject met the task goal of maintaining a simple static grasp.

Subjects performed all trials with their dominant hand [Oldfield, 1971]. Subjects were seated in a chair, with the grasping hand resting on the chair's armrest (Figure 4.1). Moreover, we asked subjects to immobilize the wrist of their grasping hand by gripping the wrist with their non-dominant hand to minimize wrist rotation and hand translation, since we were interested in the coordination of fingertip forces for steady-state static grasp.

Subjects performed steady-state static grasps under three weight and two visual conditions, for a total of 6 conditions. Three different weights, 50 g, 100 g and 200 g, were screwed to the object from below (Figure 4.1) to add to the 50 g weight of the object

itself. The torques induced by the lowered center of mass helped to minimize rotations of the object, except those about the vertical axis. In the visual feedback trials, we presented a crosshair on the screen, whose height represented total grasp force as the sum of the three normal forces (Figure 4.1). We updated the position of the crosshairs at a rate of 50 Hz. Subjects had to control normal forces such that the crosshairs would align with a horizontal target line, in addition to minimizing object translations and rotations. The visual feedback screen was placed approximately 1.5 m away from the subject, ensuring that the subject would be able to track the horizontal line.

Subjects performed static grasp trials of 68 s duration three times for each weight, and for each visual condition, for a total of 18 trials per subject (3x3x2). Between trials, subjects had one minute of rest to avoid fatigue. The different weights were attached in random order, while the nine trials involving visual feedback were always performed after the ones without, because the target line height was based on the self-selected average sum of normal forces subjects applied to the force sensors for a given weight in the non-visual condition.

4.3.2 Data preprocessing

The three-dimensional force data recorded by each transducer were sampled at 400 Hz, while the marker positions were sampled at 200 Hz (both force and motion data collection were triggered synchronously). We removed the first seven and last 1 second(s) from each trial's time series to avoid transients. Next, we downsampled both the force and motion capture time series to 100 Hz. Due to the type of data analysis we performed, we did not filter the data to avoid creating artifactual correlations (see below and Results section).

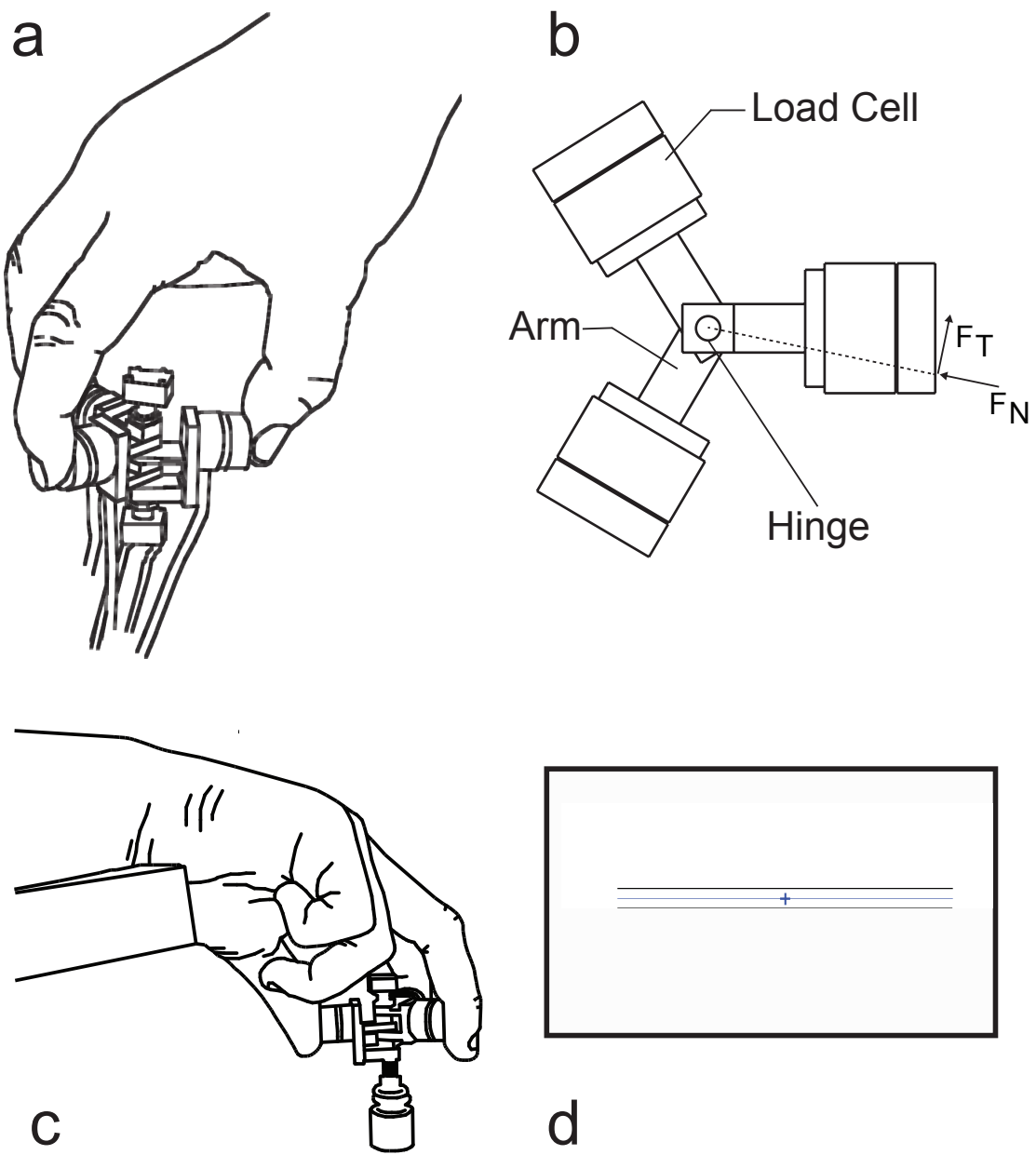


Figure 4.1: a.-b. The apparatus designed and built in our lab. It consists of three arms rotating about a common hinge. Each arm is instrumented with a 6-axis force transducer, which form the contact surfaces for tripod grasp. c. The static grasp posture during trials. In addition, subjects were asked to hold their wrist with their non-dominant hand. d. The visual feedback on the sum of normal forces. Subjects had to align the crosshair with the target line.

4.3.3 Data analysis

To analyze the spatial coordinated action among the three fingertip forces, we first performed principal component analysis (PCA) on the time series of each sensors normal forces, for each trial. PCA is a common linear method for the estimation of spatial correlation structures in data [Clewley et al., 2008]. Specifically, we computed the three principal components of the 3x3 normal force covariance matrix (q-PCA). PCA has been commonly used to estimate effective degrees of freedom in motor systems; and in the context of the Uncontrolled Manifold (UCM) hypothesis to compute task-relevant and -irrelevant latent variables, which are represented by the orthogonal PC vectors. As is commonly done [Kutch and Valero-Cuevas, 2012], we then projected the 3-dimensional normal forces (one normal force per force sensor) time series data onto the three principal components. We also tested doing this same analysis on the full 9-dimensional data sets (3 force components per force sensor) but the results are unchanged from when using only the normal force component from each sensor). As described in the Results, the first, second, and third principal components can be called the grasp, compensation and hinge modes of this task (Figure 4.3).

Next, we applied Detrended Fluctuation Analysis (DFA) to each projected time series [Kantelhardt et al., 2001]. DFA is a tool for the detection of long-range temporal correlations in non-stationary time series, and has the advantage (in particular, over the classical time-lagged autocorrelation function) that it can distinguish unwanted trends of arbitrary order, which can give rise to spurious non-zero correlations, from actual long-range correlations in non-stationary data. DFA has been used extensively for the analysis of behavioral and physiological data [Hausdorff et al., 1996a, Peng et al., 1998,

Penzel et al., 2003]. Mathematically, DFA quantifies the power-law increase of the root-mean square deviations from a trend in the time series fluctuations, once segments of increasing length n have been subtracted from it to remove trends of that length:

$$F(n) = \left[\frac{1}{L} \sum_{j=1}^L (X_j - a_j - b)^2 \right]^{\frac{1}{2}}$$

Where $X_j a_j b$ represents the residuals of the linear fit $a_j b$ to the time series segment X_j of length n . For a given segment length n , there are L overlapping segments in the process. The complete expression for $F(n)$ represents the average root mean squared deviation at segment length, or time scale, n . In a non-stationary process, this time scale is related to $F(n)$ by the relationship

$$F(n) \propto n^\alpha$$

This power-law increase in root-mean square deviation is mathematically linked to long-range temporal correlations in the data: negative correlations will, over time, lead to a smaller rate of increase than positive correlations. In particular, scaling exponents can be fit to the logarithmic plots of the time scales n vs. the $F(n)$: on the one hand, a scaling exponent $\alpha > 0.5$ indicates *persistence*, meaning that the time series increments at a particular time scale n are positively correlated with the time series increment at time scale $\Delta = 0$. In other words, a positive (negative) increment at time scale $\Delta = t$ is associated with a positive (negative) increment at time scale $\Delta = 0$. On the other hand, a scaling exponent $\alpha < 0.5$ indicates *anti-persistence*, i.e. positive (negative) increments are followed by negative (positive) increments. If $\alpha = 0.5$, there is a lack of correlation between the increments at that particular time scale Δ and the time series is equivalent to a purely diffusive and random (i.e., Brownian) walk. Because long-range

negative correlations reflect corrective actions that prevent dissipation, they are interpreted as evidence for the workings of corrective and stabilizing (i.e., negative feedback) control, while positive correlations can be interpreted as evidence of feedforward control [Collins and De Luca, 1994].

DFA reveals empirically the inherent time scales for which different temporal correlations exist in the data. We found that the steady-state static grasp data naturally contained three inherent time scales: 1-50 ms, 200-500 ms, and 3500-7000 ms (Figure ??). These time scales are found based on regions of linearity in the logarithmic plots of n vs. $F(n)$, and thus regions of actual power-law scaling.

We noticed that some trials exhibited a relaxation of the total grasp force, likely an adaptation to reduce fingertip forces when no perturbations are expected and to mitigate fatigue. Therefore, to test for reliability of our results, we repeated the DFA on the first and second half of each trial to test if normal force coordination patterns are time-varying and sensitive to the location in the trial, and in the level of total grasp force.

Note that here we do not employ DFA to determine self-similarity or fractional dimensionality in the data, as has been done in some studies [Hausdorff et al., 1996b, Hausdorff et al., 1996a]. In those studies, the linearity in the logarithmic plots needs to extend over at least one order of magnitude to count as strong evidence of fractionality [Kantz and Schreiber, 2004]. In our case the requirements for the linearity of the logarithmic plots are not as rigid because the quantification of long-range correlations applies to data where the linearity extends over shorter ranges of time scales.

4.3.4 Identification and modeling of the mechanical requirements of the task and its nullspace

Each fingertip applies a three-dimensional force $\tilde{\mathbf{f}}$ to the object. Computing the cross product of the moment arm, i.e. the vector between the point of force application and

the object's center of mass, with the fingertip force vector yields the moment applied to the object. The total 6-dimensional force and moment applied to the object can be computed with the following mapping \mathbf{W} :

$$\begin{bmatrix} \sum \mathbf{f} \\ \sum \mathbf{m} \end{bmatrix}_{6 \times 1} = \begin{bmatrix} \mathbf{I}_{3 \times 3} & \mathbf{I}_{3 \times 3} & \mathbf{I}_{3 \times 3} \\ \mathbf{M}_{\text{th}} & \mathbf{M}_{\text{ind}} & \mathbf{M}_{\text{mid}} \end{bmatrix}_{6 \times 9} \begin{bmatrix} \tilde{\mathbf{f}}_{\text{th}} \\ \tilde{\mathbf{f}}_{\text{ind}} \\ \tilde{\mathbf{f}}_{\text{mid}} \end{bmatrix}_{9 \times 1} \\ = \mathbf{W}\tilde{\mathbf{f}}$$

where $\mathbf{I}_{3 \times 3}$ is the unit matrix and $\mathbf{M}_{\{\text{th}, \text{ind}, \text{mid}\}}$ is the skew-symmetric matrix representing the cross-product between the moment arm of the finger and its force vector $\mathbf{f}_{\{\text{th}, \text{ind}, \text{mid}\}}$. Since \mathbf{W} is a mapping from 9-dimensional to 6-dimensional space, the associated null space, i.e. the space of vectors for which $\tilde{\mathbf{0}} = \mathbf{W}\tilde{\mathbf{x}}$ has 3 dimensions. Any vector $\tilde{\mathbf{x}}$ in this space represents a solution to the static grasp requirement $\begin{bmatrix} \sum \mathbf{f} \\ \sum \mathbf{m} \end{bmatrix} = \begin{bmatrix} \tilde{\mathbf{0}} \\ \tilde{\mathbf{0}} \end{bmatrix}$, i.e. that both the sum of forces and the sum of moments should be zero.

However, this is a necessary requirement only. Additionally, we require that at the finger tip contact points the tangential forces are upper-bounded through the relationship $f_{\text{tangential}} \leq \mu f_{\text{normal}}$, i.e. the tangential force cannot exceed the normal force, multiplied with the friction coefficient μ , which we have set to 0.04, the friction coefficient of teflon. This represents a lower bound on the coefficient of friction, since this coefficient is certainly greater when fingertip and teflon surface interact - the grasp under experimental conditions is actually far less constrained. The sum of tangential forces applied needs to oppose the force applied to the object by gravity. The simulated object had a weight of 100 g, hence the sum of tangential forces had to equal 0.981 N, which in turn determined the sign (positive, i.e. into the object) and the minimum magnitude of the normal forces.

We sampled vectors $\tilde{\mathbf{f}}_{\text{null}}$ from the null space of the above linear matrix by multiplying the three null space basis vectors $\tilde{\mathbf{n}}_i$ with random values a, b, c , drawn from a

standard Brownian random walk: $\tilde{\mathbf{f}}_{t_{\text{null}}} = a \cdot \tilde{\mathbf{n}}_1 + b \cdot \tilde{\mathbf{n}}_2 + c \cdot \tilde{\mathbf{n}}_3$. We then added the null space vector $\tilde{\mathbf{f}}_{\text{null}}$ to the minimum sum-of-squared-forces solution $\tilde{\mathbf{f}}_{\min \text{sq}}$ of force vectors that met all the above described static grasp constraints: $\tilde{\mathbf{f}}_t = \tilde{\mathbf{f}}_{\min \text{sq}} + \tilde{\mathbf{f}}_{t_{\text{null}}}$, using MATLAB's (Natick, MA) `quadprog()` function to determine the actual solution with minimum Euclidean distance to $\tilde{\mathbf{f}}_{\min \text{sq}} + \tilde{\mathbf{f}}_{t_{\text{null}}}$.

Constraint	Magnitude	Interpretation
$\sum \mathbf{F}$	$[0, 0, mg]^T$	Sum of forces equal and opposite to gravity force, i.e. no net force
$\sum \mathbf{M}$	$\mathbf{0}$	Sum of moments equals zero, i.e. no net moment
F_{i_T}	$\leq \mu \cdot F_{i_N}$	Tangential force at the i -th finger cannot exceed normal force

Table 4.1: List of relevant constraints in static grasp

4.4 Results

4.4.1 Principal component analysis of simulated normal forces

The three individual simulated normal forces are shown on the right in Figure 4.4. Note that despite their apparent variability, each sample represents a valid solution to the constrained problem of steady-state static grasp. Furthermore, on the left in Figure 4.4 we show the simulated normal forces plotted against each other, and it becomes obvious that the valid solutions populate a plane. Applying Principal Component Analysis (PCA) to the simulated data to determine the two basis vectors of that plane, we find that it is spanned by the vectors $[0.8, 0.4, 0.4]^T$ and $[0.0, -0.7, 0.7]^T$, explaining together 100% of data variance. Hence, if the variability of normal fingertip forces exhibits this structure in steady-state static tripod grasp, such variability will not give rise to accelerations or rotations of the grasped object and exists entirely in the null space of the task, while actual acceleration or rotation of the object is associated with normal force variability perpendicular to this plane, along the vector $[0.6, -0.5, -0.5]$.

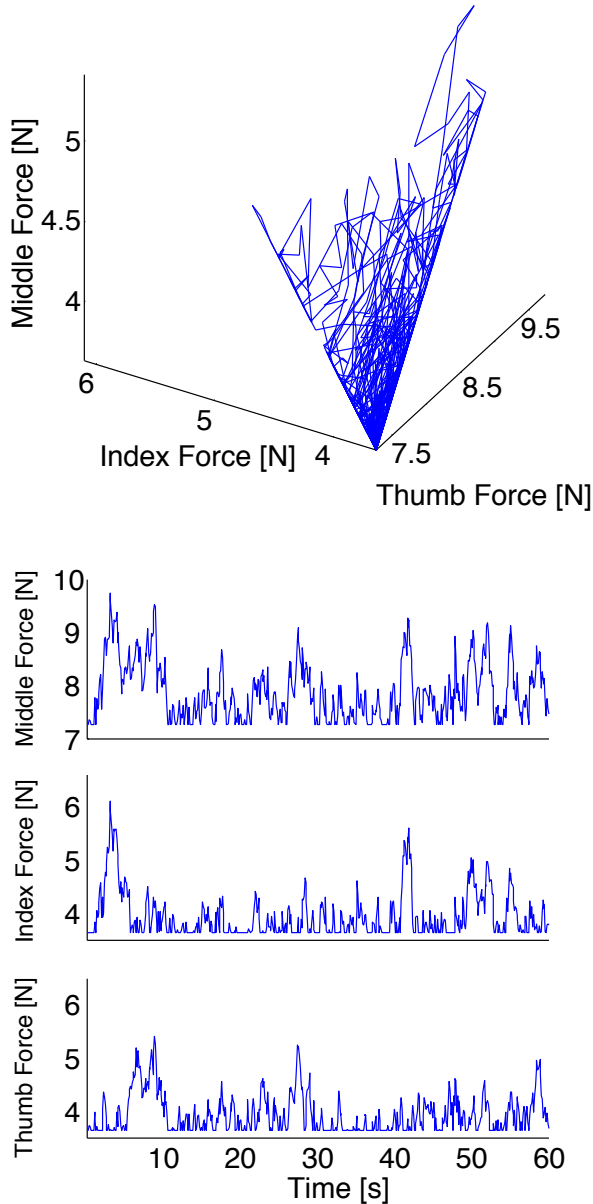


Figure 4.2: Representative plot of the simulated thumb, index and middle finger normal forces. *Top:* The three simulated normal forces plotted against each other. Note that the force fluctuations come to lie on a plane, whose orientation we compute using PCA. *Bottom:* The three simulated normal forces during a trial plotted individually. Note that the floor effect results from the minimum normal force constraint.

We refer to these three principal components found in the simulations as: (i) the grasp mode, along $[0.8, 0.4, 0.4]^T$, as it reflects synchronous increases and decreases in

the three normal forces, which are also known as grasp forces, (ii) the compensation mode, along $[0.0, -0.71, 0.71]^T$, reflecting the out-of-phase opposition, or compensation, of thumb normal force by either the index or middle finger normal force, and (iii) the hinge mode, along $[0.6, -0.5, -0.5]$, reflecting an increase (decrease) in thumb normal force accompanied by a simultaneous decrease (increase) in the index and middle finger normal forces, which would typically occur if the object was accelerated by the thumb or rotated, thus violating the mechanical task requirements of static grasp. These three normal force modes are illustrated in Figure 4.3.

Mechanically, the dynamics associated with the compensation mode reflect movement of the intersection point of the three force vectors, as shown in [Yoshikawa and Nagai, 1991, Flanagan et al., 1999]. As long as the force vectors, extended from their respective application points intersect in one common point inside the object, there will be no moment exerted on the object. This intersection point can move inside an area spanned by the friction cones without violating the task requirements. Its motion indicates that the tangential force components parallel to the grasp plane are changing, as the normal forces, in turn, need to be compensated in synchrony, to avoid both slippage of fingers and accelerations of the object.

4.4.2 Principal component analysis of experimental forces

As expected, subjects met the task requirements well but not perfectly: movements of the object markers were well within 5 mm in all directions. Object motion was significantly affected by the presence of visual feedback, but not weight. Importantly, the small but measurable object accelerations are not caused by force dynamics inside the two-dimensional manifold spanned by the grasp and compensation modes found in the simulations (above), but are due to dynamics along the hinge mode and the tangential force components.

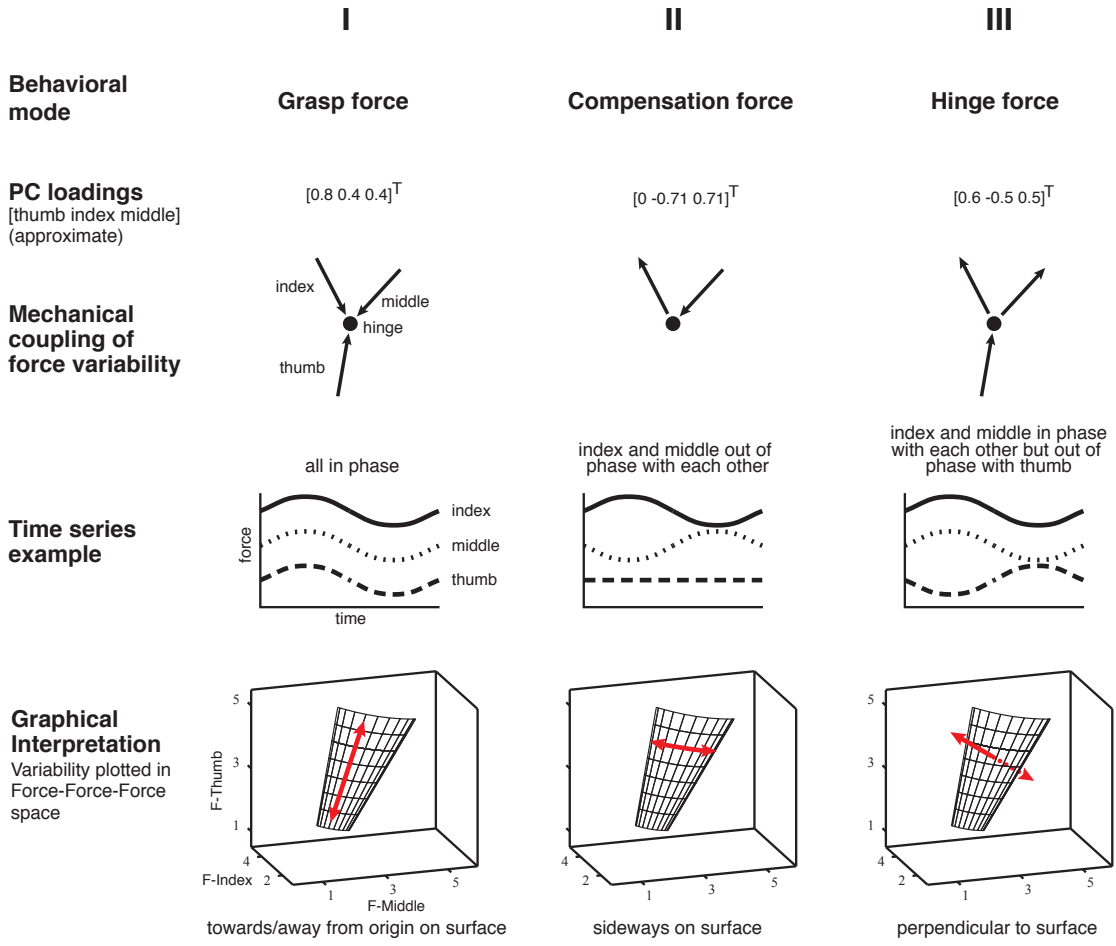


Figure 4.3: Illustration of the three normal force modes associated with the principal components computed from the data and the simulations, across all subjects and conditions.

We applied PCA to the time series of experimental normal forces (Figure 4.4 for a representative figure), and found that across all trials and subjects, and therefore regardless of task condition, normal force variability consistently exhibited a structure described by the three principal components found in the simulation: $[0.8, 0.4, 0.4]^T$, $[0.0, -0.7, 0.7]^T$ and $[0.6, -0.5, -0.5]$ (Figure 4.6). Note that the slight deviations from these directions are unlikely to reflect violations of the task requirements, since subjects performed the task well (above), but could be due to one of the following: (i) The grasp

plane formed by the three fingertips is not perfectly parallel to ground. If you consider Figure 4.1, this seems plausible. Subjects performed this task in a posture that was comfortable for them. (ii) The individual grasp mode vector components reflect the degree of opposition between thumb normal force and the other two normal forces and are therefore influenced by the apparatus arm angles and the finger tip contact points. In the experiments, we adjusted the arm angles for subjects' individual comfort and subjects decided where to place their fingertips.

As expected from a spatial variability standpoint, the grasp mode explains approximately 90% of the normal force variance, while the compensation mode approximately 5-10% and the hinge mode 1-3% (Figure 4.7). In the trials with visual feedback, grasp and compensation modes contribute equally to the normal force variance, slightly less than 50% each (Figure 4.7) and again 1-3% by the hinge mode, which means that the null space manifold is evenly populated by the normal force dynamics in these trials. The low percentage of variance explained by the hinge mode in both cases shows that subjects satisfied the task requirements of not accelerating or rotating the object.

Projecting the fingertip force time series data without visual feedback onto the grasp mode shows a very slow monotonic downward trend (Figure 4.8 for a representative trial). This slow trend is interpreted by PCA as a contributor to large spatial variability explained by this mode and is caused by the three fingers reducing their normal forces simultaneously. In trials *with* visual feedback, the grasp force mode does not exhibit such a trend (Figure 4.5 for a representative trial), which is not surprising, since keeping the sum of normal forces constant becomes a task requirement, which the subjects did meet. Thus, visual feedback has the effect of reducing the grasp mode's contribution to the overall force variability due to the absence of the above mentioned slow trend. In turn, the compensation mode now contributes a larger proportion of the overall variability (Figure 4.7). The compensation mode also exhibits a slow non-monotonic

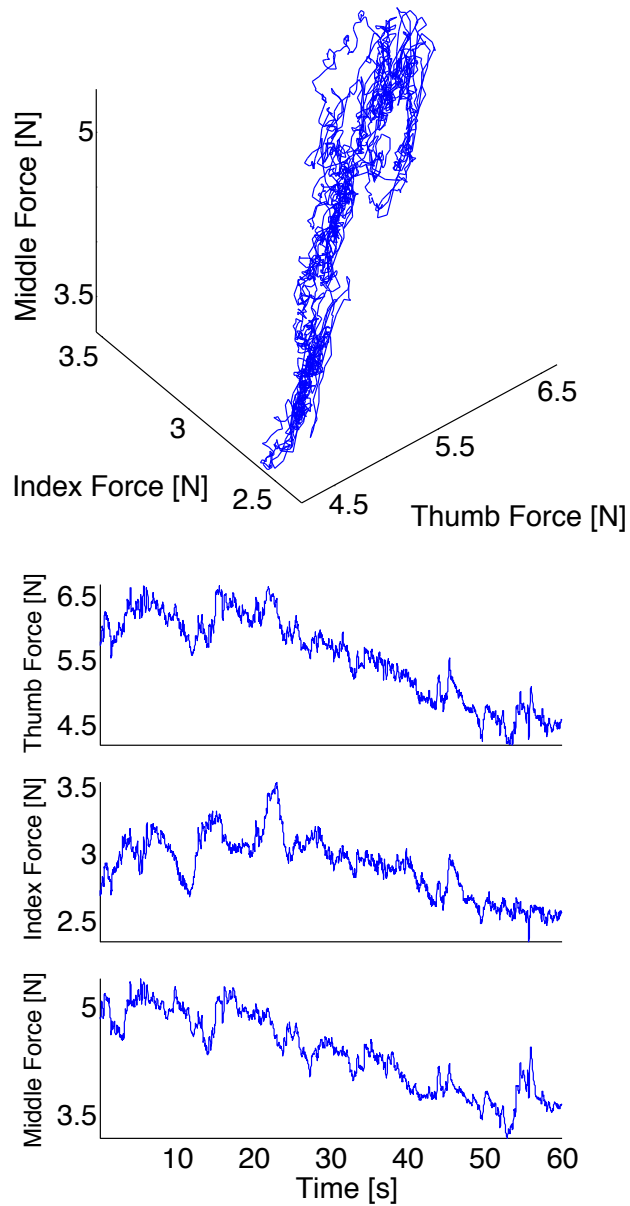


Figure 4.4: Representative plot of experimental thumb, index and middle finger normal forces recorded during one trial with a 200 g weight. *Top:* The three normal forces plotted against each other. Note that the force fluctuations come to lie on a plane, whose orientation we computed using PCA. *Bottom:* The three normal forces during a trial plotted individually. Note the common downward trend across the three fingers.

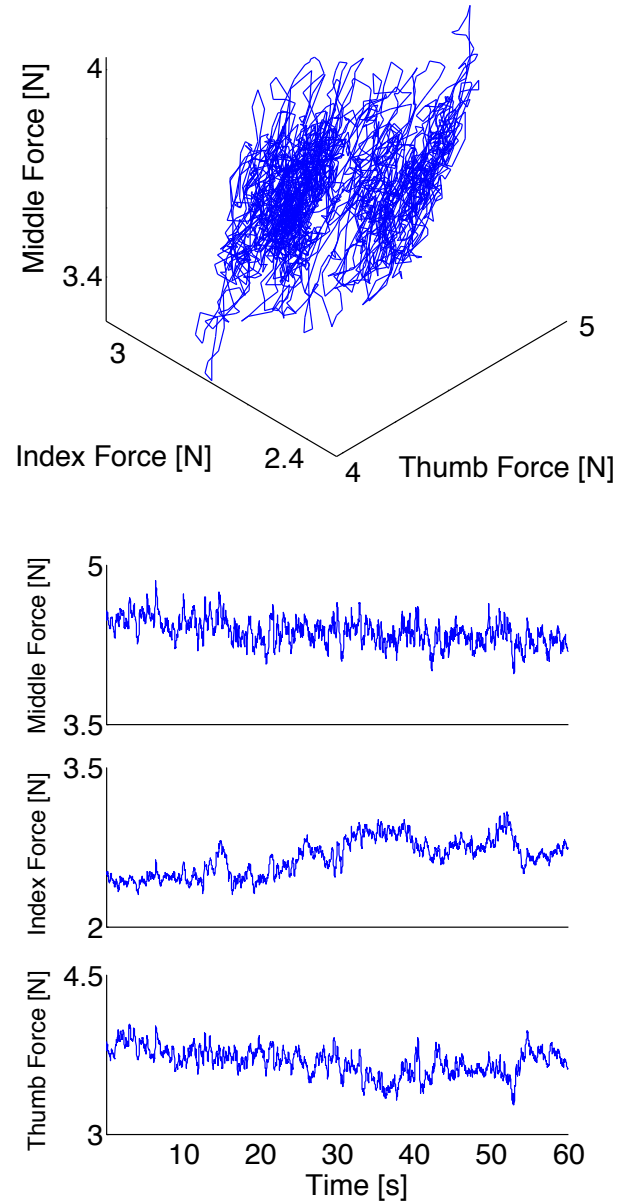


Figure 4.5: Representative plot of experimental thumb, index and middle finger normal forces recorded during one trial with a 200 g weight, when visual feedback was presented. *Top:* The three normal forces plotted against each other. Note that the force fluctuations come to lie on a plane, as in tasks without visual feedback, but the dynamics populate the plane differently. *Bottom:* The three normal forces during a trial plotted individually. Note the absence of a downward trend across the three fingers, due to the enforcement of the sum of normal forces constraint.

modulation both increasing and decreasing over time (Figure 4.8). This indicates that index and middle finger normal forces are slowly and continuously modulated, out of phase, during static grasp, unlike a white noise process. Lastly and not surprisingly, the hinge mode shows almost no variation over time.

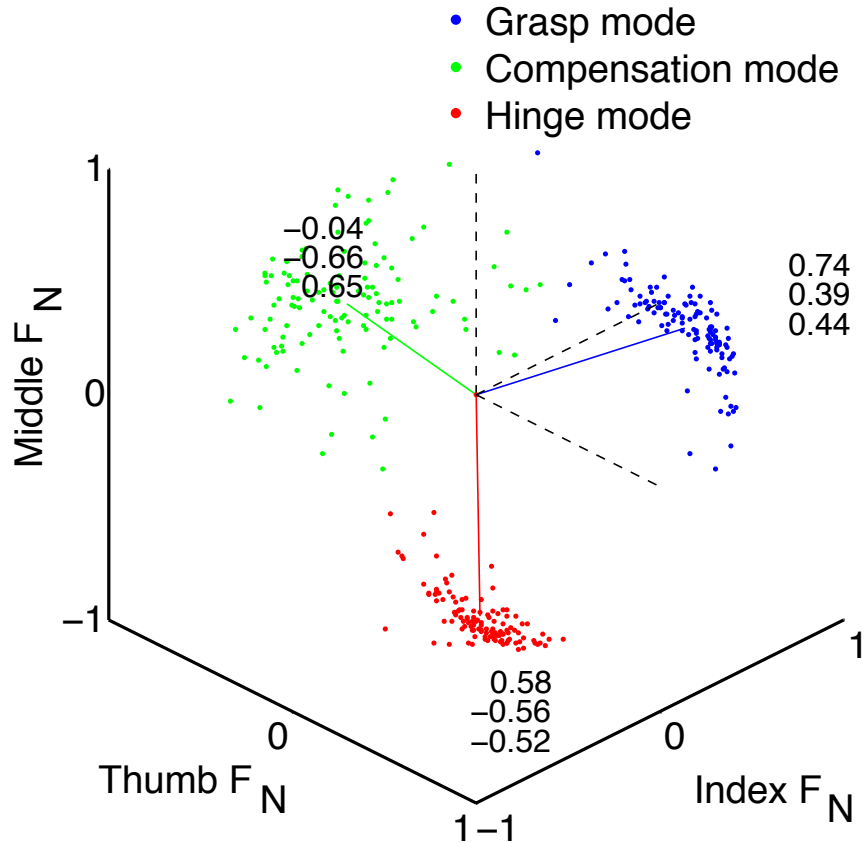


Figure 4.6: Distribution of data principal components (dots). The colored lines show the mean grasp, compensation and hinge mode directions.

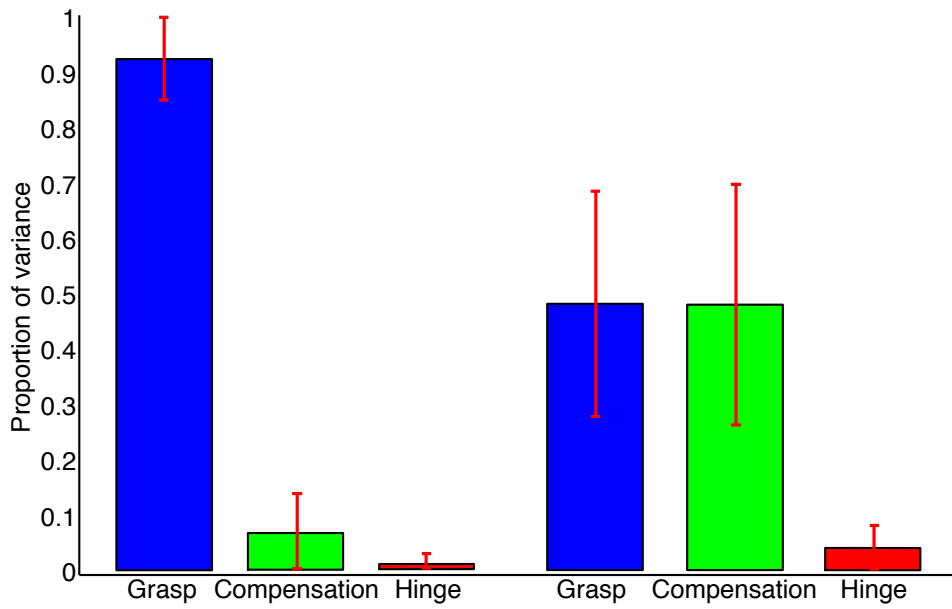


Figure 4.7: Mean proportions of variance explained by the grasp, compensation and hinge mode, respectively, in the simple trials with (*right*) and without (*left*) visual feedback. In trials without visual feedback, most variance occurs along the grasp mode, capturing the downward trend across all finger normal forces.

4.4.3 Detrended Fluctuation Analysis of time series projected onto principal components

DFA of the normal force time series projected onto the three principal components reveals long-range correlations indicative of both the presence and absence of time-delayed corrective control in all three modes. In the following, all reported changes in Hurst exponents (i.e., slopes of the log-log plots) are statistically significant at the $p < .01$ level, based on Kruskal-Wallis (across the three weight conditions) or Mann-Whitney tests (across the two visual feedback conditions).

Consider Figure 4.9, which shows the scaling exponents in the first and second halves of the trials, respectively. At short time scales (1-50 ms), the slopes associated with both the compensation and hinge mode time series are close to 0.5, indicating

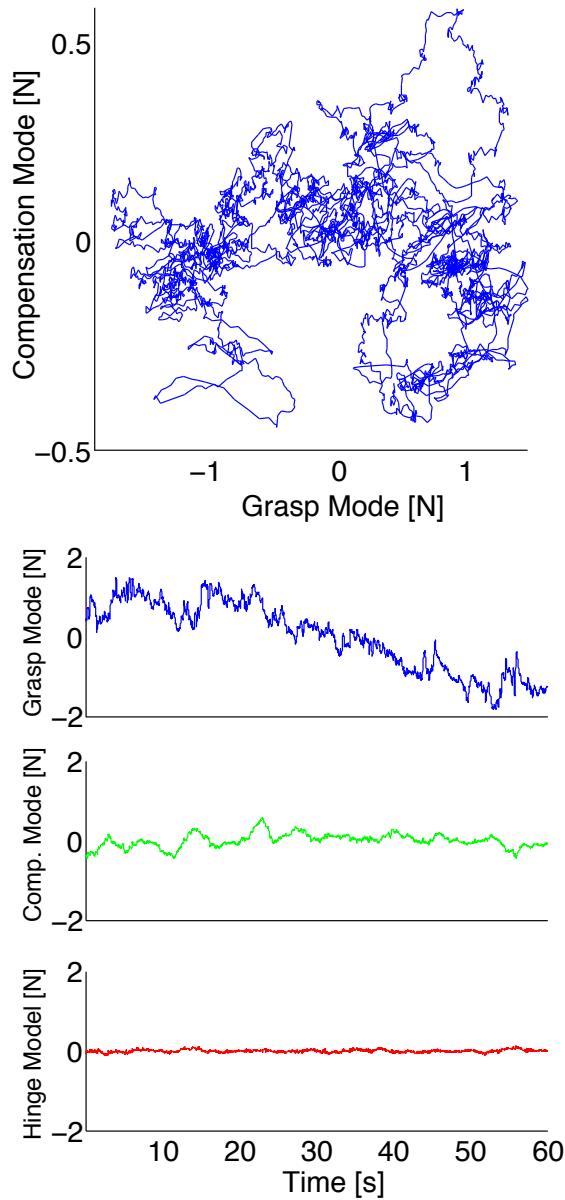


Figure 4.8: Representative plot of the above experimental normal forces projected onto the three principal components. *Top:* The force fluctuations on the plane spanned by the grasp and compensation modes. *Bottom:* The three principal component time series during a trial plotted individually. Note how the grasp mode captures the common downward trend, while the hinge mode has comparatively minimal variability.

lack of negative correlation between increments and thus absence of a corrective control

effort, while the grasp mode has a slope of 0.7, reflective of positive correlations in the time series.

At medium time scales (200-500 ms), the slope of the grasp mode decreases to 0.5, indicating lack of corrective control effort along this dimension, while the compensation mode now indicates the activity of a stabilizing or correcting effort, having decreased to a value 0.3, and the hinge mode shows a very distinct slowing down of RMS deviation scaling with exponent 0.1, indicating strong concentration around a mean level. Importantly, the 200-500 ms time delays include the shortest voluntary time scales of the sensorimotor system [Kawato, 1999].

The long time scale (3500-7000 ms) is not particularly different from the 200-500 ms time scale in terms of DFA slopes, except that the grasp mode now becomes corrective as well, with a slope having decreased to 0.3 from 0.5.

Its slope at this time scale is further reduced to 0.1 in trials with visual feedback, thus reflecting the lack of slow trends in the grasp mode, since the sum of normal forces has to be kept constant. The hinge mode is also affected by vision at long time scales, becoming slightly but significantly more corrective as it is changing from 0.13 to 0.1.

Increasing the weight has the effect that it increases the slope of the grasp mode at small time scales (1-50 ms) to 1.0, perhaps reflecting the increase in signal-dependent noise, which scales linearly with force and is observed in the 8-12 Hz frequency band of force measurements ([Jones et al., 2002], i.e. time scales of < 125 ms) and induces positive mechanical correlations across fingers due to reaction forces. Another effect of weight increase is a slight increase of the hinge mode slope with weight, possibly reflecting the increased difficulty of maintaining stable the more inert object and the increased need for corrective efforts.

Adding visual feedback also increases the slope of the grasp mode at short time scales (1-50 ms), which again might reflect the increased amount of signal-dependent

noise, since the grasp force level had to be kept constant and could not decrease, as in the trials without visual feedback.

Finally, the fact that the results are so similar between the first and the second halves of the trials indicates that the observed dynamics and the associated correlation structure depend neither on time nor the total grasp force (which can be interpreted as location in the force space; or in control terms the "state space" of the system). This in turn indicates a control strategy that is state-independent except potentially at the boundaries. While the increase in weight and the addition of visual feedback does seem to modulate the dynamics on the individual dimensions, it does not lead to a crossing of the 0.5 line and therefore not to a fundamental change in the control strategy.

Importantly, we see that each mode, both mechanically task-relevant and -irrelevant, exhibits features of control as well as the absence of control, at some time scale.

4.5 Discussion

While we cannot claim at this point that the neural controller actively controls the specific dimensions of normal force coordination determined through PCA, our simulation results nevertheless clearly indicate that the first two principal components, the grasp and compensation modes, span the null space of force dynamics associated with static grasp: variation of force inside this planar manifold does not violate the constraints of static grasp (i.e. zero net force and moment). Given however that noise is an inevitable reality in neuromuscular systems, successful task completion therefore naturally leads to the population of the null space manifold, while variability orthogonal to it will be minimal, but not necessarily zero.

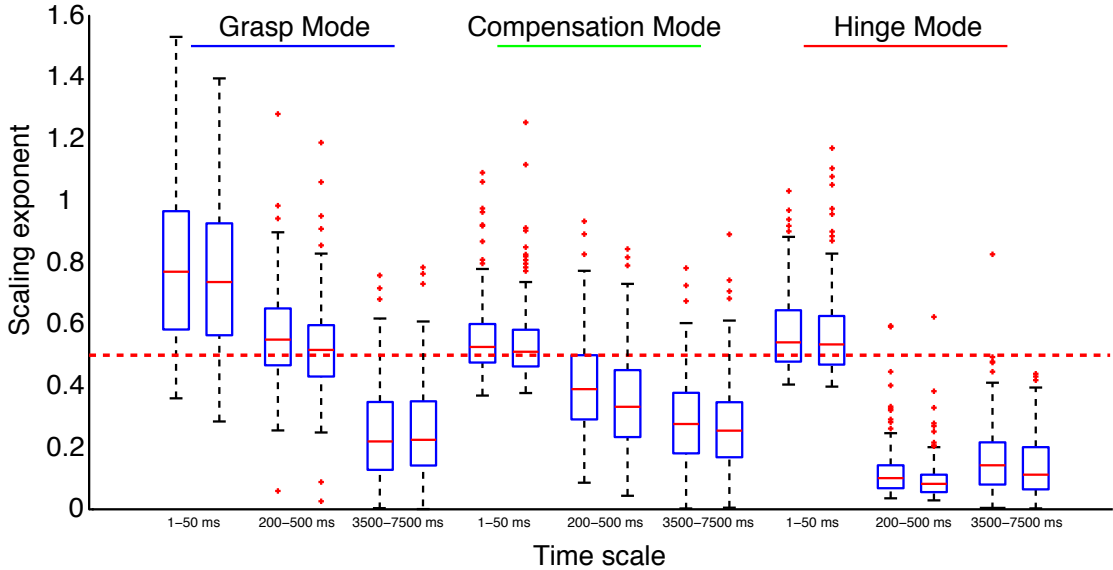


Figure 4.9: The distribution of DFA scaling exponents of the normal forces projected onto the three force modes - during the first (left box plots) and the second half (right box plots) of the trials. Note the large exponent of the grasp mode at short time scales, while the other two modes exhibit a lack of correlation at this time scale. At larger time scales, the hinge mode exponent is very close to 0, reflecting the fact that subjects hardly accelerated the object. The grasp mode, on the other hand, exhibits no correlation at the medium time scale. Importantly, there is no significant difference between scaling exponent between the first and the second half of the trials.

These results regarding the distribution of variability in space seem to agree with the Uncontrolled Manifold (UCM) Hypothesis and the Minimal Intervention Principle [Scholz and Schnier, 1999, Jordan, 2003]: that the nervous system chooses to control only the task-relevant dimensions of a task and keeping their variance small, since they interfere with the task, while allowing larger variability in directions or variables that do not affect task performance. This control strategy is reflected in the distribution of variability along different dimensions of the task. Since static tripod grasp has an associated multi-dimensional task-irrelevant manifold, on which fluctuations do not require corrective intervention, i.e. the grasp and compensation modes found here through PCA,

task-irrelevant variables not affecting the mechanical requirements of the task certainly exist.

However, the *temporal* DFA applied to task-irrelevant variables and the task-relevant hinge mode gives a much more complex picture, in which variables of both types appear to be controlled at uncontrolled, depending on the time scale considered. It is important to note that the UCM hypothesis would predict a lack of any correlation in task-irrelevant variables. On the one hand, grasp mode variability exhibits a lack of long-range correlation at medium time scales (300-1000 ms) and an absence of corrective dynamics at short time scales (1-50 ms), while the compensation mode is entirely random at short time scales (1-50 ms): being mechanically task-irrelevant, these results seems to support lack of intervention by the neural controller. Qualitatively, the grasp mode exhibits a slow downward trend in trials without visual feedback, which might be a consequence of not controlling forces at medium time scales, while the positive correlations at short time scales can be shown to be a result of the interplay between signal-dependent noise [Jones et al., 2002] and reaction forces, i.e. of purely mechanical origin.

On the other hand, the grasp mode exhibits negative correlations indicative of corrective control at large time scales and contrary to the prediction of the UCM hypothesis. These negative correlations cannot solely be attributed to control intervention when there is a risk of dropping the object due to a reduction in grasp mode force. Instead, the non-zero scaling below 0.5 observed in our experimental data, both in the first and second half of the trials (Figure 4.9), suggests control intervention independent of state-space location. Next, the task-irrelevant compensation mode exhibits negative correlations at medium and large time scales, again contrary to the UCM hypothesis prediction. Lastly, DFA exposes an absence of correlation at very short time scales in the task-relevant hinge mode, indicating an absence of control. Given the existence of loop

delays in neuromuscular systems, the absence of correlations along the hinge mode at short time scales is not surprising.

These results expose a fundamental limitation of the UCM hypothesis and the Minimum Intervention Principle: their focus on spatial aspects of motor variability and disregard for temporal aspects. "Spatial aspects" refers to latent variables, or instantaneous correlation modes of elemental variables in motor tasks, which can be revealed through the use of PCA, among other methods. "Temporal aspects" refers to the correlations over time along such latent correlation modes. In other words, due to physiological limitations, even highly task-relevant variables can be uncontrolled temporarily.

We conclude that controlled and uncontrolled dynamics vary as functions not only of spatial, but also temporal constraints of the task due to physiological and other limitations, and argue that the UCM hypothesis and the Minimum Intervention Principle need to be extended by considerations of temporal aspects of motor control, as revealed through our DFA applied to all task variables. In their current form, these theories of motor control are incommensurate with our results in that these theories assume a simple separation of task variables into relevant and irrelevant ones, entirely based on mechanical considerations. The results presented here instead suggest a continuum of task-relevance based on aspects beyond those of pure mechanics.

What aspects are potentially relevant to motor tasks, other than mechanics? One possible explanation for the observed negative correlations along the grasp and compensation modes could be that traversing this manifold is an active process, through which the CNS actually takes advantage of redundancy. Specifically, controlled dynamics along the compensation mode correspond to the regulation of the index and middle finger contributions to the opposition of thumb normal force. We speculate that the CNS is actively trying to shift the demands between the two fingers over time, which

in turn might mitigate effects of fatigue at the muscle level. By gradually varying end-point forces, the CNS achieves a change in the underlying muscle coordination pattern, which in turn will change the rates of fatiguing of individual muscles, thus allowing for improved use of available resources. Furthermore, the slow downward trend along the grasp mode direction of normal forces would fall in line with this hypothesis: a general reduction of forces generated by the muscles leads to a reduction in the fatigue rate. This intriguing hypothesis deserves further investigation.

Chapter 5

An Involuntary Stereotypical Grasp Strategy Pervades Voluntary Dynamic Multifinger Manipulation

5.1 Abstract

We used a novel apparatus with three hinged finger pads to characterize collaborative multifinger interactions during dynamic manipulation requiring individuated control of fingertip motions and forces. Subjects placed the thumb, index and middle fingertips on each hinged finger pad, and held it with constant total grasp force while voluntarily oscillating the thumbs pad. This task combines the need to (i) hold the object against gravity while (ii) dynamically reconfiguring the grasp. Fingertip force variability in this combined motion and force task exhibited strong synchrony among normal (i.e., grasp) forces. Mechanical analysis and simulation show that such synchronous variability is unnecessary and cannot be explained solely by signal dependent noise. Surprisingly, such variability also pervaded Control Tasks requiring different individuated fingertip motions and forces - but not tasks without finger individuation such as static grasp. These results critically extend notions of finger force variability by exposing and quantifying a pervasive challenge to dynamic multifinger manipulation: the need for the neural controller to carefully and continuously overlay individuated finger actions over mechanically unnecessary synchronous interactions. This is compatible with - and may

explain - the phenomenology of strong coupling of hand muscles when this delicate balance is not yet developed, as in early childhood, or when disrupted, as in brain injury. We conclude that the control of healthy multifinger dynamic manipulation has barely enough neuromechanical degrees-of-freedom to meet the multiple demands of ecological tasks, and critically depends on the continuous inhibition of synchronous grasp tendencies, which we speculate may be of vestigial evolutionary origin.

5.2 Introduction

Successful dexterous manipulation requires dynamic collaborative use of our fingers. Clearly, the neural control must actuate the system properly to satisfy the mechanical constraints of the task. Numerous studies have investigated how we adapt grasp to different friction contact [Johansson and Westling, 1984], object curvature [Jenmalm et al., 2003], fingertip positions [Baud-Bovy and Soechting, 2001], perturbations [Eliasson et al., 1995, Kim et al., 2006, van de Kamp and Zaal, 2007], object manipulations [Flanagan et al., 1999, Shim et al., 2005, Winges et al., 2008] and dexterity requirements [Johanson et al., 2001, Valero-Cuevas et al., 2003, Venkadesan et al., 2007]. These prior studies have identified voluntary and involuntary collaborative force interactions among fingertips to reduce task variability when pressing or grasping rigid objects (e.g., [Baud-Bovy and Soechting, 2001, Scholz et al., 2002, Shim et al., 2005, Latash and Zatsiorsky, 2009]; and for a review [Schieber and Santello, 2004]). This study, however, examines the behavior of collaborative, multifinger interactions during more ecological dynamic manipulation of a deformable object requiring the simultaneous control of fingertip motion and force. It is motivated by prior work aiming to clarify an apparent and long-standing paradox between the scientific concepts of muscle redundancy and robustness, vs. the clinical

reality of motor development and dysfunction [Venkadesan and Valero-Cuevas, 2008, Keenan et al., 2009, Kutch and Valero-Cuevas, 2011]. If, say, hand musculature is so redundant, why then is dynamic manipulation so vulnerable to developmental problems [Forssberg et al., 1991], mild neurological pathologies, and aging [Schreuders et al., 2006]? This paradox may arise simply because experiments and models often use simplified tasks for which the musculature is indeed redundant [Loeb, 2000]. In contrast, everyday ecological behavior often involves tasks that require meeting multiple mechanical constraints and transitioning between constraints. Our prior work on single fingers indicates that even ordinary manipulation tasks can push the neuromuscular system to its limit of performance when they require combinations of, or transitions between, motion and force constraints [Venkadesan and Valero-Cuevas, 2008, Keenan et al., 2009, Kutch and Valero-Cuevas, 2011]. Here we extend that prior work to multifinger function by investigating ordinary, yet critical, multifinger tasks: dynamic manipulation of deformable objects requiring continuous and simultaneous regulation of fingertip motions and forces.

5.3 Methods

5.3.1 Experimental procedure

We designed a novel instrumented apparatus with three hinged finger pads to be held using a tripod grasp with the thumb, index and middle fingers (Figure 5.1). Each finger pad consisted of a six-axis load cell (Nano 17, ATI/Industrial Automation, Apex, NC, USA) at one end of a rigid link to measure forces used to grasp and manipulate the object, with the other end connected by a common planar hinge instrumented to measure angles between the finger pads [Valero-Cuevas and Brown, 2006]. The grip surface of

the load cell was 30 mm from the hinge axis and covered with fine (360 grit) sandpaper. The objects mass is approximately 60 g to mitigate fatigue. Lastly, to ensure rotation of the thumb pad at the appropriate frequency, we used a software metronome (Metronome 1.1, Keaka Jackson, The World, 2008).

Mechanics dictates that the direction of fingertip force vectors for a static grasp must intersect at a point or the forces would create a net moment about the center of mass and cause a rotation (e.g., Yoshikawa and Nagai, 1991, Flanagan et al., 1999). The location of this point is arbitrary as long as the conditions imposed by the friction cones at the fingertips are satisfied, and the zero net force constraint is met. In this study, in contrast, the fingertip forces are constrained to intersect at a specified point (a central hinge) or else the finger pads will rotate. Holding the apparatus with a given total grasp force while reconfiguring the angles between the hinged finger pads requires collaborative multifinger interactions to control fingertip motions and force vectors. Thus, this apparatus explicitly distinguishes the multifinger interactions needed to hold the object against gravity (i.e., total grasp force) from those needed to dynamically reconfigure the grasp (i.e., compensating for thumb oscillations). Total grasp force is an independent task constraint from compensations in fingertip force vectors when reconfiguring the grasp: one can squeeze tighter without moving the pads, or reconfigure the grasp while producing the same total grasp force.

We tested six consenting subjects (1 female, 5 male; 21-31 years; 5 right-handed, 1 left-handed) using a protocol approved by the USC Institutional Review Board. Subjects held the test object with the thumb, middle and index fingers of the dominant [Oldfield, 1971] hand in a tripod grasp (Figure 5.1a, the subject flexed the ring and little fingers out of the way).

In the original task, subjects were instructed to maintain 10 N of total grasp force, defined as the sum of the normal forces at each fingertip, while oscillating the thumb

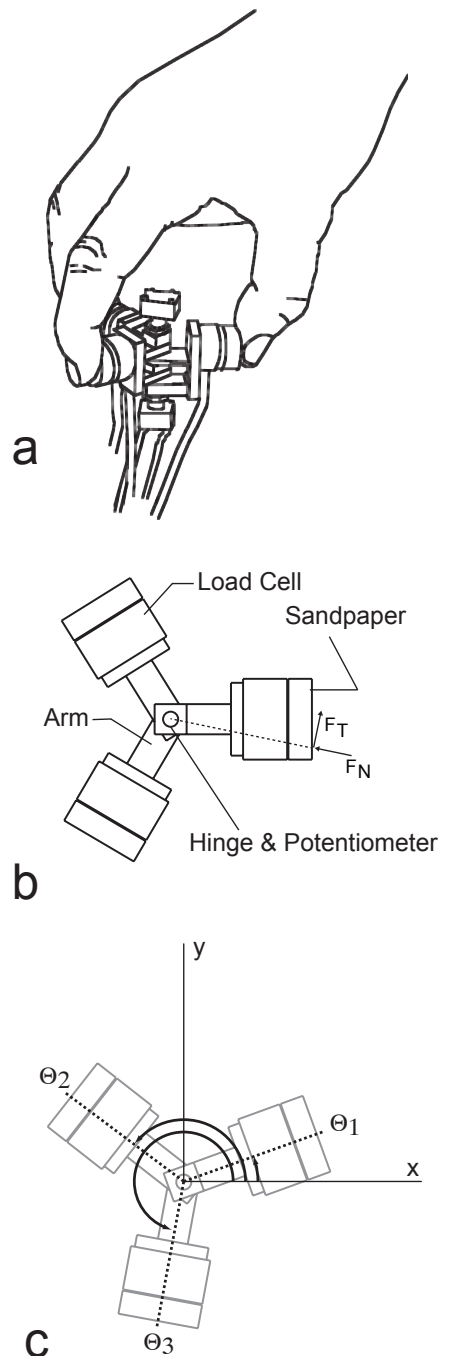


Figure 5.1: Experimental setup. *a.* Subjects held the object in a precision tripod grasp. *b.* The test object connected three load cells with a central hinge that allowed movement of the fingers. Normal force in this work is defined as the force directed at the hinge. *c.* The coordinates used in deriving the equations of motion

position in time to an audible metronome. The visual feedback consisted of a line and a crosshair presented on a computer screen at a distance approximately 1 m from the subject. The line represented the 10 N target sum of the three normal forces, which is consistent with the sum of normal forces used to lift a 400 g object with three fingers [Flanagan et al., 1999], while the crosshair represented the sum of normal forces actually applied by the subjects. Simultaneously, subjects were asked to oscillate the thumb pad of the grasping device in time with the audible metronome at 1 Hz, such that the leftmost and rightmost angular displacements of the thumb pad were reached on the metronome beat at a frequency of 0.5 Hz. The angular displacement of the thumb was left to the subjects preference. In the following, we will refer to this task as the original task.

Subjects had several practice trials, repeated with 60 s rest between trials until they reported to be comfortable with the task (from two to six repetitions, three typical). We did not do additional training because subjects reported to be very satisfied with their performance, likely because humans perform such tasks regularly and our task was designed to be similar to many ecological tasks as mentioned above. We then recorded 95 s of force and angle data at 400 samples/s (PCI 6025, National Instruments, Austin, TX) for each subject to obtain up to 47 full task cycles per subject. Data acquisition and visual feedback was provided with a program written in Matlab using the Data Acquisition Toolbox (Natick, MA, USA). Subject visual feedback on the force magnitude was updated at a rate of 50 Hz. The needed forces were so low that subjects did not report fatigue, but 60 s of mandatory rest were always enforced before each trial.

To rule out potential confounds or alternative interpretations of our results, we also studied six different Control Tasks (Table 5.1) were performed in addition to the Original Task - all of which were done in block-randomized order and repeated three times each for 95 s, and for which subjects had practice trials as in the Original Task. These Control

Tasks establish baseline performance for a variety of combinations of fingertip motion and force constraint, and were added after the initial pilot work to better understand the performance of the Original Task.

- *Control 1*: Perform the above-described Original Task, but with the instrumented object attached to ground. Doing this enabled us to distinguish force fluctuation correlations across fingers due to neuromuscular from purely mechanical causes associated with motion or reaction forces. Furthermore, this task removes the need for force dynamics that could be attributed to behavioral responses to dropping the object or vertical slip-grip responses.
- *Control 2*: The instrumented object was handheld, but we locked the pads in a configuration comfortable for the subject (making it a rigid object) and asked them to oscillate the normal force between index and middle finger at a frequency of 0.5 Hz, while holding the thumb still, thus mimicking the oscillations in normal forces the subjects needed to apply to compensate for thumb pad motion. The visual feedback in this condition consisted of two 0.5 Hz sinusoidal curves, phase shifted by 180 degrees and two crosshairs, representing the individual normal forces applied by index and middle finger. There was no explicit feedback on the total grasp force in this condition, but the amplitude of the sinusoidal curves corresponded to the amplitude of the oscillations in the Original Task. This Control Task helps to elucidate the coupling of two dimensions of force, which are at least mathematically independent [Gao et al., 2005]: the grasp force that counteracts gravity and the force compensating for thumb motion. It removes an explicit enforcement of a target total grasp force, as long as it is sufficient to hold the object.

- *Control 3*: The instrumented object was handheld but with unlocked pads and we asked subjects to oscillate the total grasp force, that is, oscillate in-phase the normal forces of thumb, index and middle finger at 1 Hz, thus voluntarily reproducing the synchronous grasp variability (i.e., Grasp Mode, see Results) observed experimentally in the Original Task. Here, the visual feedback consisted of a sinusoidal, whose amplitude we determined for each subject from his or her actual performance of the Original Task trials. While Control Task 2 above removed the target total grasp force enforcement, this task removes the requirement to modulate force variability compensating for thumb motion. It complements Control Task 2, in that it quantifies the coupling of the two force components, i.e. synchronous and compensatory normal force variability.
- *Control 4*: Control Task 3 was repeated, but this time with the pads locked as a rigid object to investigate the effect of removing the instability of the hinged pads on the Grasp Mode.
- *Control 5 and 6*: The final two tasks consisted of simple static grasps (handheld object with no oscillation of the thumb), with the target sum of normal forces to be maintained at 10 N, with pads either free (Control Task 5) or locked (Control Task 6) to separate force variability caused by visual processing from other contributors. These tasks allow us to quantify the contribution to the total force variability by corrective action vis--vis the visual feedback.

5.3.2 Mechanical Analysis

We found the closed-form analytical solution to the necessary fingertip forces and motions to perform the task. Comparing experimental forces to the analytical solution disambiguates mechanically necessary from neurally driven interactions. We modeled

Task	Hinge state	Thumb motion	Object displacement	Target force	Goal
Original	Free	0.5 Hz	Free	10 N grasp	Characterize multifinger interactions during dynamic manipulation requiring simultaneous control of fingertip motions and forces.
Control 1	Free	0.5 Hz	Fixed	10 N grasp	Same as original task, but with object fixed to ground to remove slip-grip response and behavioral fear of dropping object.
Control 2	Fixed	None	Free	0.5 Hz oscillating compensation	Voluntarily produce the compensation mode (alternating index and middle finger forces) as seen in original task, but with a locked object to remove hinge instability and voluntary finger motions.
Control 3	Free	None	Free	1 Hz oscillating grasp	Voluntarily produce the oscillations in the grasp mode (synchronous normal force modulation across fingers) as seen in original task, but without voluntary finger motions.
Control 4	Fixed	None	Free	1 Hz oscillating grasp	Same as in Control 3, but with a locked object to remove hinge instability.
Control 5	Free	None	Free	10 N grasp	Simple static grasp with visual feedback to assess effect of visuomotor feedback loop on grasp force variability.
Control 6	Fixed	None	Free	10 N grasp	Same as in Control 5, but with a locked object to remove hinge instability.
Simulation 1	Free	Oscillating	Free but stationary	10 N	Mechanical constraints of successful task performance dictate variability.
Simulation 2	Free	Oscillating	Fixed	10 N + noise	Signal-dependent noise informs force variability patterns more than the task mechanics.
Simulation 3	Free	Oscillating	Free but stationary	10 N + noise	Task mechanics govern force variability patterns.
Simulation 4	Free but stationary	None	Free but stationary	10 N + noise	Task mechanics govern force variability patterns.

Table 5.1: Explanation of tests and simulations used to support hypothesis

the system as a planar, rigid-body mechanism with five degrees of freedom: x and y location of the hinge axis on the plane, and the absolute angle of each pad. All three finger pads (which are each reduced to a point collocated with the center of pressure of the finger pad) and their links are in the horizontal plane, and gravity acts perpendicular to the plane in a downward direction, eliminating the vertical force from the analysis. The six control inputs in the plane of the finger pads are the normal (toward the hinge) and tangential components of fingertip forces for each of the three fingers. The normal and tangential forces of both the model and the experimental data are measured with respect to the hinge rather than the grip surface to reflect the task goals and to more easily separate the grasp force and compensation to thumb oscillation modes (Figure 5.1b).

5.3.3 Equations of motion for a 2-D system of three links connected via a common hinge

We derived the dynamic equations of motion for a simplified planar model of the grasper set-up using the Lagrange method (see, e.g. [Williams and Willima, 1996]). The Lagrange method requires generalized coordinates (q_i) that describe the configuration of the object. The kinetic and potential energy (T and V) are expressed as functions of the q_i and generalized forces (F_i) that act on each generalized coordinate. The Lagrangian is the kinetic minus potential energy: $L = T - V$, and is inserted into Lagranges equation:

$$\frac{d}{dt} \left(\frac{\delta}{\delta \dot{q}_i} L \right) - \frac{\delta}{\delta q_i} = F_i$$

The grasp-device system has two translational degrees of freedom (DOF) relative to an inertially fixed coordinate reference frame and three rotational DOF - one for each pad. Since we observed very limited motion in the vertical direction and rotation of the device itself, we disregarded these 4 dimensions (1 translational, 3 rotational) in our modeling analysis. For the generalized coordinates, we selected x and y position of the hinge and the absolute angle of each pad relative to the fixed coordinate system $\theta_i, i = 1, 2, 3$ (Figure 5.1c). Using these coordinates, the 2-D vector for the position of each pad is:

$$r_i = \begin{bmatrix} x \\ y \end{bmatrix} + d_i \begin{bmatrix} \cos \theta_i \\ \sin \theta_i \end{bmatrix}$$

where d_i is the distance from the hinge to the center of mass of the i -th pad. Differentiating this expression yields the velocity

$$v_i = \begin{bmatrix} \dot{x} \\ \dot{y} \end{bmatrix} + d_i \dot{\theta}_i \begin{bmatrix} -\sin \theta_i \\ \cos \theta_i \end{bmatrix}$$

where the over dot represents the derivative with respect to time. The velocity determines the kinetic energy of each body. Let m_i be the mass of the i -th pad and I_i be the scalar moment of inertia of the i -th pad about a vertical (out of the page) axis through the center of mass of link I . The kinetic energy of the system is given as the sum of the energy of the individual parts. The partial derivatives in the Lagrangian eliminate potential energy terms from the equation because gravity acts perpendicular to the system. Thus the Lagrangian is given by the kinetic energy:

$$L = T = \sum \frac{1}{2} m_i (v_i \cdot v_i) + \frac{1}{2} I_i \dot{\theta}_i^2$$

The generalized forces for this simple system are the resultant forces or torques when all generalized coordinates are fixed except one. Fixing all coordinates and allowing x to vary gives us the generalized force for x :

$$F_x = \sum F_{N_i} \cos \theta_i - F_{T_i} \sin \theta_i$$

which is all the forces in the x -direction. The forces F_{N_i} and F_{T_i} are the normal and tangent forces at the grip surface on each pad (Figure 5.1b). Likewise for the y direction, the generalized force is:

$$F_y = \sum F_{N_i} \sin \theta_i - F_{T_i} \cos \theta_i$$

The generalized forces corresponding to the angles are physically torques. The resultant torque when allowing only one angle to vary is given by:

$$T_{\theta_i} = lz \cdot F_{T_i}$$

The component parts are arranged according to Lagranges equation to arrive at the following equations of motion, written in matrix form for computational ease:

$$\begin{bmatrix} M & -m_1 d_1 s_1 & -m_2 d_2 s_2 & -m_3 d_3 s_3 \\ M & m_1 d_1 c_1 & m_2 d_2 c_2 & m_3 d_3 c_3 \\ -m_1 d_1 s_1 & m_1 d_1 c_1 & m_1 d_1^2 + I_1 & \\ -m_2 d_2 s_2 & m_2 d_2 c_2 & m_2 d_2^2 + I_2 & \\ -m_3 d_3 s_3 & m_3 d_3 c_3 & m_3 d_3^2 + I_3 & \end{bmatrix} \cdot \begin{bmatrix} \ddot{x} \\ \ddot{y} \\ \ddot{\theta}_1 \\ \ddot{\theta}_2 \\ \ddot{\theta}_3 \end{bmatrix} + \begin{bmatrix} -d_1 c_1 & -d_2 c_2 & -d_3 c_3 \\ -d_1 s_1 & -d_2 s_2 & -d_3 s_3 \end{bmatrix} \cdot \begin{bmatrix} \dot{\theta}_1^2 \\ \dot{\theta}_2^2 \\ \dot{\theta}_3^2 \end{bmatrix} =$$

$$\begin{bmatrix} c_1 & c_2 & c_3 & -s_1 & -s_2 & -s_3 \\ s_1 & s_2 & s_3 & c_1 & c_2 & c_3 \\ & & & lz & & \\ \mathbf{0} & & & lz & & \\ & & & lz & & \end{bmatrix} \cdot \begin{bmatrix} F_{N_1} \\ F_{N_2} \\ F_{N_3} \\ F_{T_1} \\ F_{T_2} \\ F_{T_3} \end{bmatrix}$$

This can be written compactly using matrix and vector notations with obvious meaning as

$$M\ddot{x} + C\dot{x}^2 = D \cdot F$$

The model takes the dynamics of the position and angles as inputs and outputs the normal and tangential forces. This gives us a one-parameter subspace of the possible forces. The grasp force is added to the equations to completely determine the forces necessary for successful completion of the experimental task. In simulation, we fix x and y at the origin, maintain the middle and index angles at 130 and 230 deg, respectively, and prescribe the grasp force as ether constant or noisy. The reduced model with these assumptions is:

$$\begin{bmatrix} -d_1 c_1 \cdot \dot{\theta}_1^2 \\ -d_1 s_1 \cdot \dot{\theta}_1^2 \\ (m_1 d_1^2 + I_1) \cdot \ddot{\theta}_1 \\ 0 \\ 0 \\ F_{\text{grasp}} \end{bmatrix} = \begin{bmatrix} c_1 & c_2 & c_3 & -s_1 & -s_2 & -s_3 \\ s_1 & s_2 & s_3 & c_1 & c_2 & c_3 \\ & & & lz & & \\ & \mathbf{0} & & & lz & \\ & & & & & lz \\ 1 & 1 & 1 & 0 & 0 & 0 \end{bmatrix} \cdot \begin{bmatrix} F_{N_1} \\ F_{N_2} \\ F_{N_3} \\ F_{T_1} \\ F_{T_2} \\ F_{T_3} \end{bmatrix}.$$

The last row of this equation comes from the definition of grasp force as the sum of the normal forces.

5.3.4 Simulations

In the closed-form inverse dynamics solution we calculate fingertip forces necessary to produce the desired motion and total grasp force. The desired motion maintains the index- and middle-finger angles fixed at 130 and 230 deg while the thumb angle oscillates through an arc with amplitude of 30 degrees following a sine function with a period of 2 s (0.5 Hz). In this way we defined a comfortable configuration that would reveal clear changes in forces, shown in Figure 5.3. For comparison, a plot of the measured angles from one representative subject is shown in Figure 5.3. Note that in the subjects data, the angle between the middle and index finger pads also changed slightly during the trial, but the motion of the thumb is much greater and the mechanical solutions retain their same form in the plot of the normal forces (Figure 5.2). The experimental apparatus was built to have very low friction at the hinge, thus the modeled and experimentally measured tangential forces are very small relative to the normal forces (3000x smaller in the frictionless model and 20x smaller in the experimental data) and were excluded from the analysis. Instead, the adaptation of the normal forces to the changing configuration

captures the relevant behavior due to the thumb oscillations. We further justify using only the three normal forces to characterize the task because they fully account for the two active degrees of freedom of the system: grasp force and compensation to thumb oscillation. A system or study designed to consider additional degrees of freedom would need to include the tangential forces for the very low frictions.

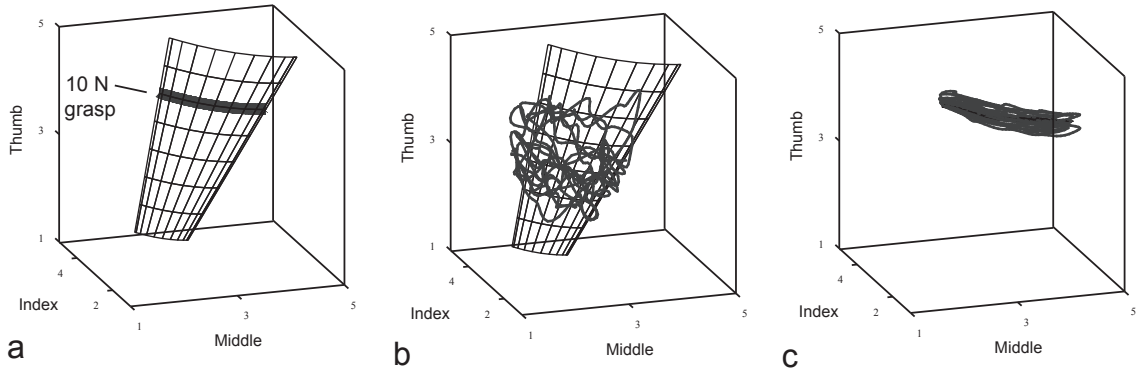


Figure 5.2: Force space. a. A perfectly executed task traverses the thick line shown here. Connecting the lines created by a variety of grasp forces (from 5 to 12 N) illustrates the manifold of allowable forces. b. The subject data lies on the manifold described by the model, but with varying grasp force magnitude. c. The subject data and the manifold have slight curvature when viewed from the [1, 1, 1] direction.

We simulated four conditions for the grasp force 5.1:

- *Simulation 1*: Idealized Original Task; where the grasp force was ideally constant, while the index and middle finger generated the exact normal forces necessary to compensate for the reconfiguration of the grasp as the thumb pad oscillated.
- *Simulation 2*: Same as Simulation 2, but with the object fixed to ground and each finger generating a zero mean Gaussian distributed noisy normal force, whose variance was adjusted such that either the grasp force magnitude or the grasp force error was reproduced. The noise was not bandlimited to the 8-12 Hz frequency band, however, with which signal-dependent noise is commonly associated. This

condition simulates the effects of signal-dependent noise [Jones et al., 2002] at each fingertip but since it does not consider reaction forces at the other fingertips, this condition in effect simulates the first Control Task in which the device was attached to ground.

- *Simulation 3*: the noisy normal forces acting on the object and inducing reaction forces in the other fingers, thus simulating correlations between fingers that would arise purely due to mechanics. This condition simulates the Original Task with noise.
- *Simulation 4*: a simple static grasp without thumb oscillations, but including the requirement to generate a 10 N sum of normal forces and correlations due to mechanics (simulating the fifth and sixth Control Tasks for simple static grasp). This condition helps to separate contributions to visual feedback error by corrective actions and by signal-dependent noise.

In Simulations 3 and 4 there is no unique mechanical solution so we computed the reaction forces by solving a underconstrained system of linear equations, solving for zero force and moment using the pseudoinverse matrix (i.e., the least-squares energy solution). In Simulation 1 we modeled constant total grasp forces ranging from 5 N to 12 N to find the full solution manifold (i.e., the set of all mechanically feasible fingertip forces to accomplish the task). This set of mechanically feasible forces is the slightly curved manifold shown as a curved surface in (Figure 5.2).

5.3.5 Data analysis

Plotting the normal component of the fingertip forces (i.e., the component of fingertip force acting on the finger pad and directed toward the hinge) against each other in the three-dimensional space of normal forces is an effective way to visualize the

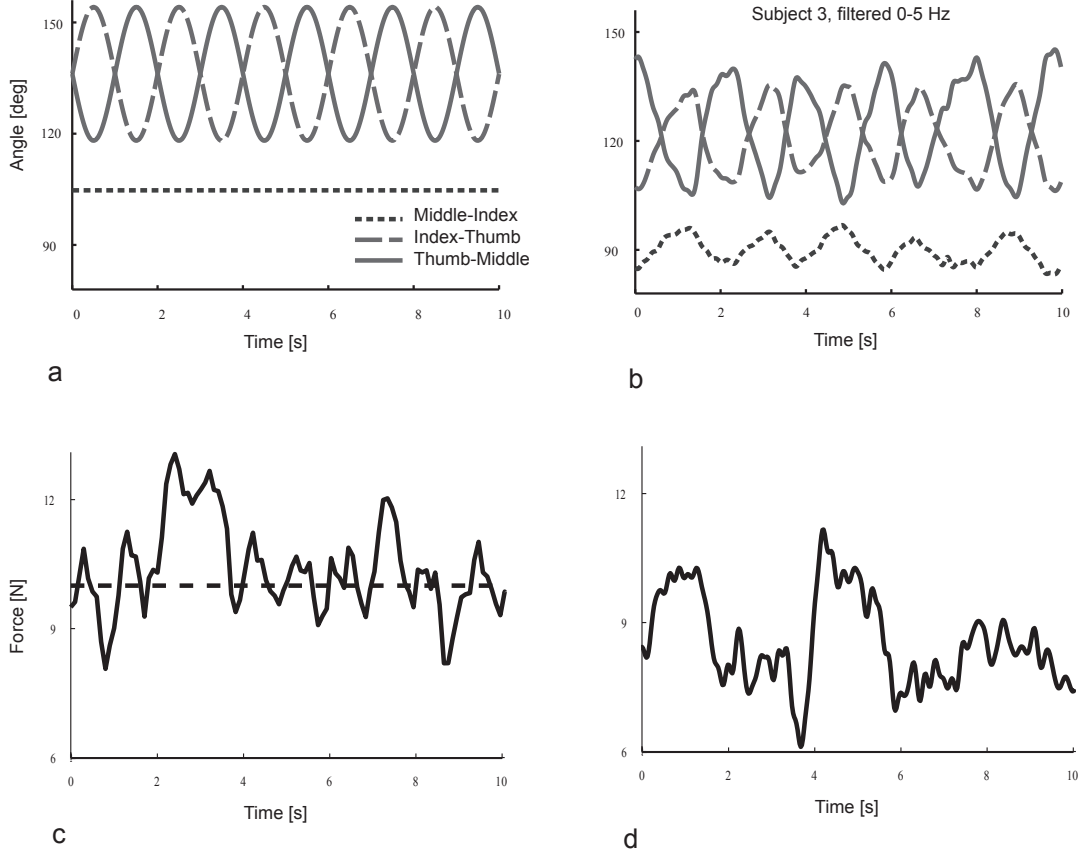


Figure 5.3: Sample time histories. *a*. The ideal inter-finger angles used in the model. The equations reference all angles to a fixed ground, but are shown relative to one another here to be consistent with the experimental data. *b*. Measured angles from a representative subjects data. *c*. The grasp force target used by the model is either constant (dashed line) or variable. *d*. Measured grasp force from the same data as *b*. Note the quasi-periodicity in the measured data.

experimental and simulation results. Each coordinate axis in this three-dimensional space represents the normal force of a given finger (thumb, index, and middle finger), and a combination of three forces is represented as a point in this space. The analytical solution to the task shows that the feasible set of fingertip forces lies on a slightly curved, nearly planar surface in force space (Figure 5.2). This is because the mechanical constraints of the task, such as the equilibrium equations for different finger pad configurations, represent lines or nearly planar surfaces in the force space. That is, only

combinations of forces that lie on the constraint lines or surfaces are valid solutions to the grasp problem, and linear analysis tools may be used, such as principal components analysis (PCA, [Clewley et al., 2008]).

We used the 3D force vector and torques on each finger pad (Figure 5.1b) to extract the center of pressure location and force components in the normal, tangent and vertical (F_N, F_T, F_V) directions relative to the hinge (Figure 5.1b). The normal force covariance patterns completely determine the grasp force and manipulation force components; the others are not included in the analysis as discussed above. The first 5 s and last 1 s of data were removed to eliminate transient behavior in the data.

The data, represented by a 3-by-N matrix, where N is the number of samples, were filtered with a sliding band pass Butterworth filter of width 1 Hz and 99% overlap between filter windows, starting from 0.1 Hz up to 10 Hz, to extract the normal force dynamics in each of these frequency bins. We performed PCA on the 3-by-3 normal force covariance matrix computed from each set of filtered data associated with a particular filter window, and computed the loadings of the three resulting principal component (PC) vectors (r-mode PCA, computed from covariances between variables) as well as the percentage of variance explained by each PC. Next, we compared the loadings of each PC to the theoretical grasp force mode and compensation-to-thumb-oscillation mode for each frequency range, by computing the angle between the experimentally observed PC and the PC associated with the mechanical simulation of the task. Lastly, to determine whether variability along a PC in the Original Task changed in a state-dependent manner, e.g. variability at the extreme points of thumb motion vs. at the middle point, we computed the variance over a window, whose length was one third of the thumb oscillation period, i.e., 0.6 s, and slid the window over the trial data. This tests the hypothesis that increased grasp force variability reflects the action of a purposeful mechanism, such as guarding against drop of the object by squeezing it at critical locations in the state space.

5.4 Results

5.4.1 Analytical Solution and Simulations

The analytical solution to the manipulation task shows that the feasible set of fingertip forces lies in a tilted and slightly curved plane in the force space (Figure 5.4). It is to be expected, therefore, that the PCA of the subjects data will naturally approximate this manifold well (Figure 5.2c) and that subjects PCs will align with the manifolds PCs, for the following reasons.

First, grasp force is the sum of the fingertip normal forces, and is equal to the projection of the current force vector $[F_{\text{middle}}, F_{\text{index}}, F_{\text{thumb}}]^T$ onto the $[1, 1, 1]^T$ direction¹ (Column I in Figure 5.4). Changes in grasp force magnitude cause movement towards or away from the origin in force space, while not moving the object. Therefore a PC of the subjects data with loadings of the same sign and similar magnitude indicates a changing grasp force. We say this PC aligns with the grasp mode.

Second, as the thumb oscillates from side to side, the relative magnitude of the middle and index fingers forces alternates to compensate for the change in direction of the thumbs force vector during the task. Thus the manipulation force is the projection of the current force vector onto the $[-1, 1, 0]^T$ direction (Column II in Figure 5.4). The changing force magnitudes of the index and middle fingers for a given thumb force magnitude causes lateral movement in force space as described by the compensations to thumb oscillation mode. The mechanics of the task result in grasp force and compensations to thumb oscillation being orthogonal modes in force space. This is the mathematical way of saying that one can produce the same magnitude of grasp force while moving

¹For the sake of clarity in the text and figures, we indicate PCs as vectors with 1s and 0s. The mathematical convention would be to present them as unit vectors. In particular, $[0.5, 0.5, 0.7]^T$ is a better approximation of the grasp mode, since index and middle finger form a smaller angle.

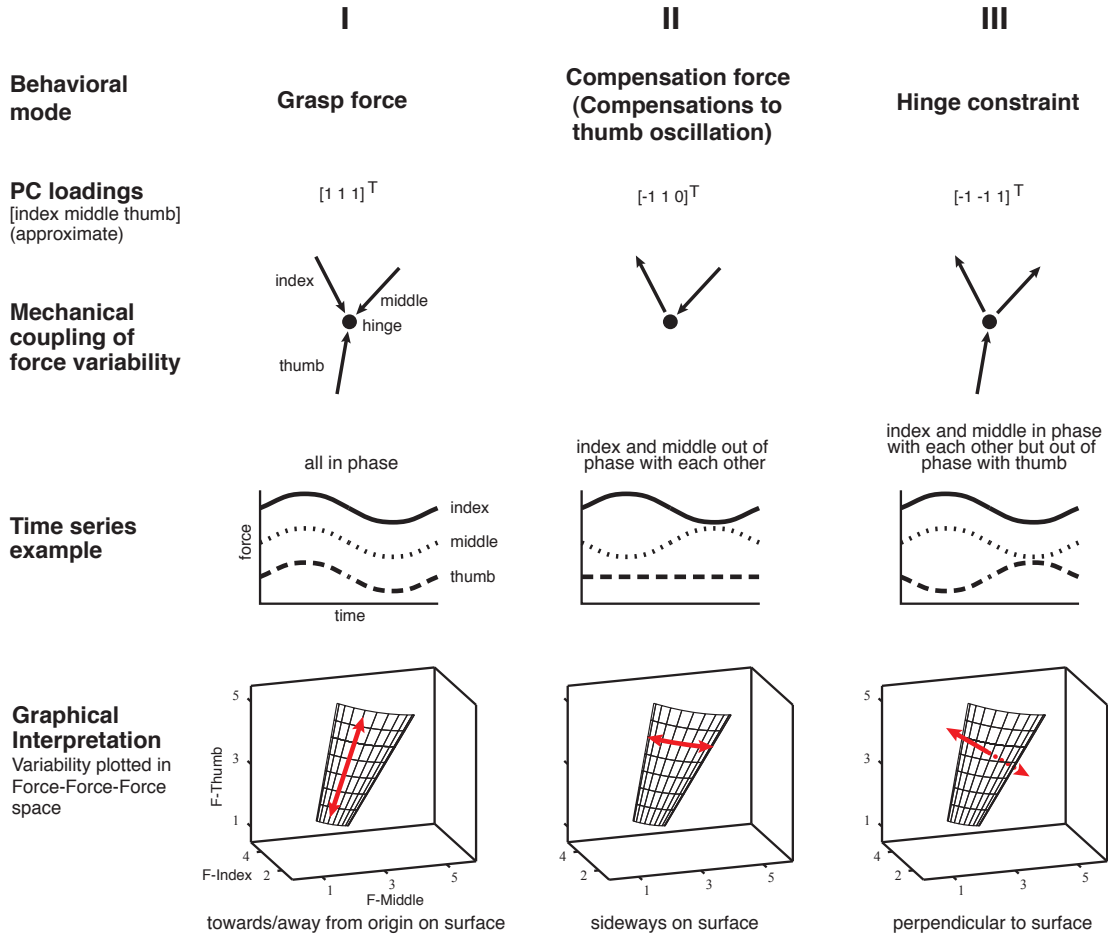


Figure 5.4: Overview over the 3 force variability modes. The Grasp force mode (column I) is the dimension of force variability that is associated with simultaneous, or in-phase, increases and decreases by all three finger normal forces. Graphically (bottom row), this can be expressed as motion along a line in 3D normal force space, which has components in every dimension. The Compensation force mode (column II), explains out-of-phase variation of index and middle finger force, with no contribution by the thumb. In 3D normal force space, this corresponds to motion at a constant thumb force level, between index and middle finger axes, along a slightly curved line. Lastly, the Hinge force mode explains that force variability whereby middle and index finger vary their normal force in-phase, while varying out-of-phase with the thumb normal force. This will lead to accelerations of the object.

the thumb or conversely, vary the grasp force without affecting the thumbs positional control. We say this PC aligns with the compensation mode.

The third mode of force interactions is variability perpendicular to the constraint plane and represents errors in maintaining the hinge constraint. Namely, the task requires that the force vectors intersect at or near the hinge, and this constraint is violated if the point of intersection of forces moves in towards or away from the thumb the $[-1, -1, 1]^T$ direction (Column III in Figure 5.4). Variability along this dimension is associated with translations and rotations of the grasped object. We say this PC aligns with the hinge mode.

5.4.2 Principal component associated with the modeled ideal performance of the task.

The fingertip forces necessary to produce motion of the thumb while maintaining a perfectly constant grasp force create a horizontal line that is slightly curved in force space (Column II in Figure 5.4), and the family of lines for a variety of grasp force magnitudes creates a slightly curved surface defining all feasible solutions to the task. For this ideal case (Simulation 1, Figure 5.7) the variability in normal forces is associated purely with compensations for movement of the thumb (i.e., column II in Figure 5.4, which is seen as traveling back and forth along the thick line as the thumb moves from side-to-side). The loadings of each PC for this ideal case are shown in the first row of column II of Figure 5.4 and, as expected, the compensation mode is the PC that explains $> 99\%$ of the variance (i.e., $[-1, 1, 0]^T$). The small contribution of the hinge constraint mode PC (i.e., $[-1, -1, 1]^T$ direction) reflects the slight curvature of the force trajectory in force space. The grasp force mode PC (i.e., $[1, 1, 1]^T$ direction) shows zero variance in the grasp force by construction (i.e., the ideal task has no variability in grasp force). This result applies equally to all frequency bands.

5.4.3 Summary of experimental PCA result and comparison with the modeled ideal performance of the task

Figure 5.5 summarizes our findings. As expected by the mechanical requirements of the task shown in Simulation 1 and Figures 5.7 & 5.2, the Compensation Mode dominates in the Original Task. But whereas Simulation 1 only shows residual levels of the Grasp and Compensation Modes (due to the linear approximation to the slightly curved solution manifold), the performance of the Original Task by the subjects was accompanied by mechanically unnecessary variability in the form of substantial amounts of the Grasp Mode; and small amounts of Hinge Mode. The Control Tasks (Table 5.1) go on to demonstrate that the Grasp Mode strongly pervaded manipulation tasks requiring different fingertip motion and force constraints (Figure 5.5 shows only Control Tasks 1 & 2 for clarity, others are presented below in detail). Only simple static grasp (Control Tasks 5 & 6) exhibits much small levels of force variability in general. Importantly, these results cannot be explained by signal dependent noise (Simulations 2-4), whether the objects is deformable vs. rigid (hinge state), or hand held vs. attached to ground (object displacement). Taken together, these results demonstrate that stereotypical grasp-and-release synchronous interactions (i.e., Grasp Mode) pervade multifinger manipulation when the manipulation task requires orchestrating individuated fingertip motions and forces, as explained in the Discussion.

5.4.4 Experimental PCA result and comparison with the modeled ideal performance of the task

We can see from Figure 5.6 (bottom plot) that on average, subjects were able to meet the 10 N sum of normal forces requirement, with a standard deviation of 0.5

N. Across the physiologically plausible frequency range for control of force production [Johansson and Birznieks, 2004], the modes observed in the experimental data match the theoretical ones quite well: the median angle difference between the experimental and theoretical modes never exceeds 30 degrees, indicating that the simulations predict the structure of variability faithfully (Figure 5.6, middle plot). Beyond 12 Hz (not shown), and thus at time scales shorter than those of the shortest sensorimotor loops for sensory mediated force production [Johansson and Birznieks, 2004], the predicted structure breaks down, i.e. it converges to a purely white noise process in a 3-dimensional space, which suggests that the structure of variability is plausibly imposed by cortically and spinally mediated drive to alpha motoneuron pools (as opposed to neural or measurement white or Gaussian noise with broad bandwidth). Figure 5.6 (top plot) shows that the magnitude of the compensation mode PC is in agreement with that found in the simulated task (Figure 5.7). The compensation mode dominates the variability below and at the oscillation frequency, then falls off sharply above. While this is not surprising, since the task determines this magnitude of variability, the magnitudes of the grasp mode show a very different picture, compared to the simulation, the modeled ideal performance of the task. The simulations suggest that there should be no grasp mode and very little hinge mode variability across the entire physiologically plausible frequency range. However, near the oscillation frequency, the grasp mode in the experimental data explains approximately 30 % of the overall normal force variance, or alternatively, has a standard deviation of almost 0.2 N. Beyond the task-relevant frequency of 0.5 Hz, the grasp mode explains most of the force variance and thus dominates its variability, even though the compensation mode magnitude does not fall off as sharply with frequency as in the simulation. The milder roll-off can be explained by imperfect matching of the task frequency by subjects over the course of an entire 95 s trial. The strong contribution of the grasp mode at all frequencies, on the other hand, is plausibly a consequence of

neural and biomechanical coupling between the control of forces which compensate for object manipulation and that of forces required to hold it.

There are two objections which can be made against the interpretation that the control of force modes is coupled: firstly, the strong contribution of the Grasp Mode to the overall normal force variability could be attributed to the interplay between mechanics of the task and signal-dependent noise at the fingertips [Jones et al., 2002], whose magnitude scales with the mean force. According to this objection, noise generated by each of the fingertips will show up as reaction force at the other two fingertips, thus giving rise to positive correlations (theoretically instantaneous but perhaps with small delay due to tissue deformation and compression) across fingertips and thereby causing the Grasp Mode variability observed in the experiments. Secondly, the large variability along the Grasp Mode direction could be attributed to the visuomotor loop involving the visual feedback, which instructed subjects to generate a constant 10 N sum of normal forces, and subjects efforts to maintain this force after seeing the visual feedback. The simplest strategy to correct for displayed deviations from the target force is to increase or decrease forces across all fingertips simultaneously, hence in alignment with the observed Grasp Mode. It should be noted, however, that i) subjects were encouraged to make their best possible effort at maintaining this force and ii) that the visuomotor loop has a defined latency and operates at time scales considerably shorter than that of the thumb oscillation frequency, and in particular, cannot be expected to be present across the entire range of frequencies. We investigate both of the above objections in the following two paragraphs.

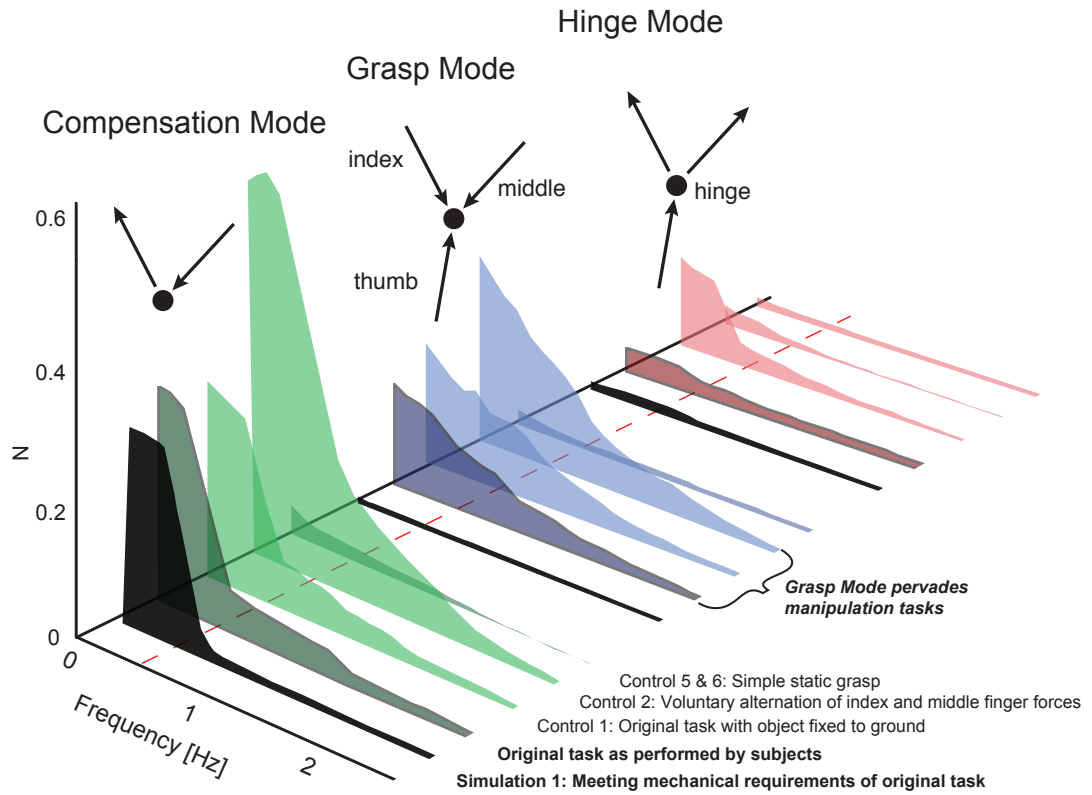


Figure 5.5: Summary figure showing the normal force variability magnitudes of the three force modes (Compensation, Grasp and Hinge Modes) across the low frequency range, found through PCA in the Original and the Control Tasks as well as Simulation 1. The results are grouped by mode and in each group, the first graph shows the magnitudes found in Simulation 1 (noiseless, ideal performance). Note that due to the curvature of the solution manifold (Figure 3), the Hinge mode is not exactly zero even in the simulation. Most importantly, the Original Task and Control Task 1 both reproduce the expected magnitude of the Compensation Mode, while they exhibit much larger Grasp Mode magnitude.

5.4.5 Comparison with the modeled imperfect performance and the experimentally grounded task

To address the first objection, we added signal-dependent noise to the simulated forces generated by each fingertip, whose magnitude was proportional to that force (simulation 2). The noise proportionality constant was chosen so that the resulting grasp force mode

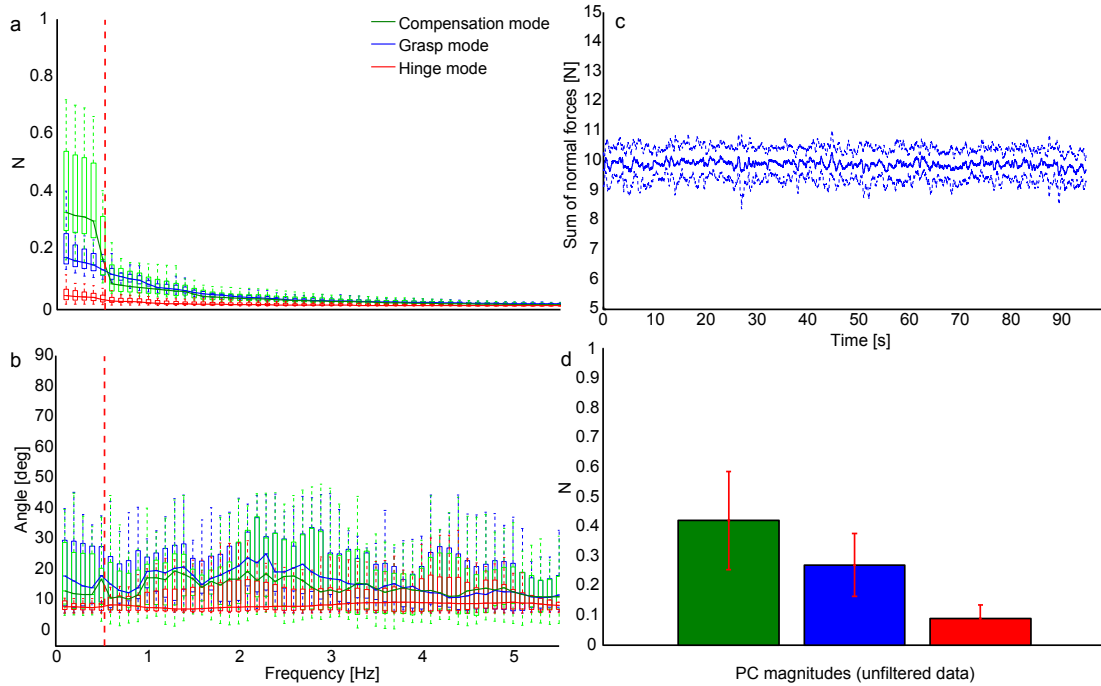


Figure 5.6: a. The measured magnitudes of the three principal components vs. frequency in the original object manipulation task. Not surprisingly, near the task-relevant frequency of 0.5 Hz (vertical red dashed line), the Compensation Mode dominates the overall force variability, as suggested by Simulation 1. However, at those frequencies, subjects exhibit considerable contributions to force variability from the Grasp Mode. Box plots indicate the distribution of these variability contributions across the 7 subjects. b. The difference in angle between the directions of the measured and the analytical principal components. The box plots reflect the fact that the three normal force correlation modes did not vary much across subjects and were closely aligned with the theoretical correlation modes. Differences across subjects and between observed and theoretical modes mostly indicate the variability of object orientation during task performance c. Average sum of normal forces across the 7 subjects in the original object manipulation task. Subjects were well able to meet the 10 N target. d. The three force mode magnitudes computed from the unfiltered data (square root of the eigenvalues), showing that overall, the Compensation Mode contributes most of the force variability and the Hinge Mode contributes the least, reflecting successful task performance. (Note that the values are in Newtons, and do not represent proportions of variance. No statistical tests are done on these data because they simply show the total variance across all frequencies.)

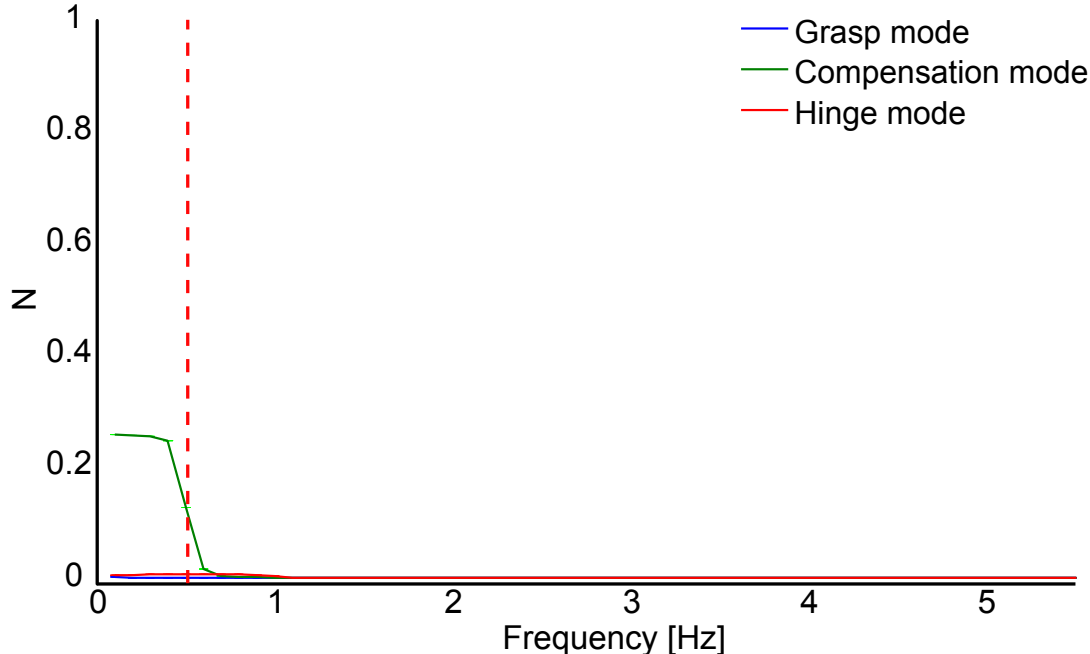


Figure 5.7: The three mode magnitudes vs. frequency in the noiseless simulation of the Original Task (Simulation 1). The Compensation Mode explains almost all the force variability and only near the task frequency of 0.5 Hz (vertical red dashed line). The remaining variability is explained by the Hinge Mode, near the task frequency, which can be attributed to the curvature of the solution manifold (Figure 5.2). The Grasp Mode does not contribute to force variability at any frequency.

variability would match experimental observations near the frequency of thumb oscillation. Since there is no connection between fingertips, neural or mechanic, principal components analysis does not reveal any correlation structure and the sum of normal forces varies wildly about the 10 N mean (results not shown). This is what we would expect in an experiment in which the device is attached to ground, and all the variability observed was due to signal-dependent noise at the fingertips. As a refinement, we introduced mechanical connection between fingertips and computed and added the reaction forces at the other fingertips (simulation 3). Figure 5.8 shows that the magnitudes of compensation and hinge modes are unaffected, while the grasp mode magnitude is increased and matches the experimental observations. However, its magnitude does not

roll off across the entire frequency range, thus differing significantly from the experimental observations. This is not surprising, since we did not band-limit the noise. However, band-limiting the noise in our simulations to the frequency range observed by [Jones et al., 2002], i.e. 8-12 Hz, does not reproduce the results either, as the tracking error is still vastly larger than in the original experimental task. More importantly, however, comparing the results of the original task with the first control task in which the device was attached to ground, we find that the experimental grasp mode magnitude is equally large (Figures 5.5 and 5.9). This is surprising because the device is attached to ground and correlations across fingertips cannot be explained by mechanical coupling (i.e., force variability and errors are shunted to ground and do not affect the other fingers), and mismatches in forces do not accelerate the object. Moreover, simulation 2 above predicted a complete absence of correlation modes. In summary, these results challenge the alternative interpretation that signal-dependent noise in conjunction with mechanics explains the experimentally observed, yet mechanically unnecessary, Grasp mode variability.

5.4.6 Comparison with the simple static hold control tasks

To investigate the second objection, that grasp mode variability is attributable solely to corrections to drifts in the visual feedback, we analyzed the normal force data of the fifth and sixth control tasks, in which subjects simply held the object statically (did not oscillate the thumb) and only tracked the 10 N sum of normal force visual feedback. As in the other experiments, the three modes of force variability match those predicted by Simulation 1, the modeled ideal performance, across the low frequency range (Figure 5.10b). Furthermore, while the compensation mode is now contributing 20 % and less to the force variability near the frequency of thumb oscillation, the variability magnitude along the grasp mode is also reduced by approximately 50 %. This can be seen in

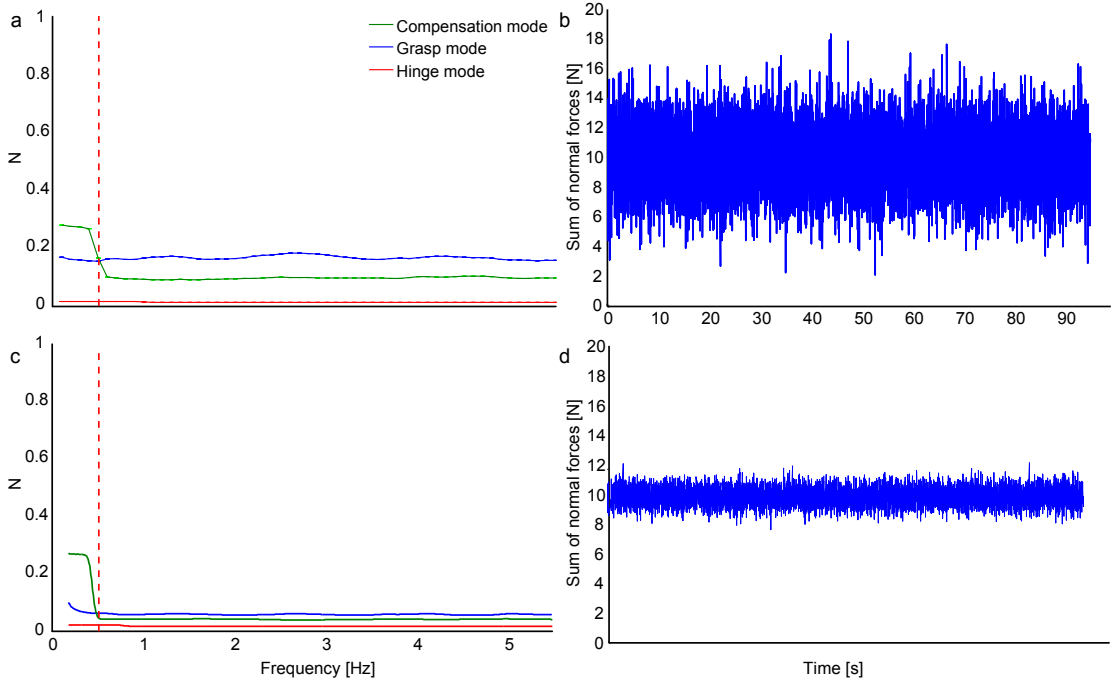


Figure 5.8: a. The simulated magnitudes of the three principal components vs. frequency in the original object manipulation task, including signal-dependent noise, whose standard deviation is proportional to the mean force. The proportionality factor was chosen such that the grasp force magnitude at the task-frequency of 0.5 Hz (vertical red dashed line) matches that measured in the Original Task. However, the noise is not band-limited to the low frequencies, since signal-dependent noise is associated with higher frequency bands, and thus the grasp force mode magnitude is considerably larger than the measured one at all other frequencies. b. The simulation also exhibits much greater variability in terms of the sum of normal forces, making signal-dependent noise an unlikely source of the grasp force variability. c and d. If, on the other hand, the signal-dependent noise magnitude is scaled to the error observed in the sum of normal forces (right plot), the resultant grasp force magnitude does not match the experimentally observed one (left plot).

(Figure 5.10a). Similarly, the standard deviation of the sum of normal forces is reduced by half (Figure 5.10c). These results suggest that voluntary (i.e., visuomotor) corrective action does explain some of the variability in the grasp mode, since this control experiment failed to abolish grasp mode variability altogether - but a large proportion (as

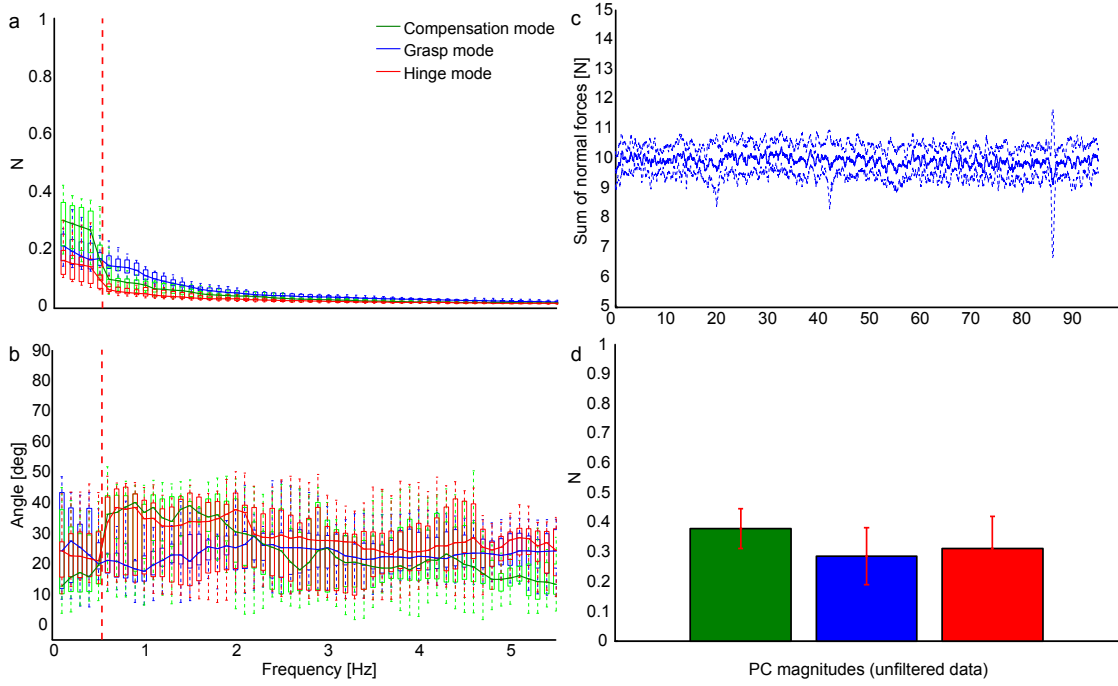


Figure 5.9: a. The measured force modes magnitudes vs. frequency in the original task, in which however, the device was attached to ground (Control task 1). Although the load cells are now mechanically decoupled and thus, noise originating at one finger does not get transmitted to the other fingers, the grasp mode contribution in this case is just as strong as in the original task. b. The measured principal component directions agree with the theoretical across the frequency range, although to a lesser extent than in the original task. Note, however, that the measured grasp mode shows the greatest agreement (vertical red dashed line indicates 0.5 Hz frequency of thumb oscillation). c. Average subject performance at maintaining the 10 N target force. d. The force variability analysis reveals that even though the object is attached to ground, and safety or signal-dependent noise is not an issue, the grasp force variability is as present as in the Original Task. Note however, that the Hinge Mode contributes stronger, too.

much as 50 %) of that variability needs to be attributed to causes other than voluntary modulation of force and the limitations of the visuomotor loop associated with it.

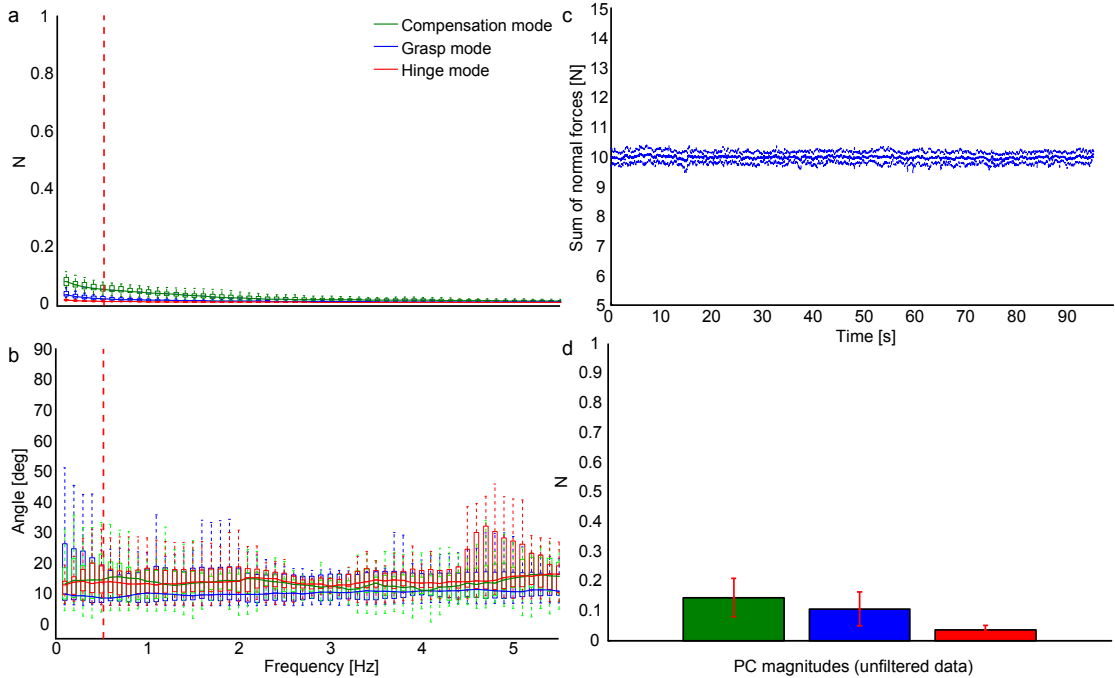


Figure 5.10: a. Force mode magnitudes vs. frequency in the simple hold task (control tasks 5 and 6). Although for this task, grasp force variability is also unnecessary, we see some contribution to force variability by it. However, it is much smaller than in the original task, suggesting that force corrections to the visual feedback are not the sole cause of grasp mode contribution. b. The measured modes agree with the hypothesized modes across all frequencies (vertical red dashed line indicates 0.5 Hz frequency of thumb oscillation). c. Subject performance at maintaining the 10 N target force in the simple hold task. d. Analyzing the unfiltered simple grasp data, we find that the order of force modes in the Original Task is preserved, but there is much less force variability. The amount of grasp force variability in this task indicates the variability arising from tracking the constant visual feedback.

5.4.7 Comparison with the alternating index/middle finger normal force task

One can argue that cognitive load may explain the higher corrective activity (i.e., dominant Grasp mode) seen when the thumb is being oscillated, since moving the thumb could consume resources that could otherwise be fully devoted to the maintenance of the task requirements. Using the range of compensation force magnitudes observed in

each subject, we asked them to voluntarily generate alternating index and middle finger forces of the same frequency and magnitude, but without oscillating the thumb and while the pads were locked into a rigid object (second Control task). Once again, the experimental force variability structure matches the predictions (Figure 5.11b). Furthermore, we see that despite the absence of any finger motion in this task, the contribution of the grasp mode is just as strong as in the original task (Figure 5.11a and 5.5). Lastly, the feedback in this control task was based on the alternation of index and middle finger normal forces and no explicit feedback about the force error was presented for the sum of normal forces. Hence, despite the absence of an explicitly enforced requirement on the grasp force, variability along this mode is just as present and thus likely to be linked to the explicitly enforced Compensation mode requirements.

5.4.8 Comparison with voluntarily oscillated grasp force

So far, we have shown that the grasp mode is present when performing a voluntary compensatory task. We then used the third and fourth control cases to test the inverse, i.e., whether voluntary grasp mode produces a corresponding involuntary compensation mode. While, for the sake of brevity, we do not show the results here, we find that such coupling is not present. In other words, generating voluntary grasp force does not increase the magnitude of compensation force variability beyond what is seen in static grasp in control cases 5 and 6 (Figure 5.10 and 5.5). This is in contrast to the voluntary production of the compensation mode, which even in the absence of thumb motion gives rise to even larger magnitudes of grasp force variability than observed in the original task (Figure 5.11 and 5.5).

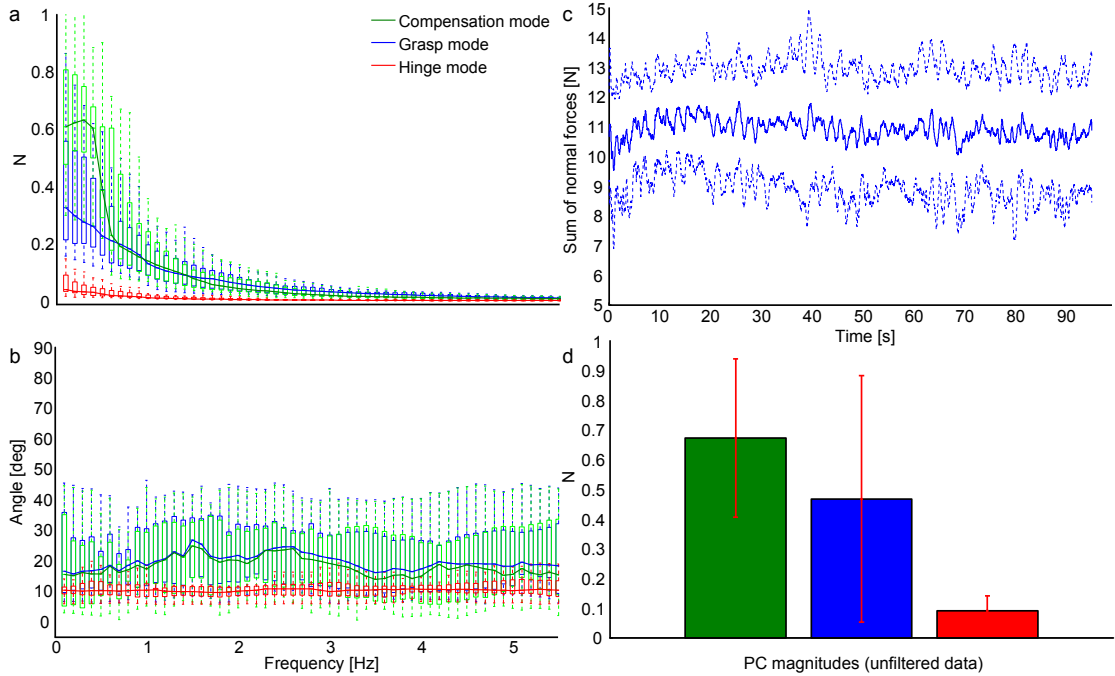


Figure 5.11: a. Force mode magnitudes vs. frequency in the index-middle finger alternating normal force task (control task 2). Since in this task production of alternating index and middle fingers was encouraged, not surprisingly, we see a large contribution from the compensation mode. There was no motion component in this task and yet, the grasp force contribution near the task frequency of 0.5 Hz (vertical red dashed line) is quite considerable, too. b. Measured force mode directions are in agreement with the simulation directions. c. The visual feedback was not explicitly given on the 10 N target force, but the sinusoids that mimicked the thumb force compensation mode. Hence, greater error on the target force is to be expected, but also a reduced need to correct via the grasp mode. d. While the magnitudes of force mode variability computed from the unfiltered data is approximately twice of that observed in the Original Task, the order of force modes in terms of magnitude and their relative magnitudes are preserved.

5.5 Discussion

While it is clear that the human nervous system has distinct adaptations that enable dexterous manipulation - a functional hallmark of our species-, we demonstrate that multifinger manipulation exposes strong limitations even for ordinary and ecological tasks requiring the simultaneous control of individuated finger motion and force, such

as unscrewing a bottle cap. We systematically explored the potential confounds that could explain our results of unnecessary grasp-and-release force variability pervading the Original Task of holding the object while reconfiguring the grasp. Now we discuss why we can now confidently argue that the underlying cause of such pervasive Grasp Mode variability is likely a context-sensitive coupling in the actual drive to the alpha motoneuron pools across fingers. Moreover, our control experiments and numerical simulations, when put in the context of seminal work by human neuroanatomists, help interpret those limitations as consequences of evolutionarily vestigial properties of cortical projections to hand muscles. We speculate that the results reveal strong competition between descending commands to grasp vs. manipulate, likely driven by competition between the phylogenetic older reticulospinal vs. the newer corticospinal tracts. This suggests that, for all its neuro-musculo-skeletal uniqueness and versatility, the healthy human hand critically depends on maintaining a delicate balance between competing descending commands. This may explain the disproportionately severe disruption of manipulation after neurological injury such as stroke, or even with healthy aging.

We begin by emphasizing that holding and reconfiguring our novel hinged apparatus defines an unstable mechanical system that requires the nervous system to generate fingertip force vectors that intersect at or close to the hinge at all times [Flanagan et al., 1999]. For a variety of magnitudes of total grasp force, the set of valid combinations of fingertip forces defines a slightly curved manifold (Figure 5.2). We provided subjects with visual feedback to produce a constant sum of 10 N of total grasp force while oscillating the thumb.

The fact that our analytical model of the task revealed the solutions to be well approximated by a linear manifold (see discussion in [Clewley et al., 2008]) both justify and motivate the use of PCA, which in turn allows us to disambiguate mechanically necessary from neurally driven variability in the experimental data [Tresch and Jarc, 2009].

Variability in the compensation mode (PC $[-1, 1, 0]^T$ in Figure 5.4) represents the instructions given to the subjects to oscillate the thumb, which results in compensatory alternating force magnitudes of the index and middle fingers as they maintain equilibrium. It is not surprising, therefore, that this PC explains the greatest variance in the data near the thumb oscillation frequency of 0.5 Hz because it is driven by the mechanical requirements of the task. On the other hand, given that the subjects succeeded at the task and did not greatly translate or rotate the object, the data exhibited the lowest variability along the hinge mode (PC $[-1, -1, 1]^T$). In fact, the mechanical requirements of the task explain both the low variability in the hinge constraint and the high variability in the compensation mode near 0.5 Hz. *Had we not modeled the analytical dynamical solution to the task, we may have been tempted to interpret the Compensation mode variability as indicative of properties of the neural controller, such as coherence modes in the control of motoneuron pools across fingers, for which there is some evidence [Schieber and Santello, 2004, Tresch and Jarc, 2009].* Contrast this to the Grasp Mode PC $[1, 1, 1]^T$, which represents unnecessary grasp-and-release force variability that is not part of the mechanical requirements of the task, which in turn leads to the population of a manifold of mechanically feasible solutions (Figure 5.4b). Its lack of mechanical relevance renders the Grasp Mode critically informative of the neural controller's performance and limitations.

5.5.1 Ruling out potential confounds

The additional six systematic control tasks, plus four simulations of mechanically driven correlations between clean and noisy fingertip forces (Table 5.1), strongly indicate that the variability along the grasp force mode cannot be attributed to signal-dependent noise and only to a limited extent - if at all - to visuomotor corrective actions along the grasp force direction at low frequencies. That is, (i) signal-dependent noise is associated with a

higher frequency band (8-12 Hz, [Jones et al., 2002]) than the one in which we observed large and unnecessary grasp force fluctuations; and (ii) the first Control Task, with the apparatus fixed to ground to abolish - by shunting to ground - any fingertip force correlations arising from reaction forces driven by signal dependent noise, exhibited the same unnecessary contribution by the Grasp Mode (Figures 5.5 and 5.9). Therefore, we conclude that signal-dependent noise in conjunction with instantaneous action-reaction mechanics cannot explain this unnecessary variability.

Secondly, simple static grasp in the fifth and sixth Control Tasks, in which a 10 N sum of normal force was to be maintained, exhibits greatly diminished variability along the Grasp Mode direction (Figures 5.5 and 5.10). This variability reflects, among other things, the corrective activity in response to visual feedback error. Its small magnitude here suggests that the much stronger presence of Grasp Mode in the Original Task is not primarily driven by the interaction with visual feedback. Importantly, Control Tasks 2, 3 and 4, involving voluntary generation of grasp and compensation forces, show that voluntary production of Compensation Mode variability leads to involuntary Grasp Mode variability, but not vice versa. We therefore conclude that the mechanically unnecessary (and potentially counterproductive?) Grasp Mode variability is of involuntary neural origin, and that such stereotypical grasp-and-release synchronous interactions pervade multifinger manipulation when the manipulation task requires individuated fingertip motions and forces.

What could be the causes of this neurally driven, context sensitive involuntary variability in the Grasp Mode? A behavioral explanation is that subjects may have simply chosen not to track the constant visual feedback in spite of our encouragement to do so. However, all subjects reported to perform the task in all conditions to the best of their ability and satisfaction with using visual feedback to explicitly help them maintain a given grasp force level (recall that we have ruled out by visuomotor corrective actions

as the main source of the Gasp Mode). Moreover, subjects are familiar with and adept at common motor tasks requiring the reconfiguration of grasp during their daily activities, such as rotating an object in the hand or unscrewing a bottle cap.

Alternatively, one can be tempted to attribute such variability to the principle of minimal intervention, giving rise to an uncontrolled manifold [Scholz and Schner, 1999, Todorov and Jordan, 2002]. Having dedicated most of its control efforts to meeting the critical constraint of not accelerating or rotating the object (hinge constraint mode PC $[-1, -1, 1]^T$) while also visibly moving the thumb (compensation mode PC $[-1, -1, 1]^T$), the nervous system may have chosen to assign the regulation of the grasp force PC $[1, 1, 1]^T$ the lowest priority. After all, varying total grasp force does not immediately lead to mechanical failure of the task and is a task variable (i.e., constraint) that might be given lower priority (i.e., an uncontrolled manifold). However, constant total grasp force is an explicit task constraint that is part of our instructions and visual feedback. In fact, Control Task 2 shows that Grasp Mode variability does not increase even when it is not an explicitly part of the instructions (i.e., demoting the relevance of the Grasp Mode does not increase it). Conversely, Control Task 1 shows that Grasp Mode variability is not decreased when the object is attached to ground either, even though there is no concern of dropping the object or involuntary slip-grip response. Therefore, the observed Grasp Mode variability arguably does not reflect controller prioritization la minimal intervention or uncontrolled manifold.

5.5.2 Grasp Mode variability reveals fundamental challenges to controlling dynamic multifinger manipulation

This leads to the intriguing third explanation that manipulating an object while dynamically reconfiguring the grasp is challenging enough to expose limitations in the neuro-muscular control of multifinger manipulation. That is, when performing certain multifinger tasks requiring individuated finger actions to meet multiple requirements (i.e., maintaining hold of an object while also reconfiguring the grasp), the nervous system is physiologically bound to violate some task constraints. We see this here as a pervasive Grasp Force variability. This is quite different from choosing to prioritize some task constraints as in the first two explanations above. In fact, this agrees well with other work with single fingers, where even ordinary manipulation tasks can push the neuro-muscular system to its limit of performance when they require combinations of, or transitions between, motion and force constraints [Venkadesan and Valero-Cuevas, 2008, Keenan et al., 2009]. Thus we are compelled to conclude that, when manipulating an object with individuated finger actions such as dynamically reconfiguring the grasp, the neural controller must carefully and continuously overlay individuated finger actions over unavoidable and mechanically unnecessary, yet strongly structured, synchronous interactions.

This superposition of the Grasp Mode should not be confused with the notion of functional coupling as in the context of the principle of superposition [Gao et al., 2005]. In that functional superposition, necessary internal forces (such as the grasp forces) are coupled to manipulation forces (required to accelerate an object) in a simultaneous, appropriate, and intentional fashion. Such coupling is determined by the goals of the task, such as the simultaneous increase of grip and load force to prevent slip, or deceleration forces at the extreme points of an oscillating motion. Here, in contrast,

we showed that our multifinger manipulation task is unavoidably accompanied by functionally unnecessary (and even inappropriate) synchrony across fingertip forces. This pervasive synchrony is neither an epiphenomenon of the task nor a desired feature of the task.

In fact, in agreement with [Schieber and Santello, 2004] who review the literature on peripheral and central limitations of multifinger manipulation, we argue that the nervous system has to superimpose finger individuation over a propensity to modulate fingertip forces in synchrony. A potential explanation for this is the emerging picture from seminal and recent work [Donald and Kuypers, 1968, Lang and Schieber, 2004, Lemon, 2008]; for a review, [Baker, 2011]) on different neural pathways that project on hand motoneuronal pools and segmental interneurons. The divergent projections to flexor muscle motoneuronal pools by the rubrospinal tract seem to be in competition with inhibitory corticospinal projections [Riddle et al., 2009]. Thus, the constant presence of the Grasp Mode perhaps reflects the inability of the (evolutionarily younger?) corticospinal tract from the neocortex to completely override projections from the reticular formation (one of the phylogenetically oldest portions of the human brain [Ranson, 1953]). Thus the strongly structured stereotypical interactions that pervade voluntary dynamic multifinger manipulation may be the modern echoes of an evolutionarily vestigial tendency for grasp so critical to brachiation or early tool use [Donald and Kuypers, 1968, Baker, 2011]. As a consequence, the human hand might not have enough neuromechanical, as opposed to strictly mechanical, degrees of freedom to meet both the constraints of grasp (i.e., holding the object steadily against gravity) and manipulation (i.e., reconfiguring the grasp).

This interpretation that, in spite of its complexity and redundancy, a neuromuscular system can run out of neuromechanical degrees of freedom if the task is sufficiently demanding has been proposed elsewhere (see,

e.g., [Loeb, 2000, Venkadesan and Valero-Cuevas, 2008, Keenan et al., 2009, Kutch and Valero-Cuevas, 2011]). That is, in spite of the evolutionary adaptations and apparent versatility and redundancy of the human hand, our results strongly suggest that the human hand has barely enough neuromechanical degrees of freedom to meet the multiple simultaneous mechanical demands of ecological tasks. This helps explain the apparent paradox [Keenan et al., 2009] that, for all the neuromechanical redundancy of the human hand, multifinger manipulation is susceptible to even mild neurological conditions, takes years to develop in childhood, and degrades in healthy with aging.

Chapter 6

Prenatal Motor Development Under Different Incubation Periods Affects Postural Control in Domestic Chick

6.1 Abstract

Domestic chicks walk within 3-4 hr after hatching following 21 days of incubation. However, differences in light exposure can significantly extend the incubation range (20 to 22 days). Based on observations that differences in incubation duration do not affect morphological measurements such as weight, height and tibial bone length, we hypothesized that chicks hatch when they are sufficiently mature to cope with the environment. However, we recently found differences in some gait measures suggesting postural control at hatching may be more advanced by light exposure during embryogenesis, so in this study we further test for potential differences and reconsider our hypothesis. Employing 3 light exposure conditions established in our earlier study and robot-assisted posturography methods, we report significant differences in several indicators of postural control as evidence that light exposure during embryogenesis advances maturation of control. Hatchlings experiencing the greatest light exposure during embryogenesis exhibited the least sway area, mean speed and distance from the center-of-pressure centroid during quiet stance. Further, when posture was randomly perturbed during quiet stance, they also recovered postural stability significantly more rapidly than hatchlings

exposed to less or no light during embryogenesis, as indicated by the fastest attenuation of perturbation-induced sway oscillations. Although all groups exhibited general postural competence, consistent with our original hypothesis, we conclude that environmental light during development not only accelerates morphogenesis but that it can also impart a developmental advantage. These findings offer new important considerations relevant to debate regarding the impact of prenatal and postnatal conditions on the development of the human fetus and infant.

6.2 Introduction

The ongoing debate on the influence of light on neonatal development and maturation during intensive care [Miller et al., 1995, Brandon et al., 2002] necessitates the testing of relevant hypotheses in a suitable animal model: in particular, the domestic chick has proved useful addressing questions of motor control development. Within a few hours after hatching, domestic chicks (*Gallus gallus*) are capable of walking, standing and resisting perturbations to quiet stance. Furthermore, chicks typically hatch at 21 days of incubation [Romijn and Roos, 1938, Hamburger and Hamilton, 1992, Noy and Sklan, 1997] but the duration of incubation can be modulated through differential light exposure. In particular, continuous light exposure will accelerate hatching, while the continuous absence of light will decelerate it, each by up to one day [Shutze et al., 1962, Siegel et al., 1969, Lauber, 1975, Ghatpande et al., 1995, Fairchild and Christensen, 2000]. Importantly, the differences in light condition and thus in incubation duration do not affect the viability of hatchlings, compared to natural conditions [Lauber and Shutze, 1964]. More specifically, morphological measures such as body weight and height and tibia bone lengths show no significant differences across conditions [Sindhurakar and Bradley, 2010]. Together, these features make chicks a

valuable model for examining the impact of light on locomotor development, since observed differences can clearly be attributed to the interplay between the nervous system, muscles and mechanics, rather than mechanics in itself.

While it is known that light exposure accelerates morphological development, among other things, by increasing the number of nuclei in the chick blastoderm [Ghatpande et al., 1995] or increasing early body weight [Lauber, 1975], and modify posthatching behavior, such as increasing the rate of feather picking between hatchlings [Riedstra and Groothuis, 2004] and attack and copulation behaviors [Zappia and Rogers, 1983], it is currently unknown if light exposure has an effect on the development of locomotor competence. On the other hand, it is known that critical neurodevelopmental events occur very shortly prior to hatching. For instance, electromyographic (EMG) and kinematic studies of leg movements during embryonic motility have provided evidence that circuits involved in locomotor control are established 1-3 days pre-hatching [Bradley et al., 2005, Bradley et al., 2008, Ryu and Bradley, 2009]. However, light seems to have little or no influence on these components of development, since intralimb EMG patterns for stepping have been shown to be expressed even in the absence of sensory or descending inputs [Jacobson and Hollyday, 1982, Bekoff et al., 1987, Bekoff et al., 1989]. Our study extends and complements previous kinematic and EMG studies of locomotor development in chicks by providing the first analyses of postural control and postural stability parameters, commonly used in human posture analysis, on the day of hatching. Our primary goal in this study was to determine if the maturation of postural control is affected by different light exposure conditions during incubation. Based on our previous kinematic study of the influence of incubation light on chick gait parameters, which found no differences between conditions as well as other studies, indicating that intra- and interlimb coordination are well established within the first day after hatching [Jacobson and Hollyday, 1982,

Johnston and Bekoff, 1992, Johnston and Bekoff, 1996], we predicted that there would be no differences in our current study. Surprisingly, the kinetic and more sensitive analysis of quiet stance and stance perturbation response showed significant differences across the three conditions, with chicks spending the shortest time inside the egg exhibiting the best stabilization performance. These results indicate an influence of incubation light condition on the development of motor skills and cast doubt on the assumption that by the time of hatching, all chicks are equally competent.

6.3 Methods

6.3.1 Subjects

We obtained fertile Leghorn chicken (*Gallus gallus*) eggs from a local hatchery and incubated them in force draft, humidified incubators at standard temperature (37.5°) and humidity (62%). Prior to the onset of incubation, we weighed the eggs and randomly assigned them to 1 of 3 incubators modified as described below. Onset of incubation was considered embryonic day E0. We moved all eggs to nonrotating shelves within the same incubator 3 days before anticipated hatching. We examined the eggs at 2 hr intervals thereafter to determine the approximate time of pipping, a crack in the shell indicating the onset of hatching, and when hatching was completed. After hatching, we weighed the chicks and moved them to a brooder (47 cm x 47 cm x 20 cm). Hatchlings were trained for and tested in only 1 of the 2 experiments of this study. All training and testing procedures were completed within 24 hours of hatching. At the end of data collection, we euthanized the animals. All procedures were approved by the University Institutional Animal Care and Use Committee.

6.3.2 Incubation Conditions

Standard industrial incubators were modified to house fluorescent lighting and/or to eliminate external sources of light without disrupting internal temperature and humidity. Fertile eggs were maintained throughout embryogenesis in a single incubator adapted to provide continuous light exposure 24 hr daily (24 L) at 4,000 - 7,000 lx; 12hr light exposure daily (12L) at 650 - 3,000 lx; or continuous dark exposure 24hr daily (24D) at \leq 1lx. The range in light intensities indicate the variation in luminance at the egg shell as the incubator shelf automatically rotated in 2 hr intervals, alternately placing the egg closer to or further from the light source (Figure 6.1).

6.3.3 Acceleration of embryogenesis through light exposure

The average duration of embryogenesis in domestic chicks (*Gallus gallus*) is 21 days. In a recent study we established 3 light exposure conditions that significantly varied the length of incubation [Sindhurakar and Bradley, 2010]. Bright light exposure throughout embryogenesis (24L conditions) reduced incubation to 20 days, whereas 12L conditions resulted in hatching at 21 days, and absence of light exposure lengthened incubation to 22 days. An array of light conditions similar to 24L exposure was also employed in earlier studies and was shown to significantly accelerate embryogenesis [Siegel et al., 1969, Lauber, 1975, Coleman and McDaniel, 1976, Ghatpande et al., 1995]. We selected 12L condition to approximate periodic indoor/outdoor light exposure during normal embryogenesis and 24D conditions as a control for light exposure.

6.3.4 Quiet Stance Training

Within 2-4 hours of hatching chicks were trained to stand upright on a platform similar to the force platform. Chicks were encouraged to stand upright without taking steps

or sitting down for at least 30 seconds at a time. If they made an attempt to escape or sit, the experimenter intervened to discourage the behavior. After each trial of training they were allowed to rest for few minutes. This procedure was repeated until the chicks stood upright without any interruptions. It typically took 3-5 trials per chick to complete the training regardless of the incubation condition. Young hatchlings are frequently distracted by the environment so the training procedure was conducted in a quiet room with dim lights. Further, hatchlings are susceptible to shivers at room temperature, which is not only uncomfortable for the chicks but also an undesirable behavior with regards to acquisition of postural control data as it might introduce noise. Thus, the training area was warmed up with a space heater. Animals were tested within 2-4 hours of training and data from the animals that were uncooperative after 2-3 trials were excluded from analysis.

6.3.5 Data collection

Quiet stance experiments

In our first experiments we sought to quantify static postural stability by recording forces during quiet stance. To collect forces applied during quiet stance, we designed and built a force platform (Figure 6.2): two square-shaped boards made from ASB material (10 cm x 10 cm x 0.9 cm) were screwed together from above and below to a 6-axis ATI Nano17 force transducer (ATI, Apex, NC). The platform surface was covered with sandpaper to minimize slippage of the feet, as the animals movements were unconstrained and to protect the load cell from dirt. We also sought to minimize postural noise due to distractions during recordings by designing a wall, consisting of four sheets made from ASB material (9 cm x 5 cm) that surrounded the chick and was mounted on the force platform. For the static postural control experiments, we collected 1 to 6 trials per chick,

with each trial of 30 s in duration. We recorded fewer than 6 trials if the chick stopped behaving or fell asleep repeatedly. Because chicks occasionally fell asleep or ceased to cooperate, care was taken ensure that we only collected data from awake chicks that maintained upright stance. We collected quiet stance trials for 10 chicks per incubation condition, for a total of 30 chicks.



Figure 6.1: The incubator. Note that the surface holding the eggs was rotated at 2-hour intervals to ensure equal light exposure.

Stance perturbation experiments

In our second experiments we sought to quantify dynamic postural stability by recording forces during random perturbations of quiet stance. For these experiments, we mounted the same force plate as in the quiet stance experiments onto the end-effector of an Adept6 300 6-degrees-of-freedom robot arm (Adept, Pleasanton, CA), where the robot can be seen in its "home" configuration, that is, its configuration prior to applying a perturbation to the force platform. The robot control software was implemented in the Adept V+ language. We used a tcp/ip client-server connection between the robot controller and a

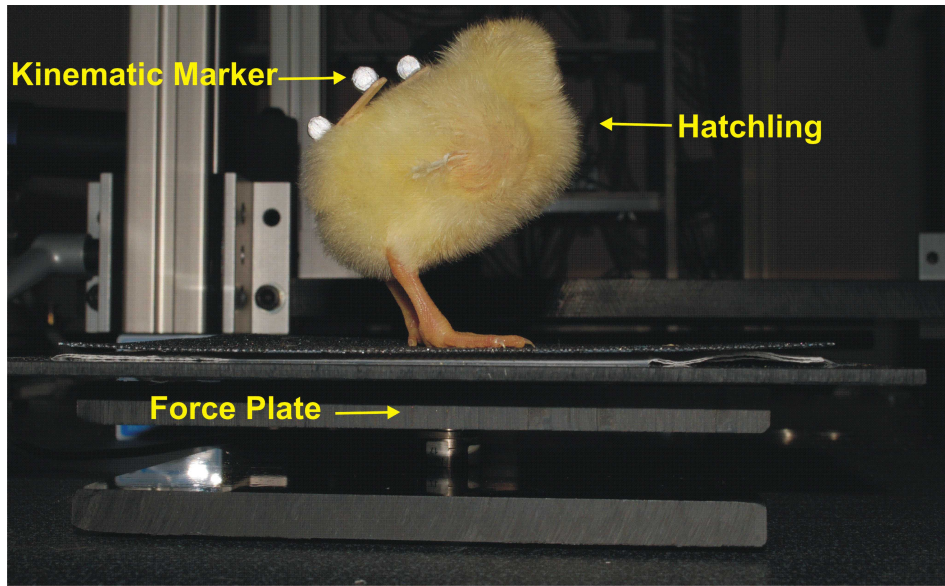


Figure 6.2: Chick on force platform. The stance platform, made from ASB material, was mounted on a ATI Nano17 force sensor. The chick was standing on a sheet of sand paper, to increase stance stability.

desktop computer to trigger perturbations from within MATLAB (Natick, MA) software we designed for data acquisition. Every 10 s, we applied a perturbation along 1 of 8 randomly selected directions in the horizontal plane at random amplitudes ranging from 0 to 25 mm. The randomized directions were drawn from a discrete uniform distribution, while the randomized amplitudes were drawn from a discretized normal distribution with standard deviation 15 mm (based on our quiet stance results). Using a mean-zero normal distribution for amplitudes effectively interspersed sham perturbations to prevent chicks from anticipating the next perturbation trial. While the maximum force platform velocity was kept constant at 2500 mm/s, the acceleration profile consisted of a step input, followed by a very slow deceleration until the final position was reached. The final position was maintained for 2 seconds, before returning the robot to its "home" configuration. Robot movement did not exhibit extraneous oscillations. We performed a total of 29 perturbations within a 5 min test session and conducted 3-4 test sessions to

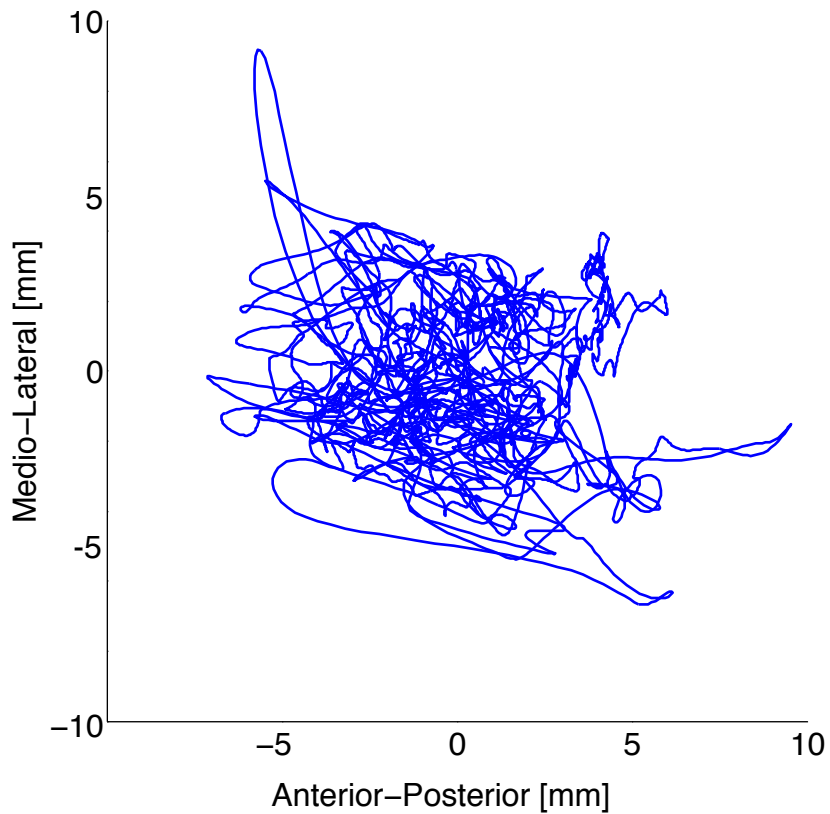


Figure 6.3: Sample 30 s center-of-pressure dynamics of one 24L chick. Coordinates are rotated so as to align with the major (anterior-posterior) and minor (medio-lateral) axes of sway.

obtain a potential sample of 87-116 perturbations. We videotaped all perturbation trials, to estimate post-trial the direction of each perturbation relative to postural orientation, because chicks typically moved about the platform during the test session. We selected perturbations for data analysis, those trials when chicks did not take a step or sit down for 1 s immediately before and after the perturbation. We successfully tested 12 chicks from 24L conditions, 11 chicks from 24D and 12 chicks from 12L conditions.

6.3.6 Data processing

We sampled force data at 1000 Hz and then down-sampled to 100 Hz for subsequent analyses. For classical posture analysis methods and analyses of stance perturbation responses the data were low-pass filtered using a 4th order bidirectional Butterworth filter with the cut-off frequency at 20 Hz and 5 Hz, respectively. However, data were left unfiltered for the drift-diffusion approach discussed below.

The x and y coordinates for center of pressure (COP) data were computed from the forces applied to the force platform as follows, for the n-th sample:

$$\begin{aligned}x[n] &= -\frac{M_y[n] + cF_x[n]}{F_z[n]} \\y[n] &= \frac{M_x[n] - cF_y[n]}{F_z[n]}\end{aligned}$$

Where $M_y[n]$ is the y moment applied to the force sensor, while $F_x[n]$, $F_y[n]$ and $F_z[n]$ are the three force components as measured by the force transducer, and c is the thickness of the force platform that was attached to the force transducer (here, $c = 9$ mm).

It was not possible to guarantee that chicks assumed identical stance orientation across trials. Therefore, we performed the subsequent data analysis not with respect to the force sensor coordinate system but instead, rotated the coordinate system so as to align with the chicks major and minor axes of sway (denoted MA and MI below). To this end, we performed Principal Components Analysis (PCA) to identify the two axes of sway directly from the COP patterns. For improved robustness, we computed the PCA on the time series of COP increments $\Delta x = x[n+1] - x[n]$, which is stationary, rather than directly on the COP data, where estimation can be affected by data clustering. For an example of the rotated COP time series, see Figure 6.3. Since PCA requires

subtraction of the mean from the data, the major and minor axis components represent the distances from the data mean along their respective associated directions.

6.3.7 Center of pressure dynamics analysis: classical approach

In [Prieto et al., 1993], a variety of metrics applicable to center of pressure measurements in humans are described. We applied the following three metrics to the chick COP measurements:

Mean distance:

$$d = \frac{1}{N} \sum_n [MA[n]^2 + MI[n]^2]^{\frac{1}{2}}$$

Mean speed:

$$v = \frac{1}{T} \sum_n [(MA[n+1] - MA[n])^2 + (MI[n+1] - MI[n])^2]^{\frac{1}{2}}$$

Sway area:

$$s = \frac{1}{2T} \sum_n |MA[n+1] \cdot MI[n] - MA[n] \cdot MI[n+1]|$$

Where n refers to the current data sample, N to the total number of samples recorded in the trial, while T is the total duration of the trial, hence $T = 30$ s. We restrict ourselves to reporting the results for the three most meaningful metrics, although most of them showed significant differences.

Center of pressure dynamics analysis: drift-diffusion approach

Assuming that the dynamics of a given system can be described by a Langevin equation [Kantz and Schreiber, 2004]:

$$\frac{\delta x}{\delta t} = f(x(t)) + g(x(t))\epsilon(t)$$

where x represents the state of a system, $x \in R^N$, while $f(x)$ describes the deterministic dynamics of the system. $g(x)$ scales, in a state-dependent way, the normally distributed noise ϵ , where $\epsilon \sim N(0, 1)$ and correlation function $E[x(t)x(t')] = K\delta(t - t')$. Due to the stochastic forcing $g(x(t))\epsilon(t)$, the state $x(t)$ follows a probability distribution $p(x, t)$, whose (deterministic) time evolution can be shown [Kantz and Schreiber, 2004] to be described by the Fokker-Planck equation, assuming the Markov property:

$$\frac{\delta p(x, t)}{\delta t} = -\frac{\delta}{\delta x}[D^1(x, t)p(x, t)] + \frac{\delta^2}{\delta x^2}[D^2(x, t)p(x, t)]$$

Where we refer to D^1 as the *drift* coefficient and to D^2 as the *diffusion* coefficient. $D^1(x, t)$ describes the state-dependent change in the mean of the probability distribution $p(x, t)$ at time t , while the diffusion term $D^2(x, t)$ describes the state-dependent change in the variance of $p(x, t)$ at time t . Since the stochastic forcing $g(x(t))\epsilon(t)$ in the Langevin equation is normally distributed, the Fokker-Planck equation fully captures the dynamics of this stochastic system with Markov property. If there were no stochastic forcing, the drift term $D^1(x, t)$ would be equivalent to the description of a deterministic system.

A novel approach for determining drift D^1 and diffusion D^2 from time series data, in particular, posture-related data, was proposed in [Gottschall et al., 2009]. The drift coefficient can be computed as follows:

$$D_i^1(x) = \langle x_i(t + \Delta t) - x_i(t) \rangle|_{x(t)=\mathbf{x}_{ref}}$$

In other words, by finding the average change in state x during a time interval Δt , and across all data samples in a suitably chosen neighborhood of a reference state x_{ref} . Next, the diffusion coefficient is computed as follows:

$$D_{ii}^2(x) = \langle (x_i(t + \Delta t) - x_i(t))^2 \rangle|_{x(t)=\mathbf{x}_{ref}}$$

I.e. by taking the average of the square of the change in state during a time interval Δt near the state x_{ref} . States can then be mapped to both the computed drift and diffusion coefficients, and polynomials fitted to this mapping. Finally, we can compute comparative statistics on the coefficients of these polynomials to quantify differences between conditions and to infer control strategies.

6.3.8 Center of pressure dynamics analysis: perturbation response

For every successful perturbation, as described above, we computed the mean m in terms of the x and y coordinates of the pre-perturbation COP time series. This mean served as the reference point for the computation of Euclidean distance ($D([n] = \sqrt{(x[n] - m_x)^2 + (y[n] - m_y)^2})$, which we used for the subsequent data analysis. We chose to analyze the dynamics of the Euclidean distance rather than those of the x and y coordinates, since it was not possible to estimate major and minor axes of sway for such short duration events. In successful perturbations, the response generally followed a

profile that consisted of two successively smaller peaks, reflecting the oscillatory nature of the perturbation response (Figure 6.4). We extracted the following metrics:

Time of first peak: $n = \arg \max_k(D[k])$

where k is the data point time index relative to the time of perturbation application.

This metric is based on the assumption that neuromuscular activity can modulate the oscillations that are purely due to mechanics; a relatively smaller n would reflect a faster response.

Magnitude of first and second peaks: $m_1 = \max_k(D[k]), m_2 = \max_k(D[k]), k > n$

Together with the previous metric, this represents the degree of preparedness of the chick and its ability to counteract perturbations.

Ratio of second and first peak: $\frac{m_2}{m_1}$

This metric quantifies how effectively the chick can attenuate the perturbation-induced oscillations.

Time difference between first and second peak: $d = t_2 - t_1$

Where a smaller difference corresponds to a higher oscillation frequency, which in turn can indicate a faster response.

Ratios of first peak or second peak and perturbation amplitude: $r = m_{1,2}/p$

This metric's value corresponds to the chick's ability to absorb a perturbation.

6.3.9 Statistical Analysis

Since the resulting distributions of these all metrics, for both the quiet stance and the stance perturbation experiments were found to be non-normally distributed by inspection of P-P and Q-Q plots, we applied Kruskal-Wallis tests to determine differences across all three incubation conditions and Mann-Whitney U tests for pairwise differences as these statistical tests are suitable for non-normal distributions. The statistical significance level was set to $p < .05$. We tested for the effects of light condition on the

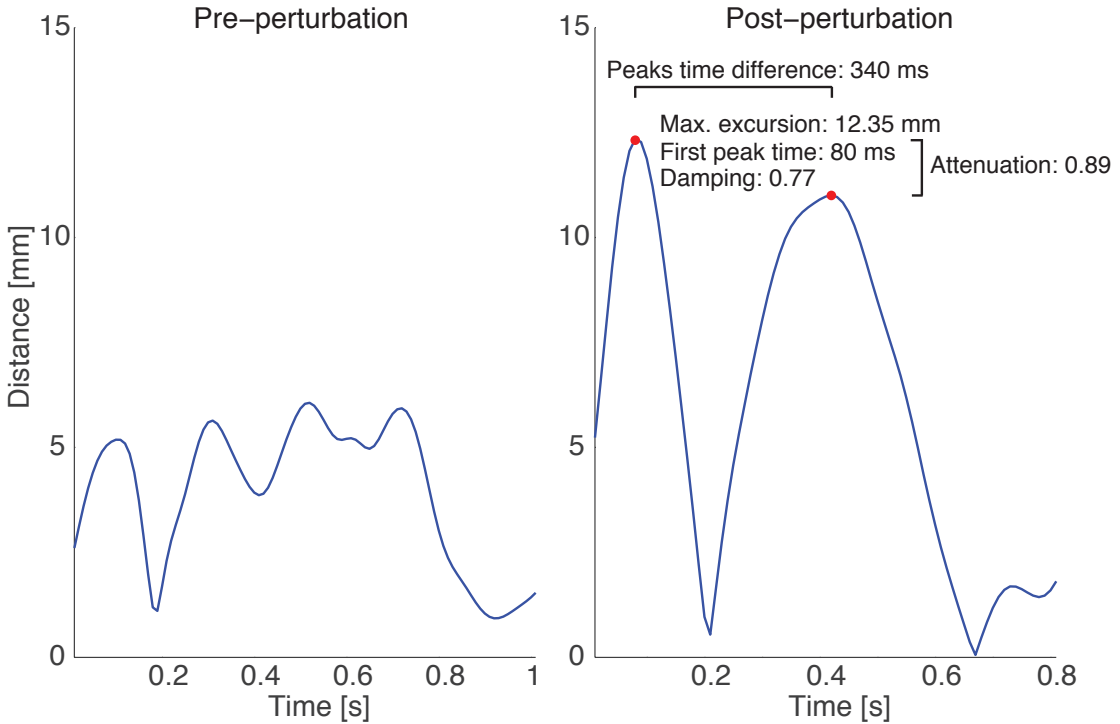


Figure 6.4: Representative example of center of pressure excursion (i.e., COP vector squared) dynamics during the second before (*left plot*) and after the perturbation (*right plot*). The right plot exhibits the typical 2-peak response profile, with the second peak smaller than the first. Also shown are the metrics we computed for each perturbation. The example shown is from a 12L condition chick, experiencing a perturbation of amplitude 16 mm.

three quiet stance metrics and the seven stance perturbation response metrics, comparing between the three groups. Furthermore, to assess the influence of perturbation direction on each of the three light conditions, we repeated the statistical comparisons (two-way design) for lateral perturbation directions (45, 90 and 135°), anterior-posterior directions (0 or 180°), assuming sagittal and frontal symmetry. To assess the influence of perturbation amplitude, we compared the metrics across the three light conditions for small (≤ 7 mm) and large perturbations (> 7 mm). We chose 7 mm as cutoff was to for equal numbers of perturbations in each subsample. Individual perturbations were removed from the analysis, if the value of one of the seven metrics exceeded its distribution by more

than two standard deviations. In total, we removed 31 perturbations from analyses, 14 perturbations from 24L condition, 13 from 24D and 11 from 12L conditions.

6.4 Results

6.4.1 Quiet stance experiment

Analyses of static postural control compared forces during quiet stance under all 3 light conditions 24D (51 trials), 12L (76 trials) and 24L (50 trials). Results indicated that all 3 classic measures of sway [Prieto et al., 1993], mean distance, mean speed and sway area (Figures 6.5-6.7), were significantly different, both across conditions as well as in pairwise comparisons. In particular, hatchlings incubated in 24L conditions swayed the smallest mean distance, at the lowest speed and over the smallest sway area, whereas hatchlings incubated in 24D conditions swayed the greatest mean distance, at the highest speed and over the largest sway area. Thus there was a consistent continuum in that all parameters for the 3 hatchling groups were negatively correlated with the extent of light exposure. Similarly, the linear coefficients of the drift function and the intercept coefficients of the diffusion function are significant across all light conditions as well as in pairwise comparisons. 24L animals had the smallest drift linear coefficient and diffusion intercept, whereas 24D animals had the largest, once again showing a consistent continuum. While the classical metrics simply suggested a difference in the sway pattern across the three incubation conditions, the drift/diffusion analysis indicated, for reasons discussed below, that the 3 groups of hatchlings employed different control strategies. Since the results nevertheless do not provide an insight into the maturity of motor competence, we performed postural perturbations to test for differences in dynamic postural control.

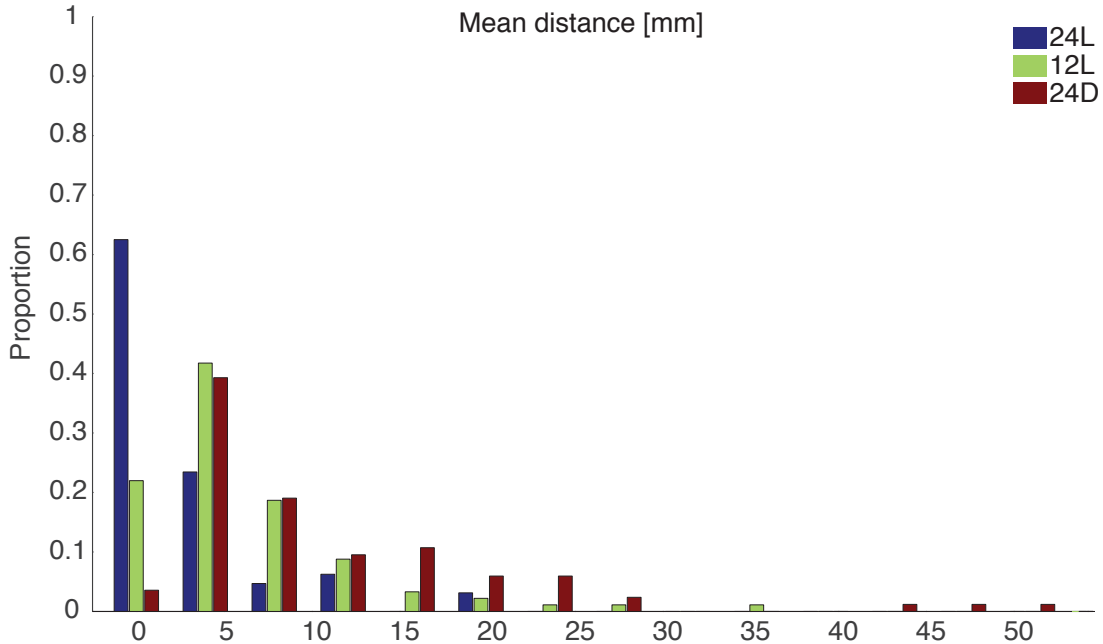


Figure 6.5: Mean distance from COP centroid distribution across the three incubation conditions. Note that while there is considerable overlap between conditions, we also observe a positive correlation between incubation duration and the magnitude of this metric, with 24D chicks exhibiting the largest mean distance.

6.4.2 Stance perturbation experiment

We recorded 586 successful perturbations in total, representing a 61% success rate for hatchlings in 24L condition; 462 successful perturbations (43% success rate) for hatchlings in 24D conditions, and 605 successful perturbations (53% success rate) for hatchlings in 12L conditions. We found significant differences across conditions in the following metrics: the amplitude of the second peak, the ratio of second and first peak amplitude, the ratio of second peak to perturbation amplitude and the area covered by the post-perturbation center of pressure (Figures 6.9-6.12). In particular, hatchlings incubated in 24L attenuated the oscillations by the largest degree, as indicated by the relatively small ratio of second to first peak magnitude. Furthermore, these chicks resisted the initial perturbation to a greater extent as evidenced by the smallest ratio of center

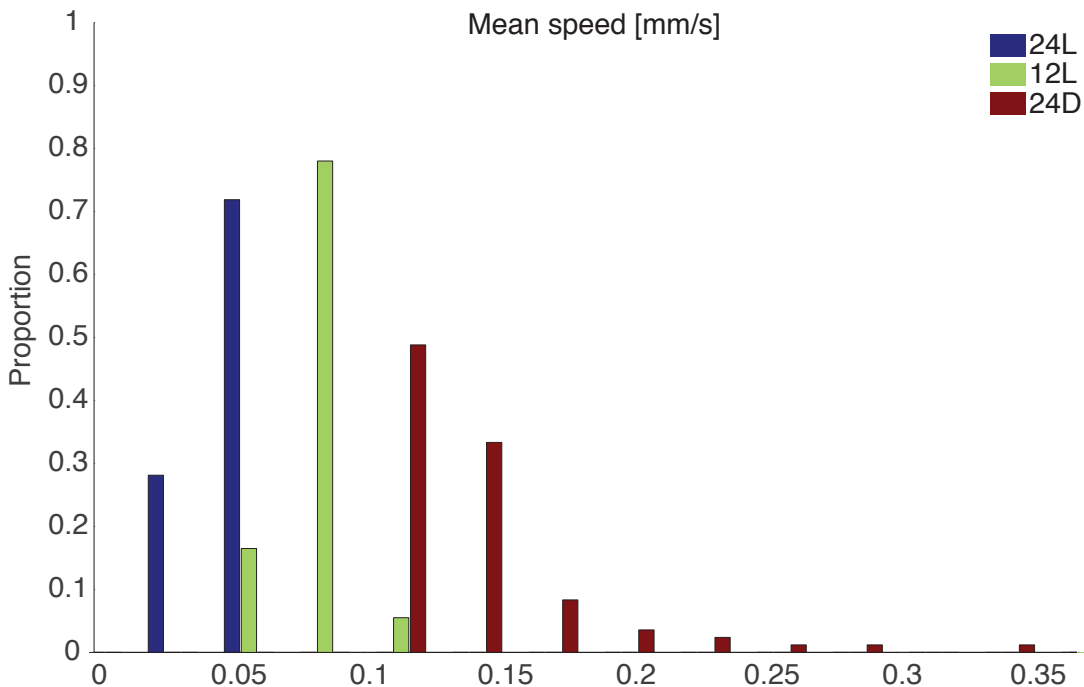


Figure 6.6: Mean speed distribution across the three incubation conditions. Unlike mean distance, the distributions for each condition are more separated, indicating the positive correlation between incubation duration and the magnitude of this metric, with 24D chicks having the largest mean speed.

of pressure maximum excursion to perturbation amplitude. As in earlier trends, hatchlings incubated in 24D conditions exhibited the greatest excursion in the second peak and the ratio of second peak to first peak amplitude. Regarding the metrics that did not exhibit significant differences: the maximum excursion value was reached at approximately the same time and the perturbation oscillations occurred at similar frequencies across hatchlings in all groups.

We then investigated the effect of perturbation direction by restricting the comparison across incubation conditions to lateral perturbations (45, 90 and 135°) and found the same significant differences as above. However, comparing anterior-posterior perturbations (0 or 180°) across light conditions, we found that the second peak excursion was

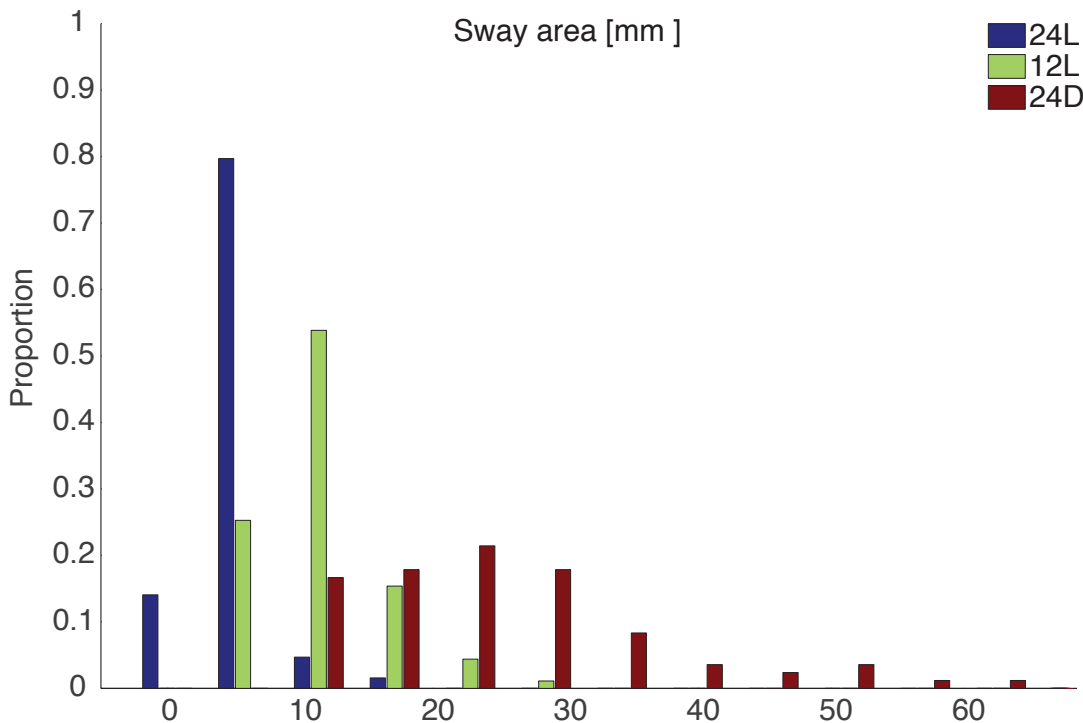


Figure 6.7: Sway area distribution across the three incubation conditions. As before, a positive correlation between incubation duration and this metric can be seen, with 24D chicks covering the largest COP area during quiet stance.

no longer significantly different across conditions. Besides perturbation direction, we also investigated the effect of perturbation amplitude, separating the data into responses to perturbations of amplitudes smaller and larger than 7 mm, and find that the above reported differences between light conditions do not change when controlling for perturbation amplitude.

6.5 Discussion

The results of this study are contrary to our null hypothesis that by the time of their hatching, domestic chicks (*Gallus gallus*) have reached a specific level of maturation that makes them equally competent at motor skills, regardless of light exposure and

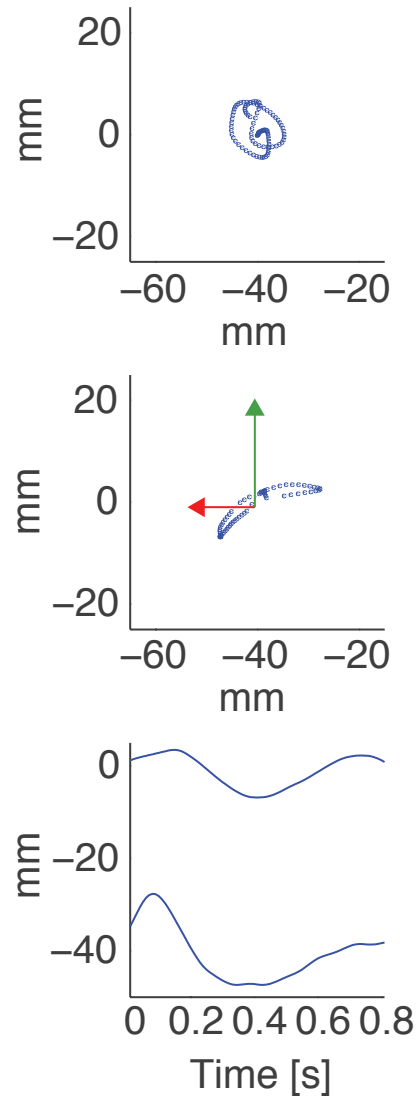


Figure 6.8: Representative example of center of pressure dynamics during the second before (top plot) and the second after the perturbation (middle plot), as well as the individual COP coordinates plotted against time (bottom plot, upper graph: y-coordinate, lower graph: x-coordinate). In the middle plot, the red arrow shows the direction of the perturbation, while the green plot shows the orientation of the chick. The example shown is from a 12L condition chick, experiencing a perturbation of amplitude 16 mm.

incubation duration. While an earlier study [Sindhurakar and Bradley, 2010] found no

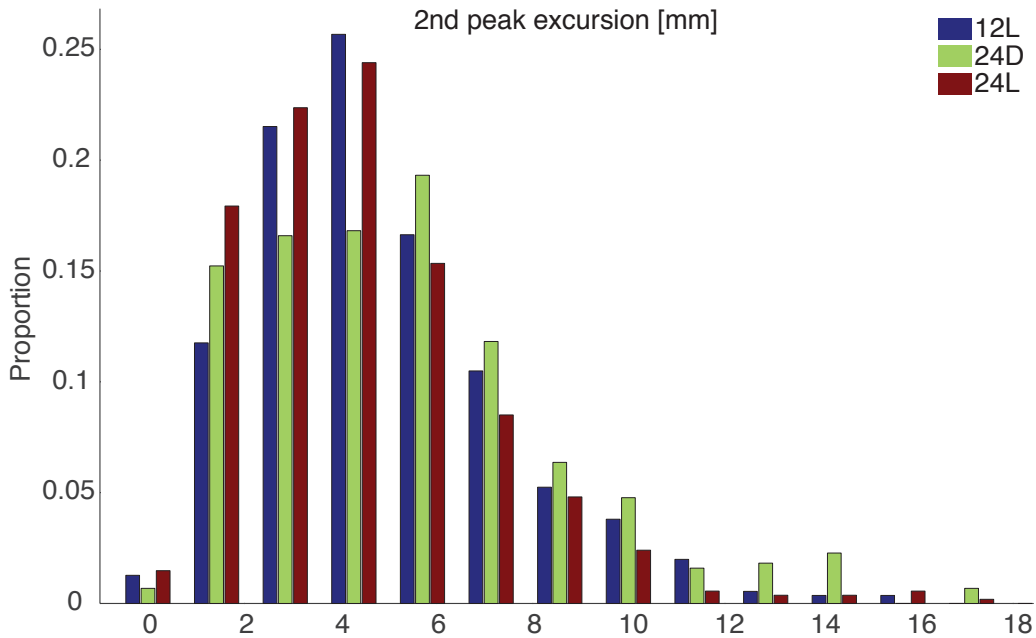


Figure 6.9: 2nd peak magnitude distribution. The values from 24L condition are most concentrated on the left.

significant differences in common gait parameters across 12L, 24D and 24L incubation light conditions, we show here that during quiet stance, light does have a significant impact on motor behavior, as measured by several common and novel metrics computed from posturographic data [Prieto et al., 1993, Gottschall et al., 2009]. Furthermore, since the quiet stance results by themselves do not allow an interpretation with regards to maturational progress, we applied force platform perturbations, using a robot. While the analysis of the perturbation response data again showed significant differences across the three conditions, they indicate, in addition, that 24L chicks return to stable stance most rapidly. This in turn suggests that under increased light exposure, the in-ovo-maturation process is improved and possibly accelerated. In the following, we will discuss and interpret the results from the two parts of the study in greater detail.

In the quiet stance experiments, chicks from the 24D condition exhibited the largest mean speed and distance from COP centroid and covered the largest sway

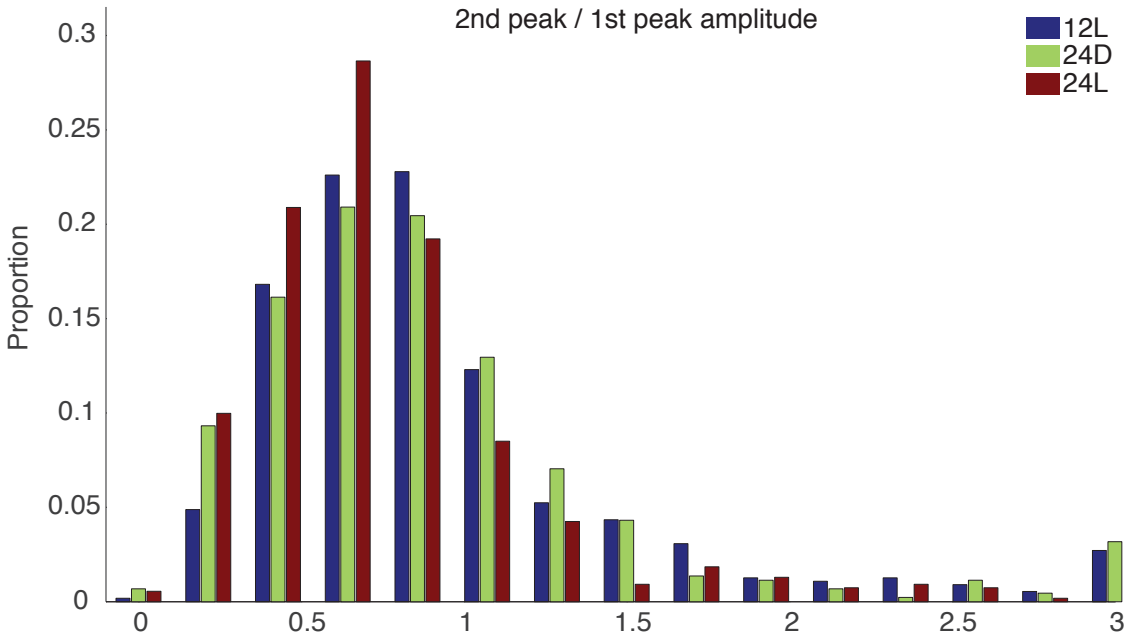


Figure 6.10: 2nd peak to 1st peak ratio distribution. The values from 24L condition are most concentrated on the left, indicating the most rapid attenuation by these chicks.

area. Traditionally, a large sway area is associated with the COP profile seen in patients suffering from neurological disorders such as paresis or Parkinson's disease [Baszczyk et al., 2007]. This would at first glance suggest that 24D chicks are the least progressed in their maturation, *despite* having had the longest incubation and thus having had the most time to develop. However, the association of large sway area and maturational deficit needs to be supported by more direct evidence. On the one hand, aging and neurological disorders lead to a greater lack of stability, as indicated by an increased fall-rate in the relevant populations [Overstall et al., 1977, Baszczyk et al., 2007]. Conversely, a larger sway area can also be indicative of superior control [Cabrera and Milton, 2004], if the objective is to minimize expenditure of computational resources - the controller would intervene only when stance reaches a critical point.

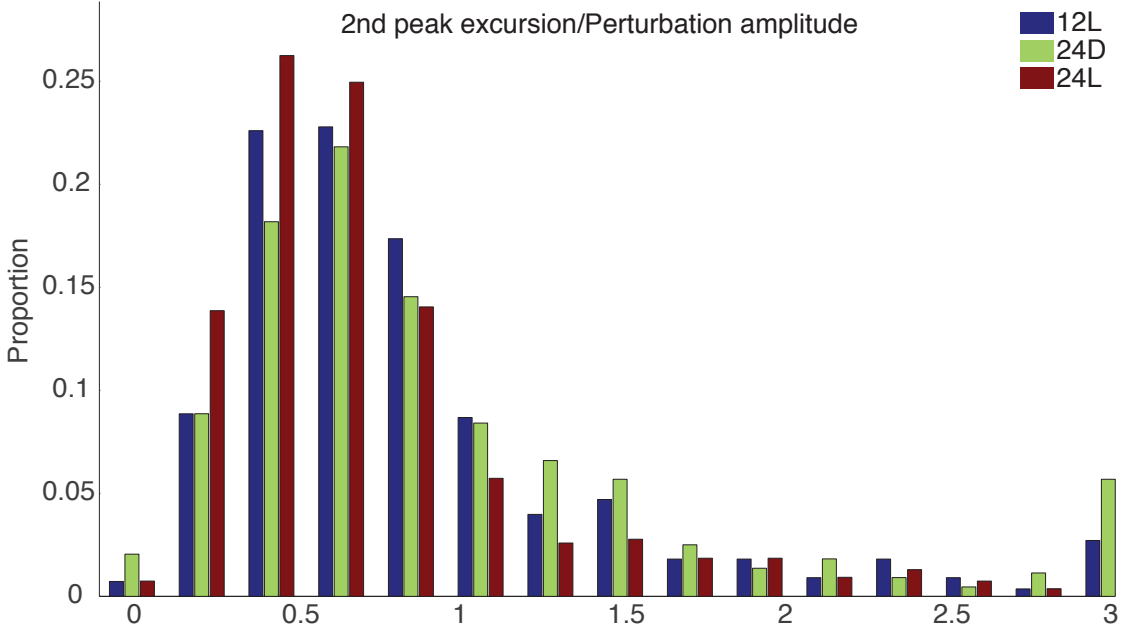


Figure 6.11: 2nd peak magnitude to perturbation magnitude ratio distribution. The values from 24L condition are most concentrated on the left, indicating that these chicks respond most effectively.

Therefore, based on the assumption that rapid attenuation of impulse-like perturbations to quiet stance reflect stabilization competence and thus the progress in maturation of motor competence, we analyzed the response to perturbations.

The lack of significant differences with regard to first peak time, peak time difference, maximum excursion and the ratio of maximum excursion to perturbation amplitude, suggests that the immediate dynamics observed after a perturbation is dominated by the purely mechanical interplay between the perturbation and the anatomy of the chick. Being morphologically equal [Sindhurakar and Bradley, 2010], chicks seem equally (un)prepared for the perturbation and reach the first peak in a similar manner. However, the later response, reflected by the properties of the second peak, is affected by the incubation condition, with 24L chicks apparently returning to a stable quiet stance most rapidly, as evidenced by the smaller magnitude of the second peak, the smaller ratio of

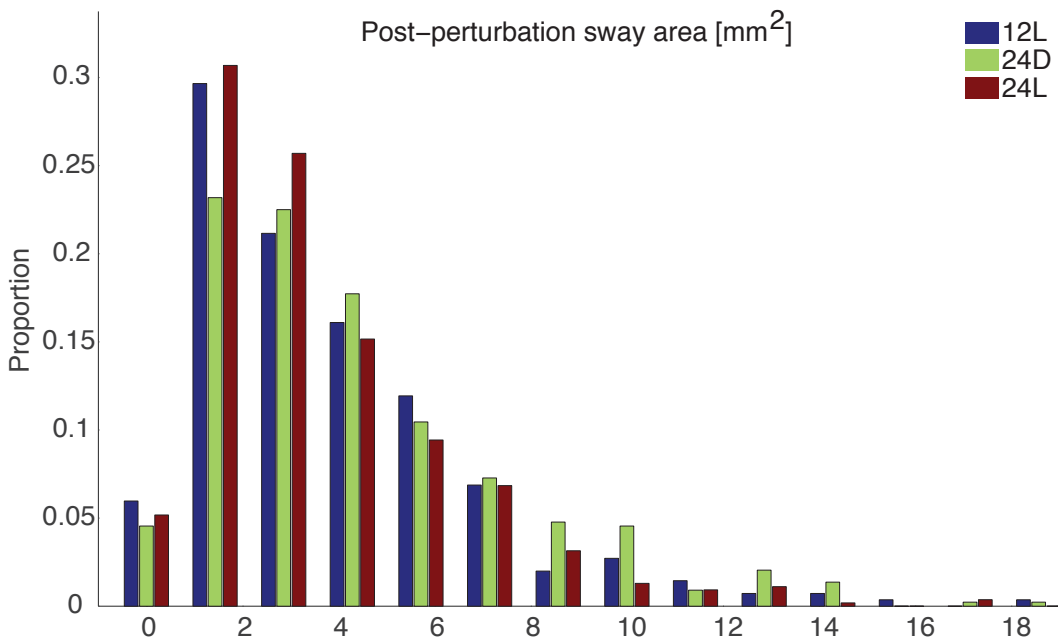


Figure 6.12: Post-perturbation sway area distribution. Chicks from 24L condition occupy the smallest area after a perturbation.

second peak to first peak and the smaller ratio of second peak to perturbation amplitude in this condition.

We conclude that by the time of hatching, chicks are not equally competent at motor skills. Instead, we assume that other developmental milestones override neurodevelopment in determining the time of hatching, thus causing chicks incubated under different light conditions to hatch at different stages of acquiring kinetic skills. Surprisingly, chicks that have spent the longest amount of time *in ovo*, 24D, appear to be the least progressed maturationally, suggesting that neuromuscular development in 24L chicks is accelerated by at least 2 days (or 10 %). We speculate that neuromuscular development is affected directly by light, which probably stimulates neurotrophic factors or encourages early *in-ovo* motor practice.

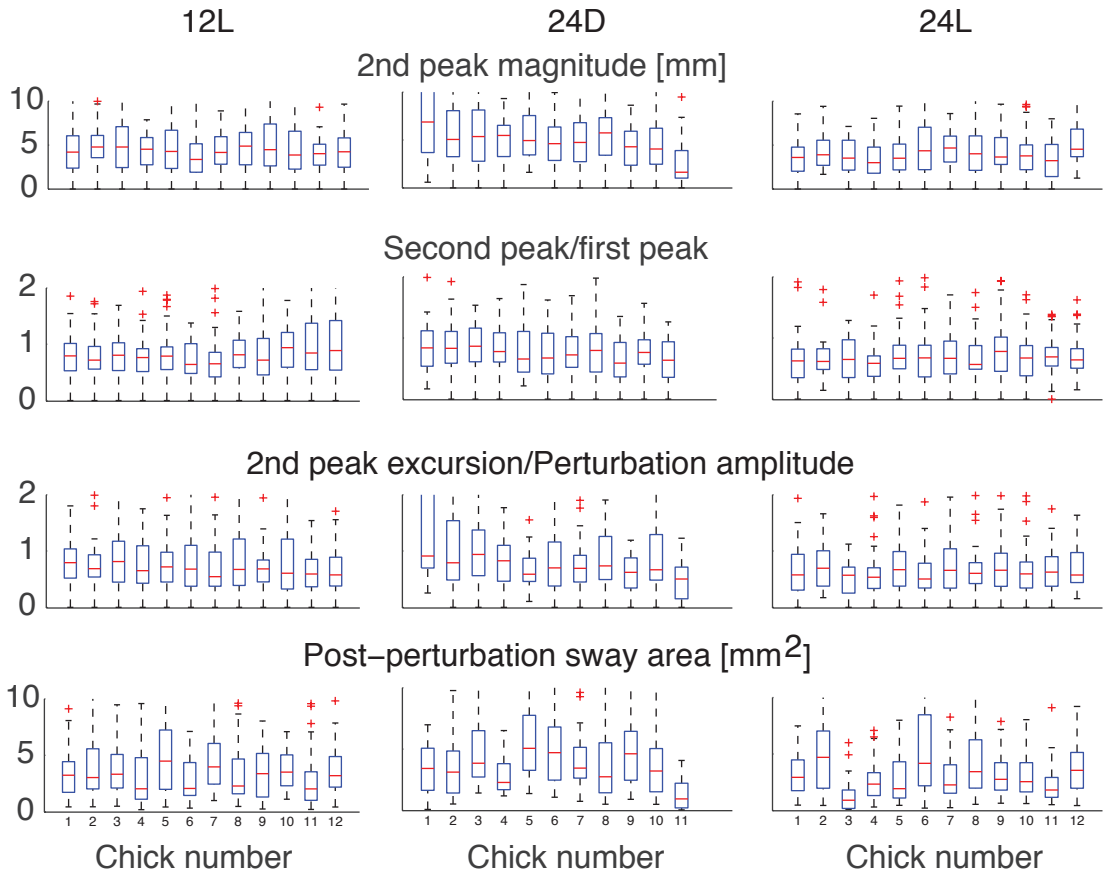


Figure 6.13: Boxplots of the metrics that were found to exhibit significant differences across incubation conditions for each chick individually. We find that chick 11 in 24D, and chicks 3 and 12 in 24L seem to exhibit behavior uncommon for their respective conditions. Removing these outliers actually enhances the difference between 24D and 24L.

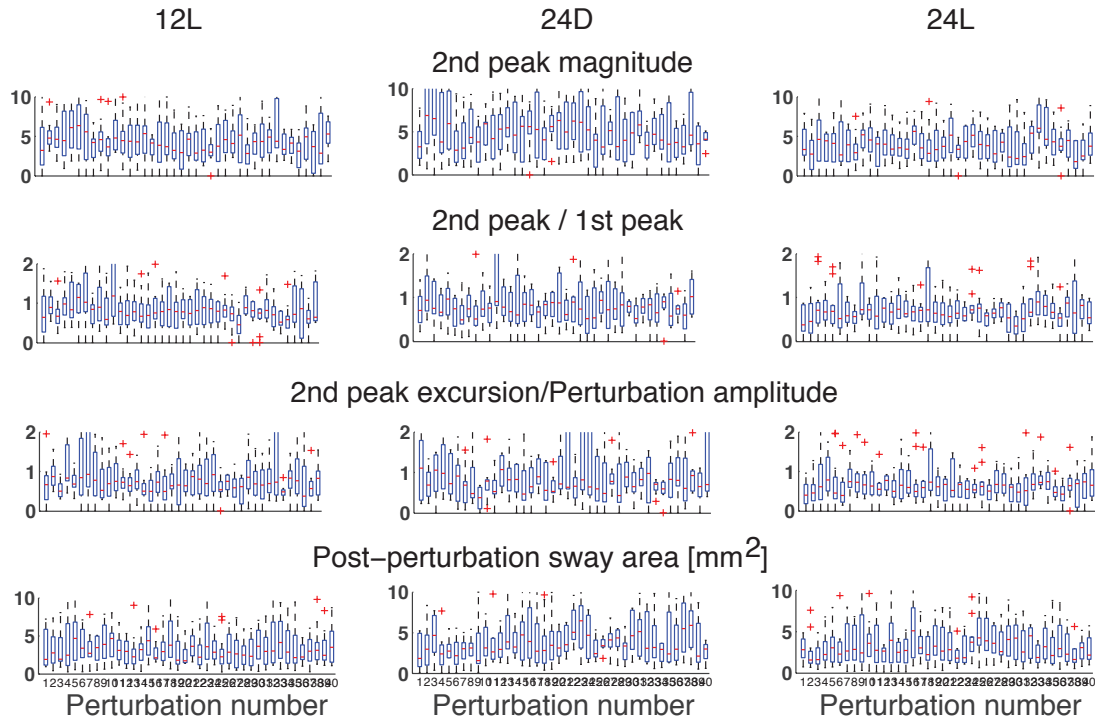


Figure 6.14: Boxplots of the metrics that were found to exhibit significant differences across incubation conditions versus the perturbation number. The lack of trends for any of the metrics indicates the absence of a learning effect.

Chapter 7

Summary and Conclusions

Having read this dissertation, I hope that the reader now understands the need for a hierarchical and successively more general view of motor redundancy, going from one level of redundancy to the next. Espousing this view aids both in the design of experiments and the interpretation of observed dynamics: for instance, it makes obvious the need to constrain the endpoint force vectors in isometric tasks to study redundancy solely at the muscle level. While this will not prevent dynamics at all more special levels of redundancy, such as motor unit redundancy, it does prevent the "leveraging" of more general redundancy levels. It can be argued that for instance, in [Danna-Dos Santos et al., 2010] not sufficient care was taken to minimize wrench dynamics in a fatiguing submaximal isometric tripod grasp. Specifically, no feedback on the tangential components of force was provided to subjects and tangential force dynamics were not analyzed, other than quantifying their mean. The authors concluded, based on fine-wire EMG measurements in 12 muscles that the nervous system employs a constant activation proportions strategy (see Chapter 2) of multi-muscle control. However, we found in Chapter 2 that following such a strategy leads to violations of the minimum tangential force constraint - in [Danna-Dos Santos et al., 2010], only a verbal encouragement was given to minimize that component. Thus, in order to enforce a synergy on the muscle level, constraints at the wrench level are by necessity violated. In conclusion, a proper design of this experiment would include feedback on the tangential component of force while a correct interpretation of the observed EMG dynamics needs to include a precise quantification of changes in tangential force.

The aforementioned term "leveraging of redundancy" implies that the nervous system takes advantage of redundancy at all levels, for instance, to mitigate effects of muscle fatigue (studied in Chapter 2 and 3) or the adaptation of tactile sensors in the skin (see below). We found here that for submaximal tasks, the nervous system not only improves its performance - in terms of endurance time - by allowing dynamics in both muscle activation and force spaces (not proportional to each other), but it is actually required to produce such dynamics for it to succeed at the motor task. Suppressing these dynamics, on the other hand, when muscle synergies are enforced, leads to immediate task failure.

We need to distinguish between necessary and optional motor redundancy dynamics. The results from the studies by Kouzaki et al. [Kouzaki et al., 2002, Kouzaki et al., 2004, Kouzaki and Shinohara, 2006] - entirely at the muscle activation level, because we cannot measure individual muscle forces - indicate that in sumaximal tasks, the nervous system goes further than just the necessary dynamics, which can be masked by the limited surface EMG resolution, in that it completely deactivates rectus femoris and the vasti in alternation, to allow for their recovery of force production ability. These optional muscle activation dynamics are very encouraging with respect to the development of medical devices that either compensate for muscle weakness or dysfunction or enhance force production in healthy humans. In a recent paper [Decker et al., 2010], it was shown that taking over the CNS' job and actively stimulating electrically, in an alternating fashion, rectus femoris and two of the vasti, in subjects with debilitating spinal cord injury significantly improved their endurance in a cycling task, compared to a protocol, where the same muscles were stimulated simultaneously. This result indicates that even the very short periods of 100 ms of deactivation allowed for muscle recovery, sufficient for task performance improvement.

Opportunities for fatigue mitigation exist at the level of wrench redundancy as well, although experimental results are currently lacking. For the task of static tripod grasp, some initial simulations suggest a benefit of varying fingertip vectors, as compared to a strategy whereby these vectors are kept constant. However, the experimentally observed dynamics (Chapter 4) of applied forces are very different: they exhibit a drift and jump behavior, whereby longer periods of slow changes (drifts) alternate with shorter periods of large changes (jumps) within the two-dimensional manifold of mechanically task-irrelevant normal force dynamics. These drift and jump dynamics are reminiscent of microsaccade dynamics, observed in another highly redundant system: vision. One suggested purpose of microsaccades is that they represent a mechanism to prevent perceptual fading, a consequence of the depletion of chemicals in photoreceptors [Skavenski et al., 1979, Rolfs, 2009]: during a "jump" event, i.e. the actual microsaccade, the sensory system switches from using one subset of photoreceptors, possibly depleted during the "drift" phase, to another subset, which is undepleted, thus allowing the previous subset to recover. Two hypotheses that emerge from this interpretation for motor systems that exhibits redundancy at the wrench level are: 1.) the drift and jump dynamics of fingertip forces serve to mitigate or prevent adaptation of tactile receptors in the fingertips by increasing and decreasing the force at each fingertip and 2.) these dynamics reflect the targeted dynamic activation of the 21 muscles actuating thumb, index and middle fingers, to mitigate fatigue and even allow recovery of some muscles. These fascinating hypotheses deserve further experimental work.

Lastly, potential benefits of redundancy have been investigated at the posture and kinematic levels as well. Most experimental studies have indeed reported kinematic changes in repeated performances of the task, such as increased coupling between arm segments or increased kinematic variability, due to repetitive movement-induced fatigue [Cote et al., 2002, Gates and Dingwell, 2008, Fuller et al., 2009]. Such fatigue

was found to be non-detrimental to task performance. Since these changes occurred long before exhaustion, it can be argued that the changes reflect a fatigue-mitigating strategy. Mathematically, the increased coupling reflects a fatigue-induced collapse of the posture solution space. Furthermore, there exist a number of modeling studies, mostly from the ergonomics research community [Ma et al., 2011], which deal with the prediction of optimal posture in a static motor task, minimizing muscle fatigue dynamically. Using a biomechanical model of the arm, with very simple dynamics of fatigue and recovery, the authors can predict fatigue and discomfort for all admissible postures and muscle activation patterns in a one-handed drilling task, and compute an optimal posture or work-rest schedule, respectively.

I conclude that there remain great opportunities for the study of beneficial dynamics at each level of motor redundancy, both in terms of modeling and experimentation. Besides, a reinterpretation of motor variability observed in previously conducted experiments, in the light of the motor redundancy hierarchy promoted here, might lead to new insights into the benefits of redundancy and the true reasons for observed failures.

Bibliography

- [Akima et al., 2002] Akima, H., Foley, J. M., Prior, B. M., Dudley, G. A., and Meyer, R. A. (2002). Vastus lateralis fatigue alters recruitment of musculus quadriceps femoris in humans. *Journal of applied physiology*, 92(2):679–684.
- [Akima et al., 2011] Akima, H., Saito, A., Watanabe, K., and Kouzaki, M. (2011). Alternate muscle activity patterns among synergists of the quadriceps femoris including the vastus intermedius during low-level sustained contraction in men. *Muscle & Nerve*.
- [Akima et al., 2007] Akima, H., Ushiyama, J., Kubo, J., Fukuoka, H., Kanehisa, H., and Fukunaga, T. (2007). Effect of unloading on muscle volume with and without resistance training. *Acta Astronautica*, 60(8):728–736.
- [Allen et al., 2008] Allen, D. G., Lamb, G. D., and Westerblad, H. (2008). Skeletal muscle fatigue: cellular mechanisms. *Physiological reviews*, 88(1):287–332.
- [An et al., 1985] An, K. N., Chao, E. Y., Cooney, W. P., and Linscheid, R. L. (1985). Forces in the normal and abnormal hand. *Journal of Orthopaedic Research*, 3(2):202–211.
- [Andersen et al., 1985] Andersen, P., Adams, R. P., Sjogaard, G., Thorboe, A., and Saltin, B. (1985). Dynamic knee extension as model for study of isolated exercising muscle in humans. *Journal of Applied Physiology*, 59(5):1647–1653.
- [Anderson and Pandy, 2001] Anderson, F. C. and Pandy, M. G. (2001). Static and dynamic optimization solutions for gait are practically equivalent. *Journal of Biomechanics*, 34(2):153–161.
- [Arnold et al., 2010] Arnold, E. M., Ward, S. R., Lieber, R. L., and Delp, S. L. (2010). A model of the lower limb for analysis of human movement. *Annals of biomedical engineering*, 38(2):269–279.
- [Avis and Fukuda, 1992] Avis, D. and Fukuda, K. (1992). A pivoting algorithm for convex hulls and vertex enumeration of arrangements and polyhedra. *Discrete & Computational Geometry*, 8(1):295–313.

- [Aymard et al., 1995] Aymard, C., Katz, R., Lafitte, C., Bozec, S., and Penicaud, A. (1995). Changes in reciprocal and transjoint inhibition induced by muscle fatigue in man. *Experimental brain research*, 106(3):418–424.
- [Baker et al., 1995] Baker, A. J., Brandes, R., and Weiner, M. W. (1995). Effects of intracellular acidosis on ca₂₊ activation, contraction, and relaxation of frog skeletal muscle. *American Journal of Physiology-Cell Physiology*, 268(1):C55–C63.
- [Baker, 2011] Baker, S. N. (2011). The primate reticulospinal tract, hand function and functional recovery. *The Journal of Physiology*.
- [Balog et al., 1994] Balog, E. M., Thompson, L. V., and Fitts, R. H. (1994). Role of sarcolemma action potentials and excitability in muscle fatigue. *Journal of Applied Physiology*, 76(5):2157–2162.
- [Baud-Bovy and Soechting, 2001] Baud-Bovy, G. and Soechting, J. F. (2001). Two virtual fingers in the control of the tripod grasp. *Journal of Neurophysiology*, 86(2):604.
- [Baylor and Hollingworth, 2003] Baylor, S. M. and Hollingworth, S. (2003). Sarcoplasmic reticulum calcium release compared in slowtwitch and fasttwitch fibres of mouse muscle. *The Journal of physiology*, 551(1):125–138.
- [Bekoff et al., 1989] Bekoff, A., Kauer, J. A., Fulstone, A., and Summers, T. R. (1989). Neural control of limb coordination. *Experimental Brain Research*, 74(3):609–617.
- [Bekoff et al., 1987] Bekoff, A., Nusbaum, M. P., Sabichi, A. L., and Clifford, M. (1987). Neural control of limb coordination. i. comparison of hatching and walking motor output patterns in normal and deafferented chicks. *The Journal of neuroscience*, 7(8):2320–2330.
- [Berme et al., 1977] Berme, N., Paul, J. P., and Purves, W. K. (1977). A biomechanical analysis of the metacarpo-phalangeal joint. *Journal of Biomechanics*, 10(7):409–412.
- [Bernstein, 1967] Bernstein, N. A. (1967). The co-ordination and regulation of movements.
- [Bevan, 1991] Bevan, L. (1991). The effect of the stimulation pattern on the fatigue of single motor units.
- [Bezanilla et al., 1972] Bezanilla, F., Caputo, C., Gonzalez-Serratos, H., and Venosa, R. A. (1972). Sodium dependence of the inward spread of activation in isolated twitch muscle fibres of the frog. *The Journal of physiology*, 223(2):507–523.
- [Bhagat and Wheeler, 1973] Bhagat, B. and Wheeler, N. (1973). Effect of amphetamine on the swimming endurance of rats. *Neuropharmacology*, 12(7):711–713.

- [Bianchi and Narayan, 1982] Bianchi, C. P. and Narayan, S. (1982). Possible role of the transverse tubules in accumulating calcium released from the terminal cisternae by stimulation and drugs. *Canadian Journal of Physiology and Pharmacology*, 60(4):503–507.
- [Bigland-Ritchie et al., 1986] Bigland-Ritchie, B., Furbush, F., and Woods, J. J. (1986). Fatigue of intermittent submaximal voluntary contractions: central and peripheral factors. *Journal of Applied Physiology*, 61(2):421–429.
- [Bigland-Ritchie et al., 1983] Bigland-Ritchie, B., Johansson, R., Lippold, O. C., and Woods, J. J. (1983). Contractile speed and EMG changes during fatigue of sustained maximal voluntary contractions. *Journal of Neurophysiology*, 50(1):313–324.
- [BiglandRitchie and Woods, 1984] BiglandRitchie, B. and Woods, J. J. (1984). Changes in muscle contractile properties and neural control during human muscular fatigue. *Muscle & nerve*, 7(9):691–699.
- [Binkofski et al., 1999] Binkofski, F., Buccino, G., Posse, S., Seitz, R. J., Rizzolatti, G., and Freund, H. J. (1999). A frontoparietal circuit for object manipulation in man: evidence from an fMRI study. *European Journal of Neuroscience*, 11(9):3276–3286.
- [Bizzi et al., 2002] Bizzi, E., d'Avella, A., Saltiel, P., and Tresch, M. (2002). Book review: Modular organization of spinal motor systems. *The Neuroscientist*, 8(5):437–442.
- [Bortolotto et al., 2000] Bortolotto, S. K., Cellini, M., Stephenson, D. G., and Stephenson, G. M. (2000). MHC isoform composition and ca²⁺-or sr²⁺-activation properties of rat skeletal muscle fibers. *American Journal of Physiology-Cell Physiology*, 279(5):C1564–C1577.
- [Bottinelli and Reggiani, 2000] Bottinelli, R. and Reggiani, C. (2000). Human skeletal muscle fibres: molecular and functional diversity. *Progress in biophysics and molecular biology*, 73(2-4):195–262.
- [Bradley et al., 2008] Bradley, N. S., Ryu, Y. U., and Lin, J. (2008). Fast locomotor burst generation in late stage embryonic motility. *Journal of neurophysiology*, 99(4):1733–1742.
- [Bradley et al., 2005] Bradley, N. S., Solanki, D., and Zhao, D. (2005). Limb movements during embryonic development in the chick: evidence for a continuum in limb motor control antecedent to locomotion. *Journal of neurophysiology*, 94(6):4401–4411.
- [Brandon et al., 2002] Brandon, D. H., Holditch-Davis, D., and Belyea, M. (2002). Preterm infants born at less than 31 weeks' gestation have improved growth in cycled light compared with continuous near darkness. *Journal of Pediatrics*, 140:192–198.

- [Brown and Loeb, 1998] Brown, I. E. and Loeb, G. E. (1998). Post-Activation Potentiation—A clue for simplifying models of muscle dynamics. *Integrative and Comparative Biology*, 38(4):743.
- [Burstedt et al., 1999] Burstedt, M. K., Flanagan, J. R., and Johansson, R. S. (1999). Control of grasp stability in humans under different frictional conditions during multidigit manipulation. *Journal of neurophysiology*, 82(5):2393.
- [Baszczyk et al., 2007] Baszczyk, J. W., Orawiec, R., Duda-Kodowska, D., and Opala, G. (2007). Assessment of postural instability in patients with parkinsons disease. *Experimental Brain Research*, 183(1):107–114.
- [Cabrera and Milton, 2004] Cabrera, J. L. and Milton, J. (2004). Human stick balancing: Tuning lvy flights to improve balance control.
- [Caldwell and Van Leemputte, 1991] Caldwell, G. E. and Van Leemputte, M. (1991). Elbow torques and EMG patterns of flexor muscles during different isometric tasks. *Electromyography and clinical neurophysiology*, 31(7):433.
- [Chao and An, 1978] Chao, E. Y. and An, K. N. (1978). Graphical interpretation of the solution to the redundant problem in biomechanics. *Journal of Biomechanical Engineering*, 100:159.
- [Chhabra and Jacobs, 2006] Chhabra, M. and Jacobs, R. A. (2006). Properties of synergies arising from a theory of optimal motor behavior. *Neural computation*, 18(10):2320–2342.
- [Clewley et al., 2008] Clewley, R. H., Guckenheimer, J. M., and Valero-Cuevas, F. J. (2008). Estimating effective degrees of freedom in motor systems. *Biomedical Engineering, IEEE Transactions on*, 55(2):430–442.
- [Cole and Abbs, 1986] Cole, K. J. and Abbs, J. H. (1986). Coordination of three-joint digit movements for rapid finger-thumb grasp. *Journal of neurophysiology*, 55(6):1407–1423.
- [Coleman and McDaniel, 1976] Coleman, M. A. and McDaniel, G. R. (1976). Light altered changes in the embryonic age versus incubation age of white leghorn embryos. *Poultry Science*, 55(6):2483–2485.
- [Collins and De Luca, 1994] Collins, J. J. and De Luca, C. J. (1994). Random walking during quiet standing. *Physical review letters*, 73(5):764–767.
- [Cote et al., 2002] Cote, J. N., Mathieu, P. A., Levin, M. F., and Feldman, A. G. (2002). Movement reorganization to compensate for fatigue during sawing. *Experimental brain research*, 146(3):394–398.

- [Crowninshield and Brand, 1981] Crowninshield, R. D. and Brand, R. A. (1981). A physiologically based criterion of muscle force prediction in locomotion. *Journal of Biomechanics*, 14(11):793–801.
- [Cutkosky, 1985] Cutkosky, M. R. (1985). *Robotic grasping and fine manipulation*. Kluwer Academic Publishers.
- [Danion et al., 2001] Danion, F., Latash, M., Li, Z. M., and Zatsiorsky, V. (2001). [Without title]. *Experimental brain research*, 138(3):322–329.
- [Danion et al., 2000] Danion, F., Latash, M. L., Li, Z. M., and Zatsiorsky, V. M. (2000). The effect of fatigue on multifinger co ordination in force production tasks in humans. *The Journal of Physiology*, 523(2):523–532.
- [Danna-Dos Santos et al., 2010] Danna-Dos Santos, A., Poston, B., Jesunathadas, M., Bobich, L. R., Hamm, T. M., and Santello, M. (2010). Influence of fatigue on hand muscle coordination and EMG-EMG coherence during Three-Digit grasping. *Journal of neurophysiology*, 104(6):3576.
- [Darling et al., 1988] Darling, W. G., Cole, K. J., and Abbs, J. H. (1988). Kinematic variability of grasp movements as a function of practice and movement speed. *Experimental Brain Research*, 73(2):225–235.
- [d'Avella et al., 2003] d'Avella, A., Saltiel, P., and Bizzi, E. (2003). Combinations of muscle synergies in the construction of a natural motor behavior. *Nature neuroscience*, 6(3):300–308.
- [Decker et al., 2010] Decker, M. J., Griffin, L., Abraham, L. D., and Brandt, L. (2010). Alternating stimulation of synergistic muscles during functional electrical stimulation cycling improves endurance in persons with spinal cord injury. *Journal of Electromyography and Kinesiology*, 20(6):1163–1169.
- [Delbono and Meissner, 1996] Delbono, O. and Meissner, G. (1996). Sarcoplasmic reticulum Ca^{2+} release in rat slow-and fast-twitch muscles. *Journal of Membrane Biology*, 151(2):123–130.
- [Dideriksen et al., 2011] Dideriksen, J., Enoka, R., and Farina, D. (2011). A model of the surface electromyogram in pathological tremor. *Biomedical Engineering, IEEE Transactions on*, (99):1–1.
- [Dideriksen et al., 2010] Dideriksen, J. L., Farina, D., and Enoka, R. M. (2010). Influence of fatigue on the simulated relation between the amplitude of the surface electromyogram and muscle force. *Philosophical Transactions of the Royal Society A: Mathematical, Physical and Engineering Sciences*, 368(1920):2765–2781.

- [Donald and Kuypers, 1968] Donald, G. L. and Kuypers, H. G. (1968). The functional organization of the motor system in the monkey: II. The effects of lesions of the descending brain-stem pathways. *Brain; a journal of neurology*, 91(1):15.
- [Duchateau et al., 2002] Duchateau, J., Balestra, C., Carpentier, A., and Hainaut, K. (2002). Reflex regulation during sustained and intermittent submaximal contractions in humans. *The Journal of physiology*, 541(3):959–967.
- [Duchateau and Hainaut, 1993] Duchateau, J. and Hainaut, K. (1993). Behaviour of short and long latency reflexes in fatigued human muscles. *The Journal of physiology*, 471(1):787–799.
- [Dul et al., 1984] Dul, J., Johnson, G. E., Shiavi, R., and Townsend, M. A. (1984). Muscular synergism—II. a minimum-fatigue criterion for load sharing between synergistic muscles. *Journal of Biomechanics*, 17(9):675–684.
- [Eccles et al., 1957] Eccles, J. C., Eccles, R. M., and Lundberg, A. (1957). The convergence of monosynaptic excitatory afferents on to many different species of alpha motoneurones. *The Journal of physiology*, 137(1):22–50.
- [Edwards et al., 1977] Edwards, R. H., Hill, D. K., Jones, D. A., and Merton, P. A. (1977). Fatigue of long duration in human skeletal muscle after exercise. *The Journal of physiology*, 272(3):769–778.
- [Ehrsson et al., 2000] Ehrsson, H. H., Fagergren, A., Jonsson, T., Westling, G., Johansson, R. S., and Forssberg, H. (2000). Cortical activity in precision-versus power-grip tasks: an fMRI study. *Journal of Neurophysiology*, 83(1):528.
- [Eliasson et al., 1995] Eliasson, A. C., Forssberg, H., Ikuta, K., Apel, I., Westling, G., and Johansson, R. (1995). Development of human precision grip. *Experimental Brain Research*, 106(3):425–433.
- [Enoka and Stuart, 1992] Enoka, R. M. and Stuart, D. G. (1992). Neurobiology of muscle fatigue. *Journal of Applied Physiology*, 72(5):1631.
- [Essen et al., 1975] Essen, B., Jansson, E., Henriksson, J., Taylor, A. W., and Saltin, B. (1975). Metabolic characteristics of fibre types in human skeletal muscle. *Acta Physiologica Scandinavica*, 95(2):153–165.
- [Fairchild and Christensen, 2000] Fairchild, B. D. and Christensen, V. L. (2000). Photostimulation of turkey eggs accelerates hatching times without affecting hatchability, liver or heart growth, or glycogen content. *Poultry Science*, 79(11):1627–1631.
- [Farina et al., 2004] Farina, D., Merletti, R., and Enoka, R. M. (2004). The extraction of neural strategies from the surface EMG. *Journal of Applied Physiology*, 96(4):1486–1495.

- [Flanagan et al., 1999] Flanagan, J. R., Burstedt, M. K., and Johansson, R. S. (1999). Control of fingertip forces in multidigit manipulation. *Journal of Neurophysiology*, 81(4):1706.
- [Forssberg et al., 1991] Forssberg, H., Eliasson, A. C., Kinoshita, H., Johansson, R. S., and Westling, G. (1991). Development of human precision grip i: basic coordination of force. *Experimental Brain Research*, 85(2):451–457.
- [Freund and Takala, 2001] Freund, J. and Takala, E. P. (2001). A dynamic model of the forearm including fatigue. *Journal of Biomechanics*, 34(5):597–605.
- [Fuglevand et al., 1993] Fuglevand, A. J., Winter, D. A., and Patla, A. E. (1993). Models of recruitment and rate coding organization in motor-unit pools. *Journal of neurophysiology*, 70(6):2470–2488.
- [Fuller et al., 2009] Fuller, J. R., Lomond, K. V., Fung, J., and Ct, J. N. (2009). Posture-movement changes following repetitive motion-induced shoulder muscle fatigue. *Journal of Electromyography and Kinesiology*, 19(6):1043–1052.
- [Gandevia, 1990] Gandevia, S. C. (1990). Neuromuscular fatigue mechanisms: central and peripheral factors affecting motoneuronal output in fatigue. *Fatigue in Sports and Exercise*, pages 9–15.
- [Gandevia, 2001] Gandevia, S. C. (2001). Spinal and supraspinal factors in human muscle fatigue. *Physiological reviews*, 81(4):1725–1789.
- [Gao et al., 2005] Gao, F., Latash, M. L., and Zatsiorsky, V. M. (2005). Internal forces during object manipulation. *Experimental brain research*, 165(1):69–83.
- [Garland, 1991] Garland, S. J. (1991). Role of small diameter afferents in reflex inhibition during human muscle fatigue. *The Journal of physiology*, 435(1):547.
- [Garland et al., 1994] Garland, S. J., Enoka, R. M., Serrano, L. P., and Robinson, G. A. (1994). Behavior of motor units in human biceps brachii during a submaximal fatiguing contraction. *Journal of Applied Physiology*, 76(6):2411–2419.
- [Garland and McComas, 1990] Garland, S. J. and McComas, A. J. (1990). Reflex inhibition of human soleus muscle during fatigue. *The Journal of physiology*, 429(1):17.
- [Gates and Dingwell, 2008] Gates, D. H. and Dingwell, J. B. (2008). The effects of neuromuscular fatigue on task performance during repetitive goal-directed movements. *Experimental Brain Research*, 187(4):573–585.
- [Ghatpande et al., 1995] Ghatpande, A., Ghatpande, S., and Khan, M. Z. (1995). Effect of different intensities of fluorescent light on the early development of chick embryos in ovo. *Cellular & molecular biology research*, 41(6):613.

- [Goddard et al., 1992] Goddard, R. E., Zheng, Y. F., and Hemami, H. (1992). Dynamic hybrid velocity/force control of robot compliant motion over globally unknown objects. *Robotics and Automation, IEEE Transactions on*, 8(1):132–138.
- [Gottschall et al., 2009] Gottschall, J., Peinke, J., Lippens, V., and Nagel, V. (2009). Exploring the dynamics of balance data—movement variability in terms of drift and diffusion. *Physics Letters A*, 373(8-9):811–816.
- [Gritti and Schieppati, 1989] Gritti, I. and Schieppati, M. (1989). Short-latency inhibition of soleus motoneurones by impulses in ia afferents from the gastrocnemius muscle in humans. *The Journal of Physiology*, 416(1):469–484.
- [Hamburger and Hamilton, 1992] Hamburger, V. and Hamilton, H. L. (1992). A series of normal stages in the development of the chick embryo. *Developmental dynamics*, 195(4):231–272.
- [Hasan and Enoka, 1985] Hasan, Z. and Enoka, R. M. (1985). Isometric torque-angle relationship and movement-related activity of human elbow flexors: implications for the equilibrium-point hypothesis. *Experimental brain research. Experimentelle Hirnforschung. Experimentation cerebrale*, 59(3):441.
- [Hausdorff et al., 1996a] Hausdorff, J. M., Purdon, P. L., Peng, C. K., Ladin, Z., Wei, J. Y., and Goldberger, A. L. (1996a). Fractal dynamics of human gait: stability of long-range correlations in stride interval fluctuations. *Journal of Applied Physiology*, 80(5):1448–1457.
- [Hausdorff et al., 1996b] Hausdorff, J. M., Purdon, P. L., Peng, C. K., Ladin, Z., Wei, J. Y., and Goldberger, A. L. (1996b). Fractal dynamics of human gait: stability of long-range correlations in stride interval fluctuations. *Journal of Applied Physiology*, 80(5):1448–1457.
- [Hayward et al., 1991] Hayward, L., Wesselmann, U., and Rymer, W. Z. (1991). Effects of muscle fatigue on mechanically sensitive afferents of slow conduction velocity in the cat triceps surae. *Journal of neurophysiology*, 65(2):360–370.
- [Henneman, 1957] Henneman, E. (1957). Relation between size of neurons and their susceptibility to discharge. *Science*, 126(3287):1345–1347.
- [Hoffer et al., 1987a] Hoffer, J. A., Loeb, G. E., Marks, W. B., O'Donovan, M. J., Pratt, C. A., and Sugano, N. (1987a). Cat hindlimb motoneurons during locomotion. i. destination, axonal conduction velocity, and recruitment threshold. *Journal of neurophysiology*, 57(2):510–529.
- [Hoffer et al., 1987b] Hoffer, J. A., Sugano, N., Loeb, G. E., Marks, W. B., O'Donovan, M. J., and Pratt, C. A. (1987b). Cat hindlimb motoneurons during locomotion. II. normal activity patterns. *Journal of neurophysiology*, 57(2):530–553.

- [Hogan, 1985] Hogan, N. (1985). The mechanics of multi-joint posture and movement control. *Biological cybernetics*, 52(5):315–331.
- [Housh et al., 1995] Housh, T. J., deVries, H. A., Johnson, G. O., Housh, D. J., Evans, S. A., Stout, J. R., Evetovich, T. K., and Bradway, R. M. (1995). Electromyographic fatigue thresholds of the superficial muscles of the quadriceps femoris. *European journal of applied physiology and occupational physiology*, 71(2):131–136.
- [Jacobson and Hollyday, 1982] Jacobson, R. D. and Hollyday, M. (1982). Electrically evoked walking and fictive locomotion in the chick. *Journal of Neurophysiology*, 48(1):257–270.
- [Jeka et al., 2004] Jeka, J., Kiemel, T., Creath, R., Horak, F., and Peterka, R. (2004). Controlling human upright posture: velocity information is more accurate than position or acceleration. *Journal of neurophysiology*, 92(4):2368–2379.
- [Jenmalm et al., 2003] Jenmalm, P., Birznieks, I., Goodwin, A. W., and Johansson, R. S. (2003). Influence of object shape on responses of human tactile afferents under conditions characteristic of manipulation. *European Journal of Neuroscience*, 18(1):164–176.
- [Johanson et al., 2001] Johanson, M. E., Valero-Cuevas, F. J., and Hentz, V. R. (2001). Activation patterns of the thumb muscles during stable and unstable pinch tasks. *Journal of hand surgery-American Volume-A*, 26(4):698–705.
- [Johansson and Birznieks, 2004] Johansson, R. S. and Birznieks, I. (2004). First spikes in ensembles of human tactile afferents code complex spatial fingertip events. *Nature Neuroscience*, 7(2):170–177.
- [Johansson and Westling, 1984] Johansson, R. S. and Westling, G. (1984). Roles of glabrous skin receptors and sensorimotor memory in automatic control of precision grip when lifting rougher or more slippery objects. *Experimental Brain Research*, 56(3):550–564.
- [Johnson et al., 1973] Johnson, M. A., Polgar, J., Weightman, D., and Appleton, D. (1973). Data on the distribution of fibre types in thirty-six human muscles:: An autopsy study. *Journal of the Neurological Sciences*, 18(1):111–129.
- [Johnston and Bekoff, 1992] Johnston, R. M. and Bekoff, A. (1992). Constrained and flexible features of rhythmical hindlimb movements in chicks: kinematic profiles of walking, swimming and airstepping. *Journal of experimental biology*, 171(1):43–66.
- [Johnston and Bekoff, 1996] Johnston, R. M. and Bekoff, A. (1996). Patterns of muscle activity during different behaviors in chicks: implications for neural control. *Journal of Comparative Physiology A: Neuroethology, Sensory, Neural, and Behavioral Physiology*, 179(2):169–184.

- [Jones et al., 2002] Jones, K. E., Hamilton, A. F., and Wolpert, D. M. (2002). Sources of signal-dependent noise during isometric force production. *Journal of neurophysiology*, 88(3):1533.
- [Jordan, 2003] Jordan, K. T. (2003). A minimal intervention principle for coordinated movement. In *Advances in Neural Information Processing Systems 15: Proceedings of the 2002 Conference*, volume 15, page 27. The MIT Press.
- [Kantelhardt et al., 2001] Kantelhardt, J. W., Koscielny-Bunde, E., Rego, H. H., Havlin, S., and Bunde, A. (2001). Detecting long-range correlations with detrended fluctuation analysis. *Physica A: Statistical Mechanics and its Applications*, 295(3):441–454.
- [Kantz and Schreiber, 2004] Kantz, H. and Schreiber, T. (2004). *Nonlinear time series analysis*, volume 7. Cambridge Univ Pr.
- [Kawato, 1999] Kawato, M. (1999). Internal models for motor control and trajectory planning. *Current opinion in neurobiology*, 9(6):718–727.
- [Keenan et al., 2009] Keenan, K. G., Santos, V. J., Venkadesan, M., and Valero-Cuevas, F. J. (2009). Maximal voluntary fingertip force production is not limited by movement speed in combined motion and force tasks. *The Journal of Neuroscience*, 29(27):8784.
- [Kim et al., 2006] Kim, S. W., Shim, J. K., Zatsiorsky, V. M., and Latash, M. L. (2006). Anticipatory adjustments of multi-finger synergies in preparation for self-triggered perturbations. *Experimental brain research*, 174(4):604–612.
- [Kouzaki, 2005] Kouzaki, M. (2005). Significant roles of synergistic muscles in human redundant and complicated activities. *International Journal of Sport and Health Science*, 3(Special Issue 2005):181–193.
- [Kouzaki and Shinohara, 2006] Kouzaki, M. and Shinohara, M. (2006). The frequency of alternate muscle activity is associated with the attenuation in muscle fatigue. *Journal of applied physiology*, 101(3):715–720.
- [Kouzaki et al., 2004] Kouzaki, M., Shinohara, M., Masani, K., and Fukunaga, T. (2004). Force fluctuations are modulated by alternate muscle activity of knee extensor synergists during low-level sustained contraction. *Journal of Applied Physiology*, 97(6):2121–2131.
- [Kouzaki et al., 2002] Kouzaki, M., Shinohara, M., Masani, K., Kanehisa, H., and Fukunaga, T. (2002). Alternate muscle activity observed between knee extensor synergists during low-level sustained contractions. *Journal of Applied Physiology*, 93(2):675–684.

- [Kuo and Zajac, 1993] Kuo, A. D. and Zajac, F. E. (1993). A biomechanical analysis of muscle strength as a limiting factor in standing posture. *Journal of Biomechanics*, 26:137–150.
- [Kutch et al., 2008] Kutch, J. J., Kuo, A. D., Bloch, A. M., and Rymer, W. Z. (2008). Endpoint force fluctuations reveal flexible rather than synergistic patterns of muscle cooperation. *Journal of neurophysiology*, 100(5):2455–2471.
- [Kutch and Valero-Cuevas, 2011] Kutch, J. J. and Valero-Cuevas, F. J. (2011). Muscle redundancy does not imply robustness to muscle dysfunction. *Journal of biomechanics*, 44(7):1264–1270.
- [Kutch and Valero-Cuevas, 2012] Kutch, J. J. and Valero-Cuevas, F. J. (2012). Challenges and new approaches to proving the existence of muscle synergies of neural origin.
- [Lamb, 1992] Lamb, G. D. (1992). DHP receptors and excitation-contraction coupling. *Journal of muscle research and cell motility*, 13(4):394–405.
- [Lamb and Walsh, 1987] Lamb, G. D. and Walsh, T. (1987). Calcium currents, charge movement and dihydropyridine binding in fast-and slow-twitch muscles of rat and rabbit. *The Journal of physiology*, 393(1):595.
- [Lang and Schieber, 2004] Lang, C. E. and Schieber, M. H. (2004). Reduced muscle selectivity during individuated finger movements in humans after damage to the motor cortex or corticospinal tract. *Journal of neurophysiology*, 91(4):1722.
- [Latash et al., 2010] Latash, M. L., Levin, M. F., Scholz, J. P., and Schoener, G. (2010). Motor control theories and their applications. *Medicina (Kaunas, Lithuania)*, 46(6):382.
- [Latash and Zatsiorsky, 2009] Latash, M. L. and Zatsiorsky, V. M. (2009). Multi-finger prehension: control of a redundant mechanical system. *Progress in Motor Control*, pages 597–618.
- [Lauber, 1975] Lauber, J. K. (1975). Photoacceleration of avian embryogenesis. *Comparative Biochemistry and Physiology Part A: Physiology*, 51(4):903–907.
- [Lauber and Shutze, 1964] Lauber, J. K. and Shutze, J. V. (1964). Accelerated Growth of embryo chicks under the influence of light. *Growth*, 28:179.
- [Lemon, 2008] Lemon, R. N. (2008). Descending pathways in motor control. *Annu. Rev. Neurosci.*, 31:195–218.
- [Loeb, 2000] Loeb, G. E. (2000). Overcomplete musculature or underspecified tasks? *MOTOR CONTROL-CHAMPAIGN*, 4(1):81–83.

- [Loeb and Ghez, 2000] Loeb, G. E. and Ghez, C. (2000). The motor unit and muscle action. *Principles of neural science*, pages 674–694.
- [Ma et al., 2011] Ma, L., Chablat, D., Bennis, F., Zhang, W., Hu, B., and Guillaume, F. (2011). Fatigue evaluation in maintenance and assembly operations by digital human simulation in virtual environment. *Virtual reality*, 15(1):55–68.
- [Macefield et al., 1991] Macefield, G., Hagbarth, K. E., Gorman, R., Gandevia, S. C., and Burke, D. (1991). Decline in spindle support to alpha-motoneurones during sustained voluntary contractions. *The Journal of physiology*, 440(1):497–512.
- [Margreth et al., 1993] Margreth, A., Damiani, E., and Tobaldin, G. (1993). Ratio of dihydropyridine to ryanodine receptors in mammalian and frog twitch muscles in relation to the mechanical hypothesis of excitation-contraction coupling. *Biochemical and biophysical research communications*, 197(3):1303–1311.
- [Merton, 1954] Merton, P. A. (1954). Voluntary strength and fatigue. *The Journal of Physiology*, 123(3):553–564.
- [Miller et al., 1995] Miller, C. L., White, R., Whitman, T. L., O’Callaghan, M. F., and Maxwell, S. E. (1995). The effects of cycled versus noncycled lighting on growth and development in preterm infants. *Infant Behavior and Development*, 18(1):87–95.
- [Milton et al., 2009] Milton, J., Cabrera, J. L., Ohira, T., Tajima, S., Tonosaki, Y., Eurich, C. W., and Campbell, S. A. (2009). The time-delayed inverted pendulum: implications for human balance control. *Chaos: An Interdisciplinary Journal of Non-linear Science*, 19(2):026110.
- [Minami et al., 1983] Minami, A., An, K. N., Cooney III, W. P., Linscheid, R. L., and Chao, E. (1983). Ligamentous structures of the metacarpophalangeal joint: a quantitative anatomic study. *Journal of orthopaedic research*, 1(4):361–368.
- [Murray et al., 1994] Murray, R. M., Li, Z., and Sastry, S. S. (1994). *A mathematical introduction to robotic manipulation*. CRC.
- [Noy and Sklan, 1997] Noy, Y. and Sklan, D. (1997). Posthatch development in poultry. *The Journal of Applied Poultry Research*, 6(3):344–354.
- [Oldfield, 1971] Oldfield, R. C. (1971). The assessment and analysis of handedness: the edinburgh inventory. *Neuropsychologia*, 9(1):97–113.
- [Overstall et al., 1977] Overstall, P. W., Exton-Smith, A. N., Imms, F. J., and Johnson, A. L. (1977). Falls in the elderly related to postural imbalance. *British Medical Journal*, 1(6056):261–264.

- [Park et al., 2010] Park, J., Kim, Y. S., and Shim, J. K. (2010). Prehension synergy: effects of static constraints on multi-finger prehension. *Human movement science*, 29(1):19–34.
- [Pascoe et al., 2006] Pascoe, M. A., Barry, B. K., Riley, Z. A., and Enoka, R. M. (2006). Identifying the source of radial nerve afferents that inhibit biceps brachii. *Med Sci Sports Exerc*, 38:S372.
- [Peng et al., 1998] Peng, C. K., Hausdorff, J. M., Havlin, S., Mietus, J. E., Stanley, H. E., and Goldberger, A. L. (1998). Multiple-time scales analysis of physiological time series under neural control. *Physica A: Statistical Mechanics and its Applications*, 249(1):491–500.
- [Penzel et al., 2003] Penzel, T., Kantelhardt, J. W., Grote, L., Peter, J. H., and Bunde, A. (2003). Comparison of detrended fluctuation analysis and spectral analysis for heart rate variability in sleep and sleep apnea. *Biomedical Engineering, IEEE Transactions on*, 50(10):1143–1151.
- [Prieto et al., 1993] Prieto, T. E., Myklebust, J. B., and Myklebust, B. M. (1993). Characterization and modeling of postural steadiness in the elderly: a review. *Rehabilitation Engineering, IEEE Transactions on*, 1(1):26–34.
- [Prilutsky et al., 1997] Prilutsky, B. I., Herzog, W., and Allinger, T. L. (1997). Forces of individual cat ankle extensor muscles during locomotion predicted using static optimization. *Journal of biomechanics*, 30(10):1025–1033.
- [Prilutsky and Zatsiorsky, 2002] Prilutsky, B. I. and Zatsiorsky, V. M. (2002). Optimization-based models of muscle coordination. *Exercise and sport sciences reviews*, 30(1):32.
- [Raibert and Craig, 1981] Raibert, M. H. and Craig, J. J. (1981). Hybrid position/force control of manipulators. *Journal of Dynamic Systems, Measurement, and Control*, 103:126.
- [Ranson, 1953] Ranson, S. W. (1953). *The anatomy of the nervous system: Its development and function*. Saunders.
- [Riddle et al., 2009] Riddle, C. N., Edgley, S. A., and Baker, S. N. (2009). Direct and indirect connections with upper limb motoneurons from the primate reticulospinal tract. *The journal of Neuroscience*, 29(15):4993–4999.
- [Riedstra and Groothuis, 2004] Riedstra, B. and Groothuis, T. G. G. (2004). Prenatal light exposure affects early feather-pecking behaviour in the domestic chick. *Animal behaviour*, 67(6):1037–1042.

- [Rolfs, 2009] Rolfs, M. (2009). Microsaccades: Small steps on a long way. *Vision research*, 49(20):2415–2441.
- [Romijn and Roos, 1938] Romijn, C. and Roos, J. (1938). The air space of the hen's egg and its changes during the period of incubation. *The Journal of Physiology*, 94(3):365–379.
- [Rudroff et al., 2010] Rudroff, T., Justice, J. N., Matthews, S., Zuo, R., and Enoka, R. M. (2010). Muscle activity differs with load compliance during fatiguing contractions with the knee extensor muscles. *Experimental Brain Research*, 203(2):307–316.
- [Ryu and Bradley, 2009] Ryu, Y. U. and Bradley, N. S. (2009). Precocious locomotor behavior begins in the egg: Development of leg muscle patterns for stepping in the chick. *PloS one*, 4(7):e6111.
- [Sale, 1987] Sale, D. G. (1987). Influence of exercise and training on motor unit activation. *Exercise and sport sciences reviews*, 15:95.
- [Sancho-Bru et al., 2001] Sancho-Bru, J. L., Perez-Gonzalez, A., Vergara-Monedero, M., and Giurintano, D. (2001). A 3-D dynamic model of human finger for studying free movements. *Journal of Biomechanics*, 34(11):1491–1500.
- [Santello and Soechting, 2000] Santello, M. and Soechting, J. F. (2000). Force synergies for multifingered grasping. *Experimental Brain Research*, 133(4):457–467.
- [Santos et al., 2010] Santos, A. D., Poston, B., Jesunathadas, M., Bobich, L. R., Hamm, T. M., and Santello, M. (2010). The influence of fatigue on hand muscle coordination and EMG-EMG coherence during three-digit grasping. *Journal of Neurophysiology*.
- [Schieber and Santello, 2004] Schieber, M. H. and Santello, M. (2004). Hand function: peripheral and central constraints on performance. *Journal of Applied Physiology*, 96(6):2293–2300.
- [Schiappati et al., 1990] Schiappati, M., Romano, C., and Gritti, I. (1990). Convergence of ia fibres from synergistic and antagonistic muscles onto interneurones inhibitory to soleus in humans. *The Journal of physiology*, 431(1):365–377.
- [Schmidt and Lipson, 2009] Schmidt, M. and Lipson, H. (2009). Distilling free-form natural laws from experimental data. *science*, 324(5923):81–85.
- [Scholz et al., 2002] Scholz, J. P., Danion, F., Latash, M. L., and Schoner, G. (2002). Understanding finger coordination through analysis of the structure of force variability. *Biological Cybernetics*, 86(1):29–39.

- [Scholz and Schner, 1999] Scholz, J. P. and Schner, G. (1999). The uncontrolled manifold concept: identifying control variables for a functional task. *Experimental Brain Research*, 126(3):289–306.
- [Schreuders et al., 2006] Schreuders, T. A., Selles, R. W., Roebroeck, M. E., and Stam, H. J. (2006). Strength measurements of the intrinsic hand muscles: a review of the development and evaluation of the rotterdam intrinsic hand myometer. *Journal of Hand Therapy*, 19(4):393–402.
- [Schuind et al., 1992] Schuind, F., Garcia-Elias, M., Cooney, W. P., and An, K. N. (1992). Flexor tendon forces: in vivo measurements. *The Journal of hand surgery*, 17(2):291–298.
- [Semmler et al., 2000] Semmler, J. G., Kutzscher, D. V., and Enoka, R. M. (2000). Limb immobilization alters muscle activation patterns during a fatiguing isometric contraction. *Muscle & nerve*, 23(9):1381–1392.
- [Seth and Pandy, 2007] Seth, A. and Pandy, M. G. (2007). A neuromusculoskeletal tracking method for estimating individual muscle forces in human movement. *Journal of biomechanics*, 40(2):356–366.
- [Shim et al., 2005] Shim, J. K., Latash, M. L., and Zatsiorsky, V. M. (2005). Prehension synergies in three dimensions. *Journal of neurophysiology*, 93(2):766.
- [Shutze et al., 1962] Shutze, J. V., Lauber, J. K., Kato, M., and Wilson, W. O. (1962). Influence of incandescent and coloured light on chicken embryos during incubation.
- [Siegel et al., 1969] Siegel, P. B., Isakson, S. T., Coleman, F. N., and Huffman, B. J. (1969). Photoacceleration of development in chick embryos. *Comparative Biochemistry and Physiology*, 28(2):753–758.
- [Sindhurakar and Bradley, 2010] Sindhurakar, A. and Bradley, N. S. (2010). Kinematic analysis of overground locomotion in chicks incubated under different light conditions. *Developmental Psychobiology*, 52(8):802–812.
- [Singh et al., 2010] Singh, T., SKM, V., Zatsiorsky, V. M., and Latash, M. L. (2010). Fatigue and motor redundancy: Adaptive increase in finger force variance in Multi-Finger tasks. *Journal of neurophysiology*, 103(6):2990.
- [Sjogaard et al., 1986] Sjogaard, G., Kiens, B., Jorgensen, K., and Saltin, B. (1986). Intramuscular pressure, EMG and blood flow during low-level prolonged static contraction in man. *Acta Physiologica Scandinavica*, 128(3):475–484.
- [Sjgaard et al., 1988] Sjgaard, G., Savard, G., and Juel, C. (1988). Muscle blood flow during isometric activity and its relation to muscle fatigue. *European journal of applied physiology and occupational physiology*, 57(3):327–335.

- [Skavenski et al., 1979] Skavenski, A. A., Hansen, R. M., Steinman, R. M., and Winterson, B. J. (1979). Quality of retinal image stabilization during small natural and artificial body rotations in man. *Vision research*, 19(6):675–683.
- [Spoor, 1983] Spoor, C. W. (1983). Balancing a force on the fingertip of a two-dimensional finger model without intrinsic muscles. *Journal of Biomechanics*, 16(7):497–504.
- [Talati et al., 2005] Talati, A., Valero-Cuevas, F. J., and Hirsch, J. (2005). Visual and tactile guidance of dexterous manipulation tasks: an fMRI study 1, 2. *Perceptual and motor skills*, 101(1):317–334.
- [Tamaki et al., 1998] Tamaki, H., Kitada, K., Akamine, T., Murata, F., Sakou, T., and Kurata, H. (1998). Alternate activity in the synergistic muscles during prolonged low-level contractions. *Journal of Applied Physiology*, 84(6):1943–1951.
- [Theeuwen et al., 1994] Theeuwen, M., Gielen, C. C., Miller, L. E., and Doorenbosch, C. (1994). The relation between the direction dependence of electromyographic amplitude and motor unit recruitment thresholds during isometric contractions. *Experimental brain research*, 98(3):488–500.
- [Todorov and Jordan, 2002] Todorov, E. and Jordan, M. I. (2002). Optimal feedback control as a theory of motor coordination. *Nature neuroscience*, 5(11):1226–1235.
- [Tresch and Jarc, 2009] Tresch, M. C. and Jarc, A. (2009). The case for and against muscle synergies. *Current opinion in neurobiology*, 19(6):601–607.
- [Trinh and Lamb, 2006] Trinh, H. H. and Lamb, G. D. (2006). Matching of sarcoplasmic reticulum and contractile properties in rat fast- and slow-twitch muscle fibres. *Clinical and experimental pharmacology and physiology*, 33(7):591–600.
- [Tseng and Scholz, 2005] Tseng, Y. W. and Scholz, J. P. (2005). The effect of workspace on the use of motor abundance. *Motor control*, 9(1):75.
- [Valero-Cuevas, 2000] Valero-Cuevas, F. J. (2000). Predictive modulation of muscle coordination pattern magnitude scales fingertip force magnitude over the voluntary range. *Journal of Neurophysiology*, 83(3):1469–1479.
- [Valero-Cuevas, 2005] Valero-Cuevas, F. J. (2005). An integrative approach to the biomechanical function and neuromuscular control of the fingers. *Journal of Biomechanics*, 38(4):673–684.
- [Valero-Cuevas, 2009] Valero-Cuevas, F. J. (2009). A mathematical approach to the mechanical capabilities of limbs and fingers. *Progress in Motor Control*, pages 619–633.

- [Valero-Cuevas and Brown, 2006] Valero-Cuevas, F. J. and Brown, D. (2006). *Device and method for quantifying and extracting sensorimotor circuitry*. Google Patents.
- [Valero-Cuevas et al., 2009a] Valero-Cuevas, F. J., Hoffmann, H., Kurse, M. U., Kutch, J. J., and Theodorou, E. A. (2009a). Computational models for neuromuscular function. *Biomedical Engineering, IEEE Reviews in*, 2:110–135.
- [Valero-Cuevas et al., 2003] Valero-Cuevas, F. J., Johanson, M. E., and Towles, J. D. (2003). Towards a realistic biomechanical model of the thumb: the choice of kinematic description may be more critical than the solution method or the variability/uncertainty of musculoskeletal parameters. *Journal of Biomechanics*, 36(7):1019–1030.
- [Valero-Cuevas et al., 2009b] Valero-Cuevas, F. J., Venkadesan, M., and Todorov, E. (2009b). Structured variability of muscle activations supports the minimal intervention principle of motor control. *Journal of neurophysiology*, 102(1):59–68.
- [Valero-Cuevas et al., 1998] Valero-Cuevas, F. J., Zajac, F. E., and Burgar, C. G. (1998). Large index-fingertip forces are produced by subject-independent patterns of muscle excitation. *Journal of Biomechanics*, 31(8):693–704.
- [van de Kamp and Zaal, 2007] van de Kamp, C. and Zaal, F. T. (2007). Prehension is really reaching and grasping. *Experimental Brain Research*, 182(1):27–34.
- [Venkadesan et al., 2007] Venkadesan, M., Guckenheimer, J., and Valero-Cuevas, F. J. (2007). Manipulating the edge of instability. *Journal of biomechanics*, 40(8):1653–1661.
- [Venkadesan and Valero-Cuevas, 2008] Venkadesan, M. and Valero-Cuevas, F. J. (2008). Neural control of motion-to-force transitions with the fingertip. *The journal of Neuroscience*, 28(6):1366–1373.
- [Vollestad, 1997] Vollestad, N. K. (1997). Measurement of human muscle fatigue. *Journal of Neuroscience Methods*, 74(2):219–227.
- [Ward et al., 2009] Ward, S. R., Eng, C. M., Smallwood, L. H., and Lieber, R. L. (2009). Are current measurements of lower extremity muscle architecture accurate? *Clinical Orthopaedics and Related Research*, 467(4):1074–1082.
- [Westgaard and De Luca, 1999] Westgaard, R. H. and De Luca, C. J. (1999). Motor unit substitution in long-duration contractions of the human trapezius muscle. *Journal of neurophysiology*, 82(1):501–504.
- [Williams and Willima, 1996] Williams, J. H. and Willima, J. H. (1996). *Fundamentals of applied dynamics*. Wiley.

- [Winges et al., 2008] Winges, S. A., Eonta, S. E., Soechting, J. F., and Flanders, M. (2008). Multi-digit control of contact forces during rotation of a hand-held object. *Journal of neurophysiology*, 99(4):1846–1856.
- [Winges et al., 2009] Winges, S. A., Eonta, S. E., Soechting, J. F., and Flanders, M. (2009). Effects of object compliance on three-digit grasping. *Journal of neurophysiology*, 101(5):2447–2458.
- [Winges et al., 2006] Winges, S. A., Johnston, J. A., and Santello, M. (2006). Muscle-pair specific distribution and grip-type modulation of neural common input to extrinsic digit flexors. *Journal of neurophysiology*, 96(3):1258.
- [Yoshikawa, 1990] Yoshikawa, T. (1990). *Foundations of robotics: analysis and control*. The MIT Press.
- [Yoshikawa and Nagai, 1991] Yoshikawa, T. and Nagai, K. (1991). Manipulating and grasping forces in manipulation by multifingered robot hands. *Robotics and Automation, IEEE Transactions on*, 7(1):67–77.
- [Zappia and Rogers, 1983] Zappia, J. V. and Rogers, L. J. (1983). Light experience during development affects asymmetry of forebrain function in chickens. *Developmental Brain Research*, 11(1):93–106.
- [Zatsiorsky et al., 2000] Zatsiorsky, V. M., Li, Z. M., and Latash, M. L. (2000). Enslaving effects in multi-finger force production. *Experimental brain research. Experimentelle Hirnforschung. Experimentation cerebrale*, 131(2):187.